MATHEMATICAL MODELING OF TRANSMISSION CHANNELS AND LINK BUDGET FOR ULTRA WIDEBAND IMPULSE RADIO SYSTEMS

PICHAYA SUPANAKOON

A THESIS SUBMITTED IN PARTIAL FULFILLMENT
OF THE REQUIREMENT FOR THE DEGREE OF
DOCTOR OF ENGINEERING IN ELECTRICAL ENGINEERING
FACULTY OF ENGINEERING
KING MONGKUT'S INSTITUTE OF TECHNOLOGY LADKRABANG
2012

KMITL-2012-EN-D-018-019

หัวข้อวิทยานิพนธ์	การทำแบบจำลองเชิงคณิตศาสตร์ของช่องสัญญาณการส่งผ่านและการเชื่อมโยงสำหรับระบบวิทยุอิมพัลส์แถบกว้างยิ่ง
นักศึกษา	นายพิชญ สุพรรณกูล
รหัสประจำตัว	53610123
ปริญญา	วิศวกรรมศาตรดุษฎีบัณฑิต
สาขาวิชา	วิศวกรรมไฟฟ้า
พ.ศ.	2555
อาจารย์ที่ปรึกษาวิทยานิพนธ์	ดร.สถาพร พรหมวงศ์
อาจารย์ที่ปรึกษาวิทยานิพนธ์ร่วม	ศ.ดร.จุนอิชิ ทาคาดะ

บทคัดย่อ

วิทยานิพนธ์ฉบับนี้นำเสนอการทำแบบจำลองเชิงคณิตศาสตร์ของช่องสัญญาณการส่งผ่านและการเชื่อมโยงสำหรับระบบวิทยุอิมพัลส์แถบกว้างยิ่ง (Ultra Wideband Impulse Radio: UWB-IR) สำหรับการทำแบบจำลองช่องสัญญาณการส่งผ่าน ได้ทำแบบจำลองเชิงคณิตศาสตร์การสูญเสียเชิงวิถีอวกาศว่างและการสะท้อนพื้นโดยได้นำเสนอวิธีการหาที่มาแบบใหม่ สูตรที่ได้อยู่บนพื้นฐานของรูปคลื่นแถบผ่านสี่เหลี่ยมและสูตรการส่งผ่านของฟรีสในรูปแบบเชิงซ้อน นอกจากนั้น ได้หานิพจน์การสูญเสียเชิงวิถีในรูปแบบปิดที่มีพื้นฐานอยู่บนการสูญเสียกำลังเฉลี่ยและการสูญเสียกำลังค่ายอดสำหรับช่องสัญญาณอวกาศว่างและการสะท้อนพื้น หลังจากนั้นได้นำเสนอพารามิเตอร์เชิงขนาดใหม่ขึ้นมา คืออัตราการสูญเสียค่ายอดต่อการสูญเสียเฉลี่ย และทำเป็นสูตรในรูปแบบปิดสำหรับระบบ UWB-IR รวมทั้งได้ทำสูตรในรูปแบบปิดของสัมประสิทธิ์สหสัมพันธ์ที่ใช้เครื่องรับสหสัมพันธ์ที่มีต้นแบบรูปคลื่นส่ง และได้ทำการวัดเพื่อนำผลมาเปรียบเทียบสำหรับช่องสัญญาณการสะท้อนพื้น จากผลที่ได้สูตรที่ได้นำเสนอทั้งหมดสอดคล้องเป็นอย่างดีกับผลการวัด ดังนั้น แบบจำลองที่นำเสนอมีความเที่ยงตรงและสามารถนำมาใช้ทำแบบจำลองช่องสัญญาณอวกาศว่างและการสะท้อนพื้น UWB-IR สำหรับการเชื่อมโยง ได้กล่าวถึงแบบจำลองการเชื่อมโยงที่เป็นแบบทั่วไปมากขึ้นสำหรับศึกษาความเพี้ยนของรูปคลื่นที่เกิดจากสายอากาศบนการส่งผ่านอวกาศว่าง ได้พัฒนาแบบแผนการประเมินผลการเชื่อมโยงอวกาศว่างในเทอมของฟังก์ชันถ่ายโอนความถี่สำหรับระบบ UWB-IR โดยได้พิจารณารูปคลื่นส่ง ความเพี้ยนที่เกิดจากสายอากาศ ช่องสัญญาณ และเครื่องรับสหสัมพันธ์ แบบจำลองนี้มีพื้นฐานอยู่บนสูตรการส่งผ่านของฟรีสดัดแปลงมาใช้สำหรับระบบการส่งผ่าน UWB-IR รูปคลื่นส่งได้ใช้รูปคลื่นแถบผ่านสี่เหลี่ยมและรูปคลื่นแถบผ่านรากการเพิ่มแบบโคไซน์ ได้ทำการประเมินผลเชิงการวัดสำหรับสายอากาศไดโพลรายคาบล็อก (Log-Periodic Dipole Antenna: LPDA) ได้หาที่มาและแสดงปริมาณความเพี้ยนในเทอมของความเพี้ยนของรูปคลื่นและอัตราขยายการส่งผ่าน แบบแผนนี้จะมีประสิทธิภาพมากโดยเฉพาะประเมินผลสายอากาศที่ใช้จริงซึ่งมีคุณสมบัติทางความถี่ของการสูญเสียย้อนกลับและสภาพเจาะจงทิศทางไม่เป็นไปตามอุดมคติ โดยที่ประสิทธิภาพทั้งหมดสามารถประเมินผลโดยใช้เพียงเทอมของอัตราขยายการส่งผ่าน UWB-IR

Thesis	Mathematical Modeling of Transmission Channels and Link Budget for Ultra Wideband Impulse Radio Systems
Student	Mr. Pichaya Supanakoon
Student ID.	53610123
Degree	Doctor of Engineering
Program	Electrical Engineering
Year	2012
Thesis Advisor	Dr. Sathaporn Promwong
Thesis Co-Advisor	Prof. Dr. Jun-ichi Takada

ABSTRACT

This thesis proposes the mathematical modeling of transmission channels and link budget for ultra wideband impulse radio (UWB-IR) systems. For transmission channel modeling, free space and ground reflection path losses are mathematically modeled. The novel method of derivation is proposed. The formula is based on rectangular passband waveform and complex form of Friis' transmission formula. In addition, the closed forms of path loss expressions are derived based on both average and peak power losses for free space and ground reflection channels. After that, the novel quantitative parameter, peak to average loss ratio, is proposed and derived in the closed form formula for UWB-IR systems. Moreover, the closed form formulas of correlation coefficient using correlation receiver with transmitted waveform template are derived. The measurement was done and compared for the ground reflection channel. From the results, all of proposed formulas correspond very well with measurement. Therefore, the proposed models are accurate and can be the choices for modeling the UWB-IR free space and ground reflection channels. For link budget, a more generalized link budget model for studying the waveform distortion due to antenna on free space transmission is discussed. The free space link budget evaluation scheme in the term of frequency transfer function that takes into account the transmitted waveform, its distortion due to the antennas, the channel and the correlation receiver is developed. This model is based on Friis' transmission formula, adapted to the UWB-IR transmission systems. The rectangular and root raised cosine passband waveforms are used as the transmitted waveform. Experimental investigations are done for log-periodic dipole antenna (LPDA). The distortion quantities in the term of waveform distortion and transmission gain are defined and shown. This link budget evaluation scheme may be effective, especially to evaluate the deployable antenna with non-ideal frequency characteristics of return loss and directivity, as the overall performance can be evaluated only by the term of UWB-IR transmission gain.

ACKNOWLEDGEMENTS

This thesis is the final submission to accomplish the Doctor of Engineering of Electrical Engineering at King Mongkut's Institute of Technology Ladkrabang, Bangkok, Thailand. During the time I have been working on my thesis, I have been received very well support, assistance and encouragement from many people as below. Therefore, I would like to take this opportunity to express my sincere thanks to those who have contributed directly or indirectly to bring this thesis to the final format.

I would like to express my gratitude to my advisor, Dr. Sathaporn Promwong, for accepting me as his doctoral student. His willingness to teach attitude and unfailing patience has been a great motivation for me to excel in my work. Without his guidance and invaluable time spent with me in this research, this thesis would not have been completed successfully.

In addition, I would like to express my gratitude to my co-advisor, Prof. Dr. Jun-ichi Takada, for his expert and kind discussion, suggestion and proof reading of my research papers. He gives me a good research experience to achieve new performance goals for my thesis. Without his kindly help, this thesis would not finish.

Moreover, I would like to thank those who have helped me throughout this whole research, especially these guys from Ultra Wideband Radio Systems (UWBRS) Laboratory for their helpful discussions and friendship.

Furthermore, I would love to express my gratefulness and appreciation to all of my family members. Most importantly, I would never be who I am and what I am without them. I am proud to give a credit to them who are totally the main reason to drive me to be at this point. Without their support encouragement, stimulation and enthusiasm, I would never get this far.

Finally, it is my wish that this thesis will be a valuable source of data for those who are interested in this field.

Pichaya Supanakoon

TABLE OF CONTENTS

TABLE OF CONTENTS (CONTINUE)

TABLE OF CONTENTS (CONTINUE)

LIST OF TABLES

LIST OF FIGURES

LIST OF FIGURES (CONTINUE)

LIST OF FIGURES (CONTINUE)

LIST OF ABBREVATIONS

Additive White Gaussian Noise	AWGN
Direct Sequence Ultra Wideband	DS-UWB
European Telecommunications Standard Institute	ETSI
Federal Communications Commission	FCC
High Rate Wireless Personal Area Network	HR-WPAN
International Telecommunication Union	ITU
King Mongkut's Institute of Technology Ladkrabang	KMITL
Line-of-Sight	LOS
Log-Periodic Dipole Antenna	LPDA
Low Rate Wireless Personal Area Network	LR-WPAN
Ministry of Internal Affairs and Communications	MIC
Multi-Band Orthogonal Frequency Division Multiplexing	MB-OFDM
Phase Locked Loop	PLL
Power Spectral Density	PSD
Root Mean Square	RMS
Radio Frequency	RF
Signal-to-Noise Ratio	SNR
Ultra Wideband Impulse Radio	UWB-IR
Vector Network Analyzer	VNA
Wireless Body Area Network	WBAN
Wireless Sensor Networks	WSN

CHAPTER 1
INTRODUCTION

1.1 Background

Ultra wideband impulse radio (UWB-IR) technology becomes an important topic for wireless system due to its potentials to offer very high capacity, low cost and low power consumption properties [1]-[3]. The interested advantages of UWB-IR systems are low cost resulted from low complexity of system, low signal power spectral density (PSD) with same as or below than noise level, resistant to multi-path fading and high time resolution for localization [4].

The Federal Communications Commission (FCC) of USA first specified that UWB-IR signal could be transmitted at the frequency spectrum ranging from 3.1 to 10.6 GHz [5]. Similarly, in Europe, European Telecommunications Standard Institute (ETSI) and International Telecommunication Union (ITU) first proposed UWB-IR signal regulation same FCC spectrum rage with slope spectral mask [6] and then modified to frequency spectrum ranging from 6.0 to 8.5 GHz [7]. In Japan, Ministry of Internal Affairs and Communications (MIC) specified the UWB-IR signal has two frequency spectrum ranges, lower band form 3.4 to 4.8 GHz and upper band from 7.25 to 10.25 GHz [8]. Recently, UWB-IR signal regulation has been approved in other regions as well. There is common frequency available among FCC, ETSI and MIC, that is from 7.25 to 8.5 GHz [9].

UWB-IR system was first adopted for IEEE 802.15.3a high rate wireless personal area networks (HR-WPANs) with distance up to 10 meters [10] but this standard was withdrawn in January 2006. Moreover, UWB-IR system is also adopted for IEEE 802.15.4a low rate wireless personal area networks (LR-WPANs) enabling wireless sensor networks (WSN) with transmission distance up to several hundred meters [11] and IEEE 802.15.6 for low power communication between body nodes to provide medical and non-medical applications [12].

1.2 Motivation

Path loss model is necessary tool for designing and deploying any wireless systems including UWB-IR systems. For UWB-IR transmission, very high peak short pulse with very low duty cycle allows to obtain the ultra low power consumption. The peak power loss and average power loss from transmitter and receiver are equal for the distortionless condition. However, the distortion of UWB-IR waveform due to frequency and time dispersions of channel causes the difference. Therefore, both

path losses based on average and peak power losses should be modeled. Furthermore, the ratio between path loss based on peak and average power losses can be defined as the distortion quantity of UWB-IR waveform. For UWB-IR correlation receiver with transmitted template signal, the correlation coefficient used to identify the receiver efficiency. The correlation coefficient is equal to 1 means the efficiency is 100%. In other words, that is the special case of correlation receiver, which is called as matched filter receiver. The transmitted template signal is identical with received signal. The correlation coefficient is decreased when the template signal is more differ. If the correlation coefficient is equal to 0, that means the template signal is orthogonal with received signal. There is no signal that can be detected from the receiver. The correlation coefficient is also applied to analyze the waveform distortion.

In UWB-IR systems, antennas usually act as significant pulse shaping filters and cause extreme waveform distortion. Moreover, low cost, geometrically small and still efficient antennas are required for the UWB-IR applications. Therefore, the link budget that considers the distortion due to antennas is important to design and improve the performance of UWB-IR systems.

1.3 Previous Work

The Friis' transmission formula is widely used to evaluate the free space of narrowband wireless system [13]. However, it is not directly applicable to the UWB-IR systems because the bandwidth of signal is extremely wide. Therefore, the extension of Friis' transmission formula in complex from was developed for UWB-IR systems [14]-[15]. The free space path loss model based on average power loss was proposed for UWB-IR systems [16]. After that, the model based on peak power loss was also proposed [17]. Moreover, the models based on average and peak power losses and considered the receivers were proposed [18]. Although these models were derived in the closed form formulas, there was no consideration about the difference between both definitions of path loss. There were some researches about ground reflection path loss models for UWB-IR systems [19]-[23]. The path loss was modeled in the integral form of narrow band signal but it was not derived in the closed form formula [20]. Despite the fact that few models were derived as simple closed form formulas, they were not considered multi-path fading [19], [22]. Some models based on average power loss were derived but they were not considered model based on peak power loss [19]-[20], [23]. On the other hand, the model based on peak power loss was proposed but it was not compared with model based on average power loss and was not verified by measurement results [21]-[22]. All of these models were

no consideration about the quantity of waveform distortion in the closed form formula.

For link budget of UWB-IR systems, several researches such as [24] claimed that the received waveform at receiver antenna terminal is simply considered in the term of derivative of transmitted waveform at transmitter antenna terminal. These models are easy and provide initial vision of received waveform but they are not sufficient for analysis and design. There are some researches about more accurate modeling of link budget for UWB-IR systems [25]-[32]. The link budget model, which composed of input admittance of transmitter, transmission impedance and frequency transfer function of receiver, was proposed in [25]. The other models, which factorized in the term of the frequency transfer functions of transmitter and receiver antennas based on radar-range equation, was proposed in [26]. The model, which composed of frequency transfer function of transmitter antenna with channel and receiver antenna, was proposed in [27]. Next, the models in the term of the antenna frequency transfer functions in transmission with reciprocity theorem were developed in [28]-[30]. The other models, which composed of frequency transfer function of transmitter antenna, channel and receiver antenna, were proposed in [31]-[32]. Note that these models have the same significance but have the different notation, factorization and definition of each factor. Moreover, the most models do not consider a correlation receiver [25]-[27], [29]-[32]. Although the correlation receiver is included in the model of [28], it does not consider the optimum correlation receiver, which can be considered as the upper boundary of best performance.

1.4 Objectives and Scope of Research

The objective of this thesis is to mathematically model transmission channels and evaluate link budget for UWB-IR systems. For transmission channel modeling, free space and ground reflection path losses are mathematically modeled. The novel method of derivation is proposed. The formula is based on rectangular passband waveform, which is the simple UWB-IR waveform [33], and complex form of Friis' transmission formula [14]-[15]. In addition, the closed forms of path loss expressions are derived based on both average and peak power losses for free space and ground reflection channels. After that, the novel quantitative parameter, peak to average loss ratio, is proposed and derived in the closed form formula for UWB-IR transmissions [34]. The peak to average loss ratio is defined as the ratio between peak power loss and average power loss from transmitter to receiver. Moreover, the closed form formulas of correlation coefficient using correlation receiver with

transmitted waveform template are derived [35]. The measurement was done and compared for the ground reflection channel. Moreover, the ground reflection path loss based on average power loss is compared with the model in [20].

For link budget, a more generalized link budget model for studying the waveform distortion due to antenna on free space transmission is discussed. The free space link budget evaluation scheme in the term of frequency transfer function that takes into account the transmitted waveform, its distortion due to the antennas, the channel and the correlation receiver is developed. This model is based on Friis' transmission formula, adapted to the UWB-IR transmission systems [14]-[15]. The rectangular and root raised cosine passband waveforms are used as the transmitted waveform. Experimental investigations are done for log-periodic dipole antenna (LPDA). The distortion quantities in the term of waveform distortion and transmission gain are defined and shown [36].

1.5 Thesis Organization

This thesis is organized into six chapters. The topic of Chapter 1 is Introduction. This chapter provides background, motivation, previous works, objectives and scope of research and thesis organization.

The topic of Chapter 2 is Ultra Wideband Impulse Radio Systems. This chapter provides introduction, advantages, definition of UWB-IR signal, regulation of UWB-IR signal, standards of UWB-IR systems and conclusion.

The topic of Chapter 3 is Mathematical Modeling of Free Space Channel. This chapter describes introduction, transmitted waveform, free space channel, received waveform, path loss, peak to average loss ration, correlation coefficient, results and conclusion.

The topic of Chapter 4 is Mathematical Modeling of Ground Reflection Channel. This chapter describes introduction, transmitted waveform, free space channel, received waveform, path loss, peak to average loss ration, correlation coefficient, measurement, results and conclusion.

The topic of Chapter 5 is Link Budget. This chapter describes introduction, model and theory of link budget evaluation, experimental evaluation of example UWB-IR antenna link, results and conclusion.

Finally, the topic of Chapter 6 is Conclusion and Future Works. This chapter gives the conclusions and recommendations for future works.

CHAPTER 2
ULTRA WIDEBAND IMPULSE RADIO SYSTEMS

2.1 Introduction

Wireless communication technologies have became important role due to they are very comfortable to communicate between equipment in an indoor, office and home. These wireless communication technologies require high data rate. Therefore, there are continuous developments to meet this requirement. Ultra wideband impulse radio (UWB-IR) technology is developed to support this requirement. UWB-IR technology has very high capacity, low cost and low power consumption properties [1]-[3].

2.2 Advantages

The interested advantages of UWB-IR systems are as follow [4].

1) UWB-IR systems have low cost resulted from low complexity of system. Unlike conventional narrowband systems, UWB-IR systems directly send baseband pulse. There is no requirement about radio frequency (RF) stage such as modulator, demodulator, up converter, down converter, local oscillator and phase locked loop (PLL).

2) UWB-IR signal has low power spectral density (PSD) with same as or below than noise level. This makes unintended detection quite difficult. Therefore, UWB-IR transmission does not cause significant interference to other narrowband systems.

3) UWB-IR systems are resistant to multi-path fading due to ultra wide bandwidth of signal obtains huge frequency diversity. This property is suitable for secure and military applications.

4) UWB-IR signal has high time resolution due to very narrow pulse width in time domain that obtains good timing precision for localization. This property is suitable for short-range radar applications such as rescuer and anti-crime operations, surveying and mining industry.

2.3 Definition of UWB-IR Signal

The Federal Communications Commission (FCC) of USA is defined the UWB-IR signal that must have main PSD ranging from 3.1 to 10.6 GHz. In addition, the UWB-IR signal must have occupied bandwidth more than or equal to 500 MHz, or fractional bandwidth more than or equal to 0.2. The occupied bandwidth f_b and fractional bandwidth are respectively defined as [5]

$$f_b = f_H - f_L, \tag{2.1}$$

$$\text{fractional bandwidth} = \frac{2(f_H - f_L)}{f_H + f_L}, \tag{2.2}$$

where f_L and f_H are the lowest and highest frequencies that PSD of signal decreased 10 dB from maximum level, respectively.

2.4 Regulations of UWB-IR Signal

One of important topic in UWB-IR signal is the frequency regulation, which is radiation limit and spectral mask. FCC specified the regulation in USA [5]. Similarly, European Telecommunications Standard Institute (ETSI) and International Telecommunication Union (ITU) specified the regulation in Europe [6]-[7] and Ministry of Internal Affairs and Communications (MIC) specified the regulation in Japan [8]. Recently, there is common regulation among FCC, ETSI and MIC [9].

2.4.1 Regulation in USA

FCC allows license-free use of UWB-IR system along the application types of UWB-IR equipments. The regulation is strictly specified to confirm that UWB-IR signal would not interference with other narrowband systems.

For radiation limits, FCC specified the limits of PSD radiation for indoor and outdoor communication applications as shown in Table 2.1. Spectral masks specified by FCC for indoor and outdoor communication applications are shown in Figure 2.1 [5].

Table 2.1 Radiation limits specified by FCC for indoor and outdoor communication applications [5].

Frequency (MHz)	PSD (dBm/MHz) Indoor communication	PSD (dBm/MHz) Outdoor communication
Below 960	-41.3	-41.3
960-1610	-75.3	-75.3
1610-1990	-53.3	-63.3
1990-3100	-51.3	-61.3
3100-10600	-41.3	-41.3
Above 10600	-51.3	-61.3

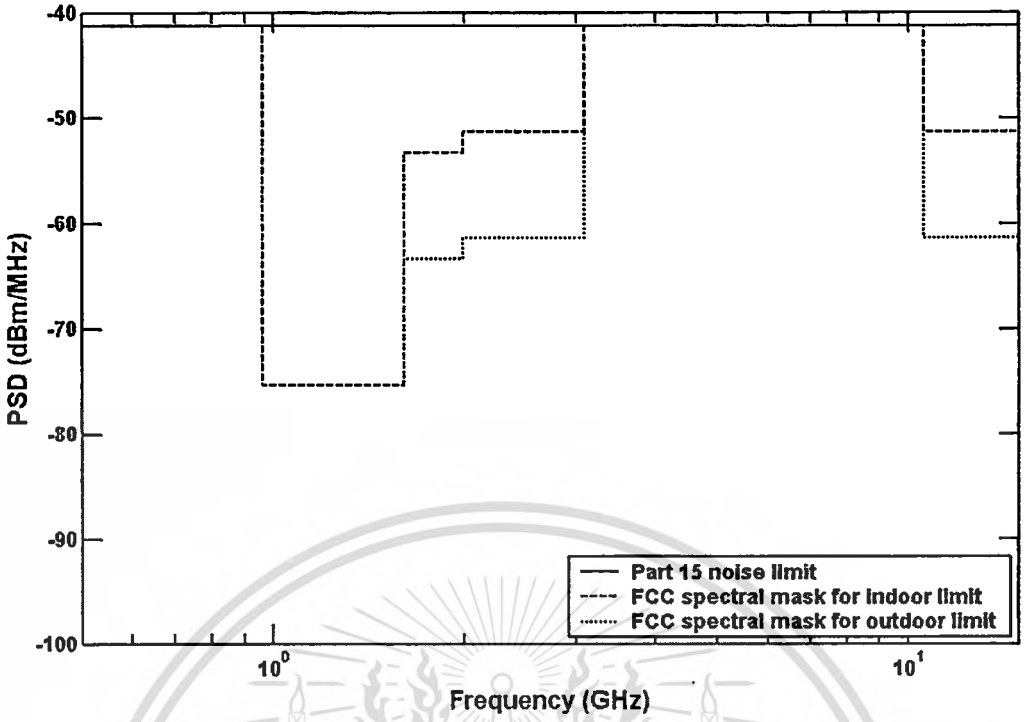

Figure 2.1 Spectral masks specified by FCC for indoor and outdoor communication applications [5].

2.4.2 Regulation in Europe

Beside the radiation limits and spectral masks specified by FCC, There are other institutes that specified radiation limits and spectral masks of UWB-IR signal. One is ETSI that specified regulation of UWB-IR applications in Europe. First regulation specifies PSD radiation raging form 3.1 to 10.6 GHz for indoor and outdoor communication applications same as FCC, but other frequency ranges are linear slope decreased logarithmically along frequency as shown in Table 2.2. First spectral masks specified by ETSI for indoor and outdoor communication applications are shown in Figure 2.2 [6].

Table 2.2 First radiation limits specified by ETSI for indoor and outdoor communication applications [6].

Frequency f (GHz)	PSD (dBm/MHz) Indoor communication	PSD (dBm/MHz) Outdoor communication
Below 3.1	$-51.3+87\log(f/3.1)$	$-61.3+87\log(f/3.1)$
3.1-10.6	-41.3	-41.3
Above 3.6	$-51.3+87\log(10.6/f)$	$-61.3+87\log(10.6/f)$

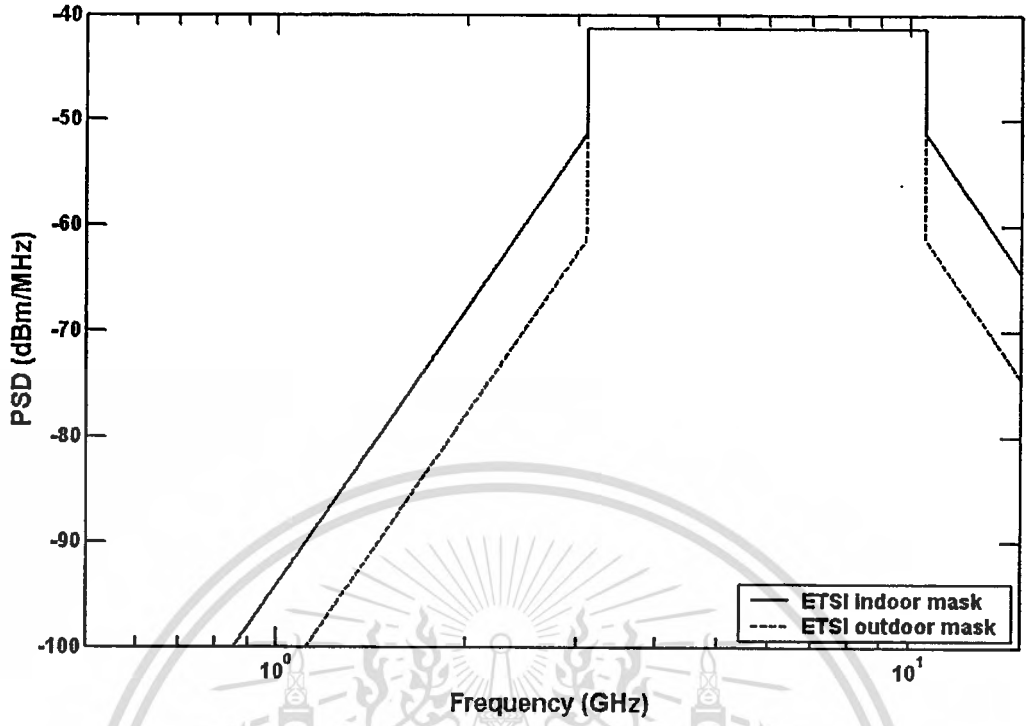

Figure 2.2 First spectral masks specified by ETSI for indoor and outdoor communication applications [6].

Currently, ETSI modified the radiation limits and spectral masks to be stricter. New regulation of PSD radiation allows UWB-IR equipments using for only indoor application. The main frequency rage is reduced to be from 6.0 to 8.5 GHz as shown in Table 2.3. Current spectral mask specified by ETSI for indoor application is shown in Figure 2.3 [7].

Table 2.3 Current radiation limit specified by ETSI for indoor application [7].

Frequency (GHz)	PSD (dBm/MHz)
Below 1.6	-90
1.6-3.8	-85
3.8-6.0	-70
6.0-8.5	-41.3
8.5-10.6	-65
Above 10.6	-85

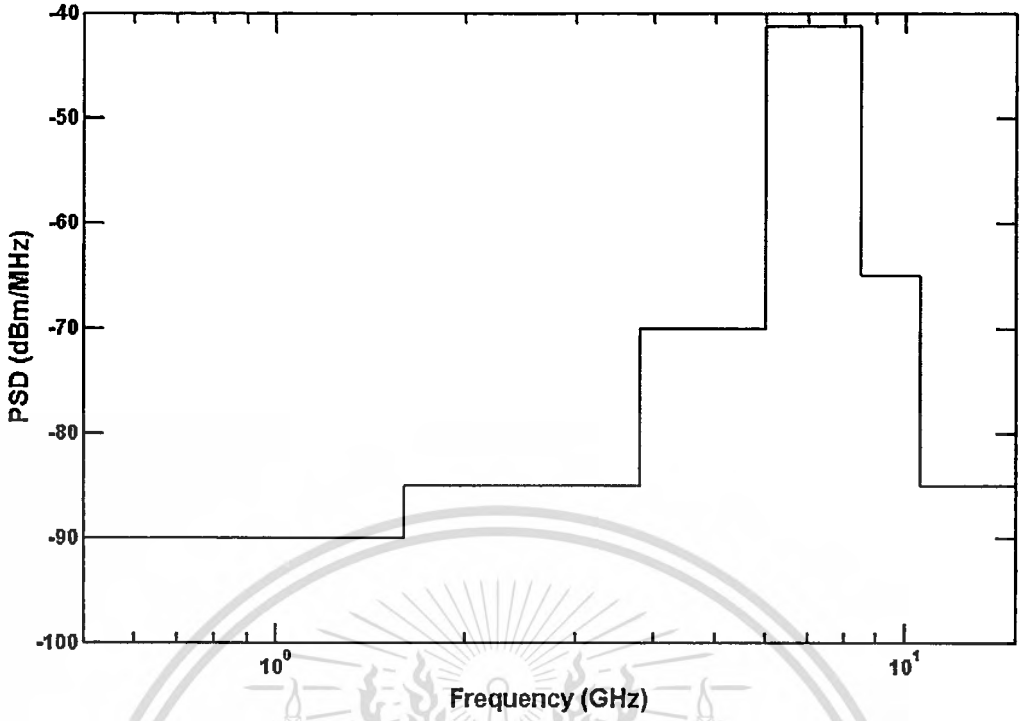

Figure 2.3 Current spectral mask specified by ETSI for indoor application [7].

2.4.3 Regulation in Japan

In Japan, MIC specified the UWB-IR signal has two frequency spectrum ranges, lower band form 3.4 to 4.8 GHz and upper band from 7.25 to 10.25 GHz, for only indoor application as shown in Table 2.4. The spectral mask specified by MIC for indoor application is shown in Figure 2.4 [8].

Table 2.4 Radiation limit specified by MIC for indoor application [8].

Frequency (GHz)	PSD (dBm/MHz)
Below 1.6	-90
1.6-2.7	-85
2.7-3.4	-70
3.4-4.8	-41.3
4.8-7.25	-70
7.25-10.25	-41.3
Above 10.25	-70

Figure 2.4 Spectral mask specified by MIC for indoor application [8].

2.4.4 Common Regulation

Recently, UWB-IR signal regulation has been approved in other regions as well. There is common frequency available among FCC, ETSI and MIC. The regulation of PSD radiation is satisfied all FCC, ETSI and MIC regulations and allows using only indoor application. The main frequency rage is from 7.25 to 8.5 GHz, while the lowest frequency of 7.25 GHz is satisfied MIC regulation and highest frequency of 8.5 GHz is satisfied ETSI regulation as shown in Table 2.5. The common frequency band spectral mask for indoor application is shown in Figure 2.5 [9].

Table 2.5 Radiation limit of common frequency band for indoor application [9].

Frequency (GHz)	PSD (dBm/MHz)
Below 1.6	-90
1.6-3.8	-85
3.8-7.25	-70
7.25-8.5	-41.3
8.5-10.25	-65
10.25-10.6	-70
Above 10.6	-85

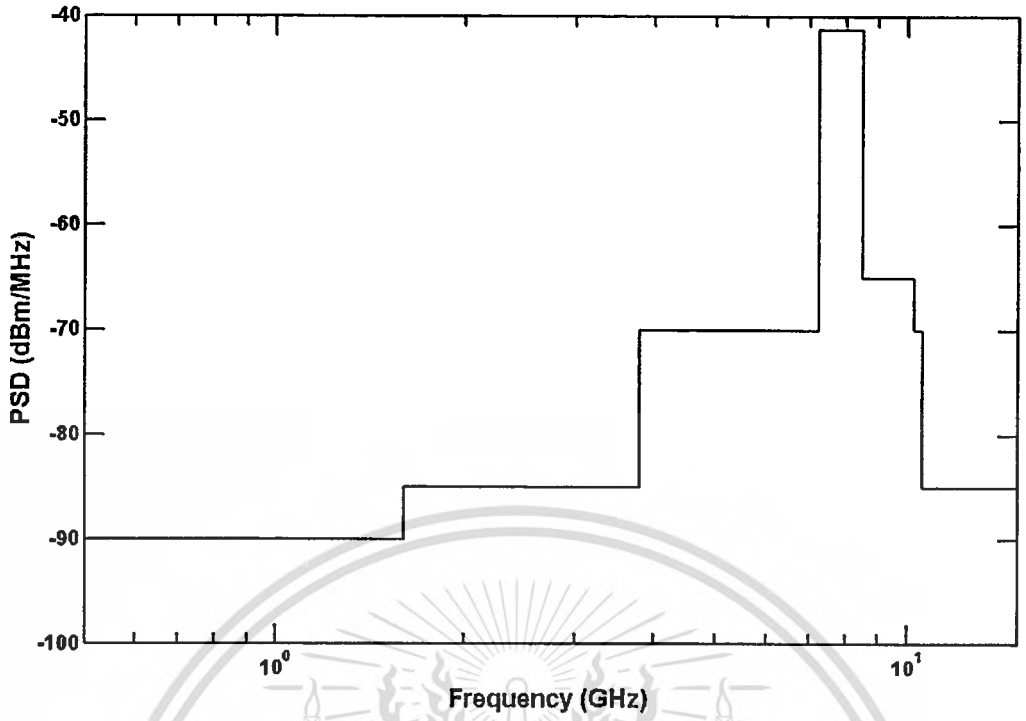

Figure 2.5 Common Frequency band spectral mask for indoor application [9].

2.5 Standards of UWB-IR Systems

There are three standards of UWB-IR: IEEE 802.15.3a for high rate wireless personal area networks (HR-WPANs) [10], IEEE 802.15.4a for low rate personal wireless area networks (LR-WPANs) [11] and IEEE 802.15.6 for wireless body area networks (WBANs) [12].

2.5.1 IEEE 802.15.3a Standard

IEEE 802.15.3a standard improved the data rate of IEEE 802.15.3 standard by using UWB-IR technique for HR-WPANs with short distance up to 10 m and high data rate up to 480 Mbps [10]. IEEE 802.15.3a standard was withdrawn in January 2006 because the members of task group were not able to decide between two technologies, multi-band orthogonal frequency division multiplexing (MB-OFDM) and direct sequence ultra wideband (DS-UWB).

2.5.2 IEEE 802.15.4a Standard

IEEE 802.15.4a standard utilizes UWB-IR technique for LR-WPANs with long distance up to about 100 m and low data rate. This standard uses for new applications that require only moderate data throughput and low cost, but long

battery life such as wireless sensor networks and high accuracy localization systems. The transmitted signal is based on very short pulse and estimated to impulse, which causes the name of UWB-IR [11].

2.5.3 IEEE 802.15.6 Standard

IEEE 802.15.6 standard is new standard for WBANs. This standard is focus on medical and consumer electronics applications such as health examination, diagnose system and pathogen controlling. WBANs operate with low power communication between body nodes to provide medical and non-medical applications [12].

2.6 Conclusion

UWB-IR systems can be utilized for variety types of wireless applications with many advantages such as low cost, low PSD, resistant to multi-path fading and high time resolution. FCC defined the UWB-IR signal as the signal must have occupied bandwidth more than or equal to 500 MHz, or fractional bandwidth more than or equal to 0.2. Moreover, FCC, ETSI and MIC strictly specified regulation of UWB-IR signal to confirm that UWB-IR signal would not interference with other narrowband systems. Three standards of UWB-IR systems are IEEE 802.15.3a, IEEE 802.15.4a and IEEE 802.15.6 for HR-WPANs, LR-WPANs and WBANs, respectively.

CHAPTER 3
MATHEMATICAL MODELING OF FREE SPACE CHANNEL

3.1 Introduction

In this chapter, the free space channel is mathematically modeled for ultra wideband impulse radio (UWB-IR) systems. The novel method of derivation is proposed. For free space model, the rectangular passband waveform [33] is used as transmitted waveform and complex form of Friis' transmission formula [14]-[15] is used to characterize free space channel. Next, the received waveform is computed. In addition, the closed forms of path loss expressions are derived based on both average and peak power losses. After that, the novel quantitative parameter, peak to average loss ratio, is proposed and derived in the closed form formula [34]. Moreover, the closed form formulas of correlation coefficient using correlation receiver with transmitted waveform template are derived [35]. The results are shown along minimum to maximum bandwidth of signal.

3.2 Transmitted Waveform

UWB-IR transmitted waveform is rectangular passband waveform and its spectral density V_t can be written as [33]

$$V_t(f)=\begin{cases}\dfrac{A}{2f_b} & \|f|-f_c|\le\dfrac{f_b}{2}\\ 0 & \|f|-f_c|>\dfrac{f_b}{2}\end{cases}, \tag{3.1}$$

where f is frequency, A is maximum amplitude of waveform and $f_c=(f_H+f_L)/2$ is center frequency. The spectral density of rectangular passband waveform is shown in Figure 3.1. Spectral density is rectangular in frequency ranging from $-f_H$ to $-f_L$ and from f_L to f_H with constant magnitude of $A/(2f_b)$. Area under this graph is equal to A, which corresponds to maximum amplitude of waveform at time of 0.

Rectangular passband waveform in time domain v_t is calculated by using inverse Fourier transform of its spectral density and it can be written as

$$v_t(t)=\mathscr{F}^{-1}\{V_t(f)\}=\int_{-\infty}^{\infty}V_t(f)e^{j2\pi ft}\,df, \tag{3.2}$$

where t is time and $\mathscr{F}^{-1}\{\cdot\}$ is inverse Fourier transform operator.

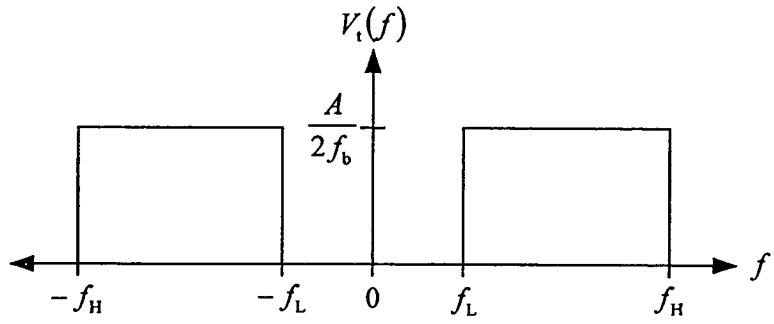

Figure 3.1 Spectral density of rectangular passband waveform.

From Equations (3.1) and (3.2), rectangular passband waveform in time domain can be derived as

$$\begin{aligned}
v_t(t) &= \frac{A}{2f_b}\left(\int_{-f_H}^{f_H} e^{j2\pi ft}\,df - \int_{-f_L}^{f_L} e^{j2\pi ft}\,df\right) \\
&= \frac{A}{2f_b}\left(\frac{1}{j2\pi t}e^{j2\pi ft}\Big|_{f=-f_H}^{f_H} - \frac{1}{j2\pi t}e^{j2\pi ft}\Big|_{f=-f_L}^{f_L}\right) \\
&= \frac{A}{2f_b}\left[\frac{1}{\pi t}\frac{1}{j2}\left(e^{j2\pi f_H t} - e^{-j2\pi f_H t}\right) - \frac{1}{\pi t}\frac{1}{j2}\left(e^{j2\pi f_L t} - e^{-j2\pi f_L t}\right)\right] \\
&= \frac{A}{2f_b}\left[\frac{1}{\pi t}\sin(2\pi f_H t) - \frac{1}{\pi t}\sin(2\pi f_L t)\right] \\
&= \frac{A}{f_b}\left[\frac{f_H}{2\pi f_H t}\sin(2\pi f_H t) - \frac{f_L}{2\pi f_L t}\sin(2\pi f_L t)\right] \\
&= \frac{A}{f_b}\left[f_H\,\mathrm{sinc}(2f_H t) - f_L\,\mathrm{sinc}(2f_L t)\right],
\end{aligned} \tag{3.3}$$

where function $\mathrm{sinc}(x) = \sin(\pi x)/(\pi x)$.

Two cases of waveform, minimum and maximum bandwidths, are considered. The rectangular passband waveform in time domain and its spectral density with minimum bandwidth $f_b = 500$ MHz, center frequency $f_c = 6.85$ GHz, lowest frequency $f_L = 6.60$ GHz, highest frequency $f_H = 7.10$ GHz and maximum amplitude $A = 1$ V are shown in Figures 3.2 and 3.3, respectively. For maximum bandwidth case, Figures 3.4 and 3.5 respectively show rectangular passband waveform in time domain and its spectral density with bandwidth $f_b = 7.50$ GHz, center frequency $f_c = 6.85$ GHz, lowest frequency $f_L = 3.10$ GHz, highest frequency $f_H = 10.60$ GHz and maximum amplitude $A = 1$ V.

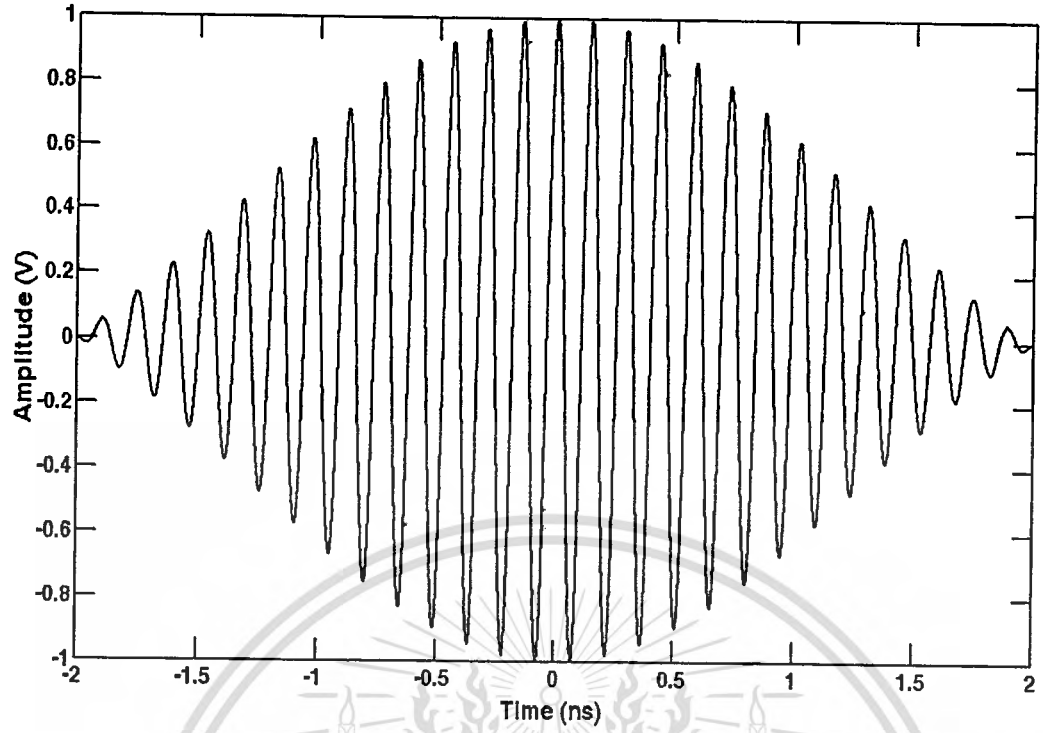

Figure 3.2 Rectangular passband waveform in time domain with minimum bandwidth case.

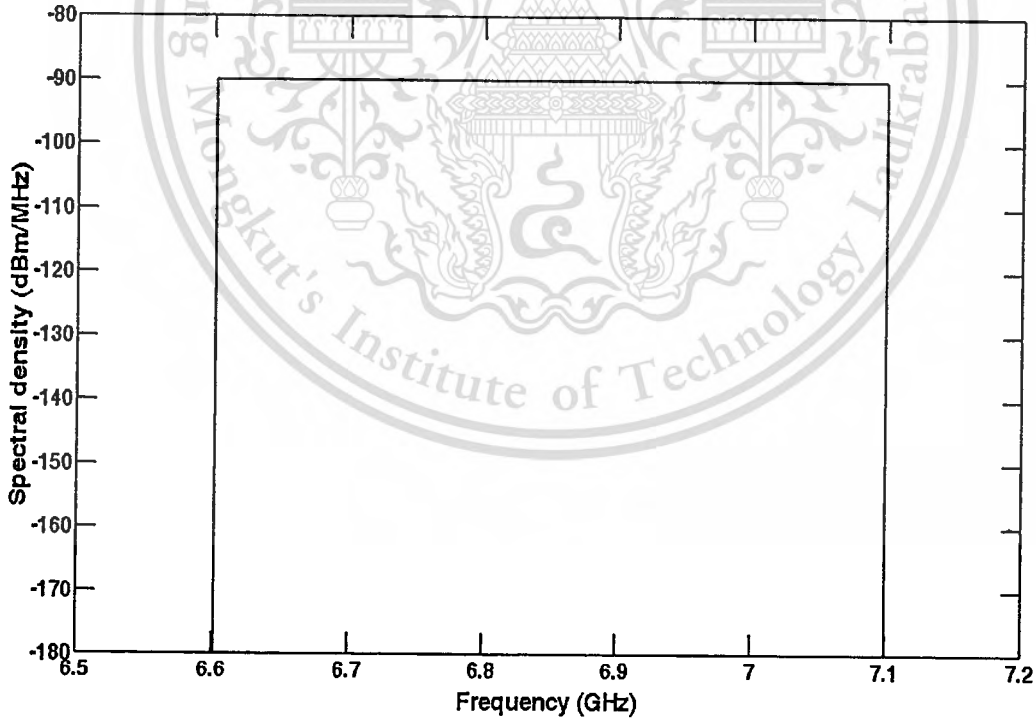

Figure 3.3 Spectral density of rectangular passband waveform in time domain with minimum bandwidth case.

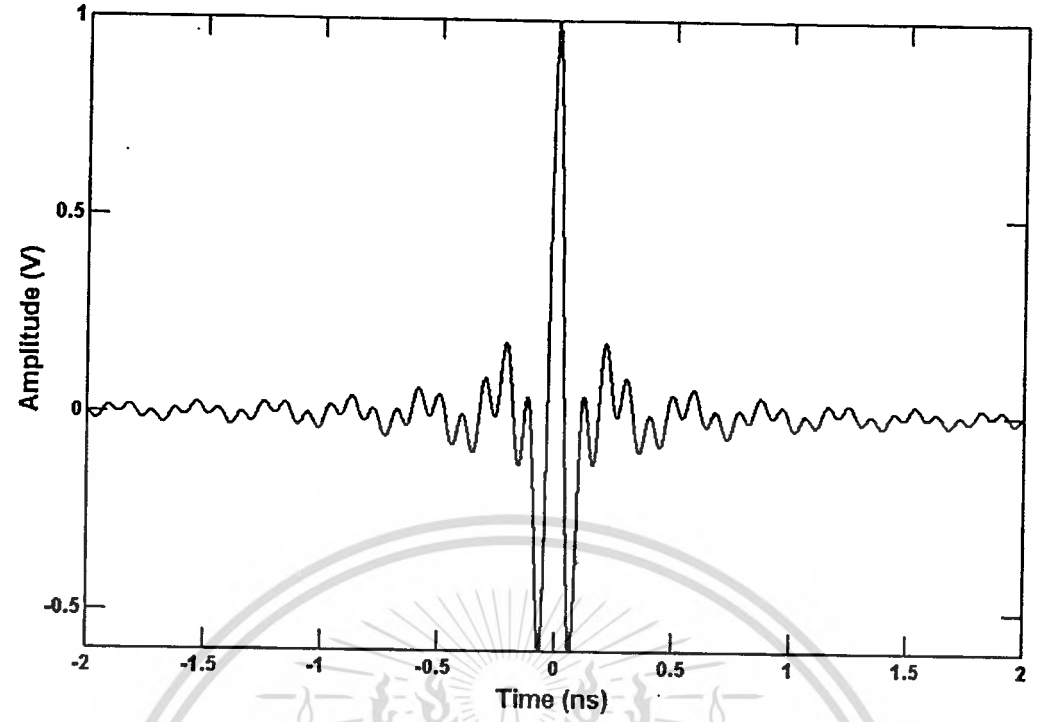

Figure 3.4 Rectangular passband waveform in time domain with maximum bandwidth case.

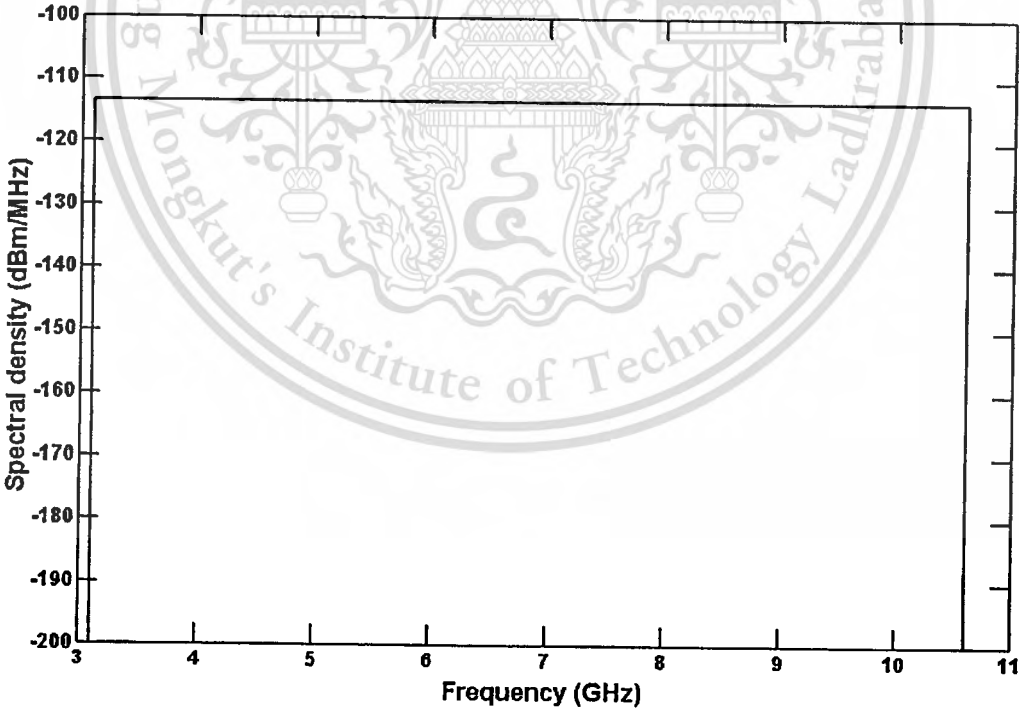

Figure 3.5 Spectral density of rectangular passband waveform in time domain with maximum bandwidth case.

3.3 Free Space Channel

For modeling the free space channel, transmitter and receiver antennas are assumed to be isotropic antenna with gains of 1. Therefore, frequency transfer function of free space channel H_f in the term of complex form of Friis' transmission formula can be written as [14]-[15]

$$H_f(f) = \frac{c}{4\pi |f| d} e^{-j2\pi f d/c}, \tag{3.4}$$

where d is distance between transmitter and receiver antennas and c is velocity of light. This equation is satisfied for both positive and negative frequencies as it satisfies the causality.

The magnitude and phase of free space channel transfer function with distance $d = 1$ m are shown in Figures 3.6 and 3.7, respectively. The magnitude is decreased when frequency is higher and phase is linear.

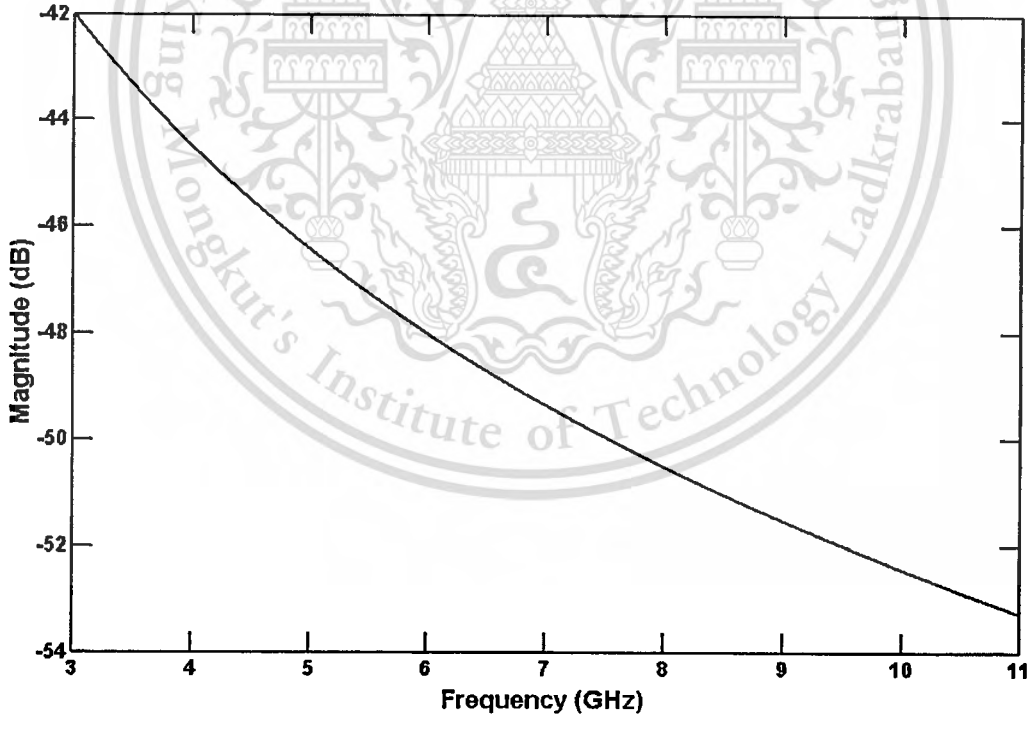

Figure 3.6 Magnitude of free space channel transfer function with distance $d = 1$ m.

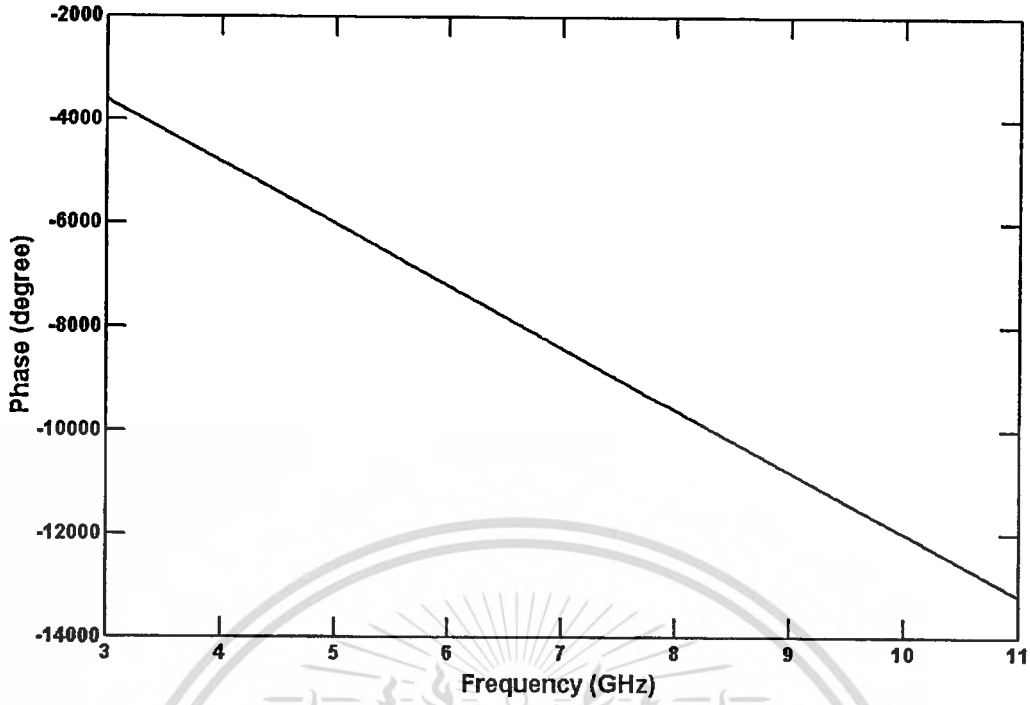

Figure 3.7 Phase of free space channel transfer function with distance $d = 1$ m.

3.4 Received Waveform

The spectral density of received waveform for free space channel $V_{r,f}$ is calculated by using the multiplication between free space channel transfer function H_f and spectral density of transmitted waveform V_t and it obtains

$$V_{r,f}(f) = H_f(f) \cdot V_t(f). \tag{3.5}$$

From Equations (3.1), (3.4) and (3.5), the spectral density of received waveform can be written as

$$V_{r,f}(f) = \begin{cases} \dfrac{cA}{8\pi f_b \mid f \mid d} e^{-j2\pi f d/c} & \mid\mid f \mid - f_c \mid \leq \dfrac{f_b}{2} \\ 0 & \mid\mid f \mid - f_c \mid > \dfrac{f_b}{2} \end{cases}. \tag{3.6}$$

The received waveform in time domain $v_{r,f}$ is calculated by using inverse Fourier transform of its spectral density and it can be written as

$$v_{r,f}(t) = \mathcal{F}^{-1}\{V_{r,f}(f)\} = \int_{-\infty}^{\infty} V_{r,f}(f) e^{j2\pi ft} \mathrm{d}f . \tag{3.7}$$

From Equations (3.6) and (3.7), it obtains

$$\begin{aligned} v_{r,f}(t) &= \frac{cA}{8\pi f_b d}\left(\int_{-f_H}^{-f_L} \frac{1}{|f|} e^{j2\pi f(t-d/c)} \mathrm{d}f + \int_{f_L}^{f_H} \frac{1}{|f|} e^{j2\pi f(t-d/c)} \mathrm{d}f \right) \\ &= \frac{cA}{8\pi f_b d}\left(\begin{array}{l} \int_{-f_H}^{-f_L} \frac{1}{|f|} \cos\left[2\pi f\left(t-\frac{d}{c}\right)\right] \mathrm{d}f + j \int_{-f_H}^{-f_L} \frac{1}{|f|} \sin\left[2\pi f\left(t-\frac{d}{c}\right)\right] \mathrm{d}f \\ + \int_{f_L}^{f_H} \frac{1}{|f|} \cos\left[2\pi f\left(t-\frac{d}{c}\right)\right] \mathrm{d}f\mathrm{d}f + j \int_{f_L}^{f_H} \frac{1}{|f|} \sin\left[2\pi f\left(t-\frac{d}{c}\right)\right] \mathrm{d}f\mathrm{d}f \end{array} \right) \\ &= \frac{cA}{4\pi f_b d} \int_{f_L}^{f_H} \frac{1}{f} \cos\left[2\pi f\left(t-\frac{d}{c}\right)\right] \mathrm{d}f . \end{aligned} \tag{3.8}$$

From Equation (3.8) and setting $t = d/c$, it obtains

$$v_{r,f}(t) = \frac{cA}{4\pi f_b d} \int_{f_L}^{f_H} \frac{1}{f} \mathrm{d}f = \frac{cA}{4\pi f_b d} \ln(f)\Big|_{f=f_L}^{f_H} = \frac{cA}{4\pi f_b d} \ln\left(\frac{f_H}{f_L}\right). \tag{3.9}$$

From Equation (3.8) and setting $t \neq d/c$, it obtains

$$\begin{aligned} v_{r,f}(t) &= \frac{cA}{4\pi f_b d} \int_{f_L}^{f_H} \frac{1}{f} \cos\left[2\pi f\left(t-\frac{d}{c}\right)\right] \mathrm{d}f \\ &= \frac{cA}{4\pi f_b d} \mathrm{C_i}\left[2\pi f\left(t-\frac{d}{c}\right)\right]\Big|_{f_L}^{f_H} \\ &= \frac{cA}{4\pi f_b d}\left\{ \mathrm{C_i}\left[2\pi f_H\left(t-\frac{d}{c}\right)\right] - \mathrm{C_i}\left[2\pi f_L\left(t-\frac{d}{c}\right)\right] \right\}, \end{aligned} \tag{3.10}$$

where $\mathrm{C_i}(x)$ is cosine integral function defined as

$$C_i(x) = -\int_x^{\infty} \frac{1}{\tau}\cos(\tau)\,d\tau .$$

Combining Equations (3.9) and (3.10), the received waveform in the term of closed form formula can be derived as

$$v_{r,f}(t) = \begin{cases} \dfrac{cA}{4\pi f_b d}\ln\left(\dfrac{f_H}{f_L}\right) & t = \dfrac{d}{c} \\ \dfrac{cA}{4\pi f_b d}\left\{C_i\left[2\pi f_H\left(t-\dfrac{d}{c}\right)\right] - C_i\left[2\pi f_L\left(t-\dfrac{d}{c}\right)\right]\right\} & t \neq \dfrac{d}{c} \end{cases} \quad (3.11)$$

The received waveform in time domain and its spectral density for minimum bandwidth case are shown in Figures 3.8 and 3.9, respectively. Figures 3.10 and 3.11 show the received waveform and its spectral density for maximum bandwidth case, respectively.

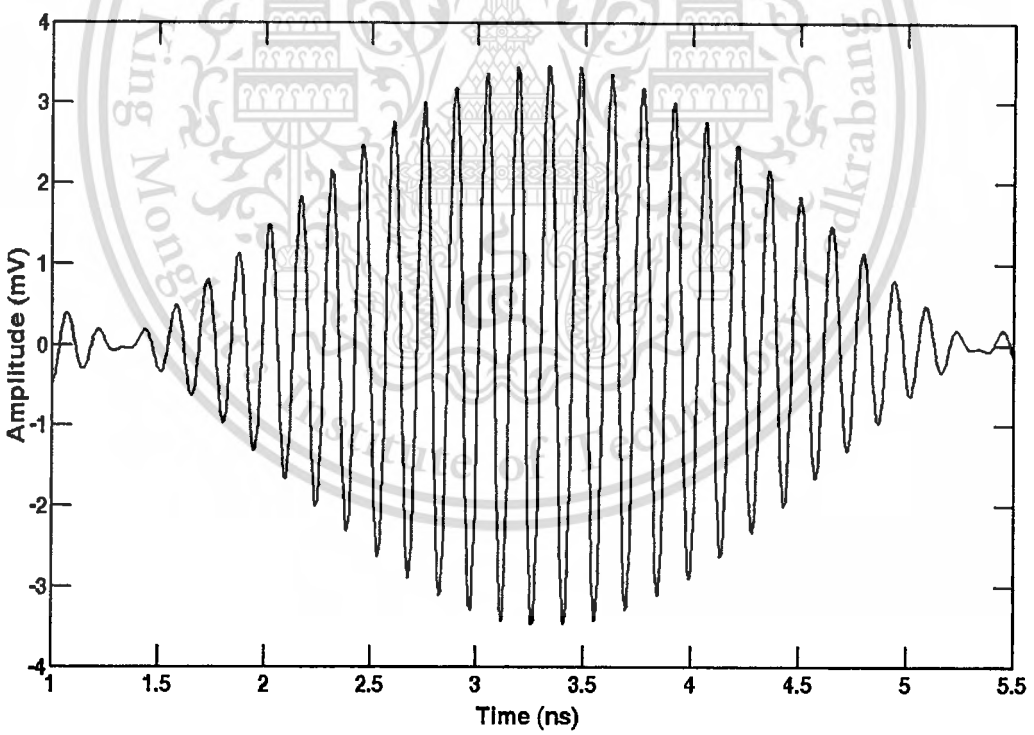

Figure 3.8 Received waveform with minimum bandwidth case for free space channel.

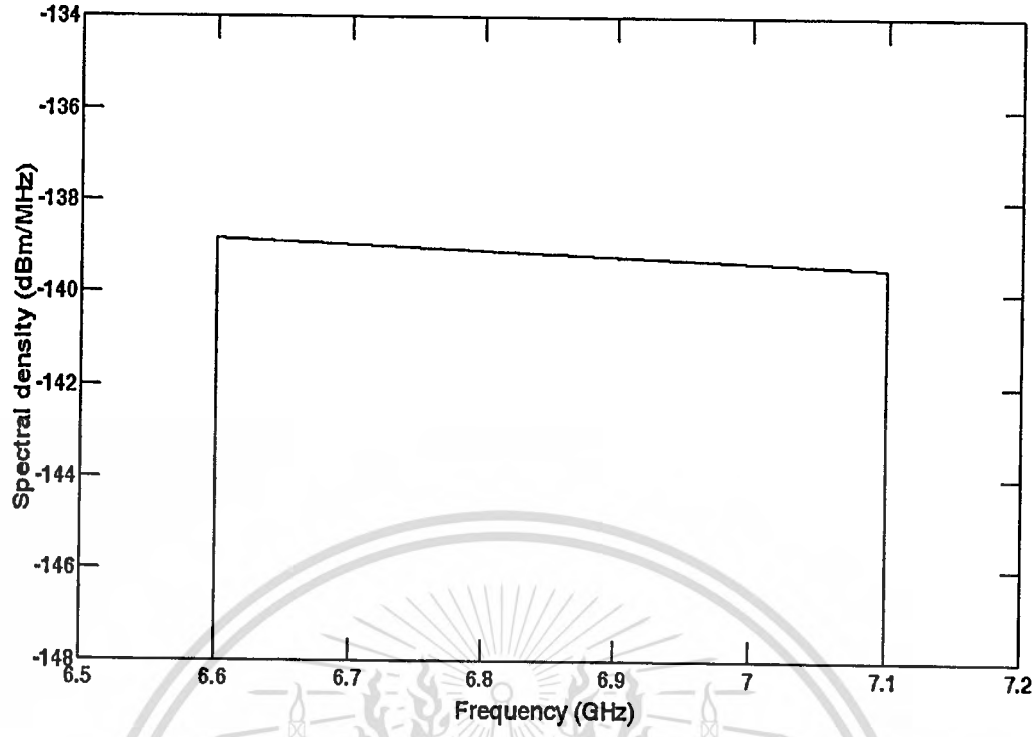

Figure 3.9 Spectral density of received waveform with minimum bandwidth case for free space channel.

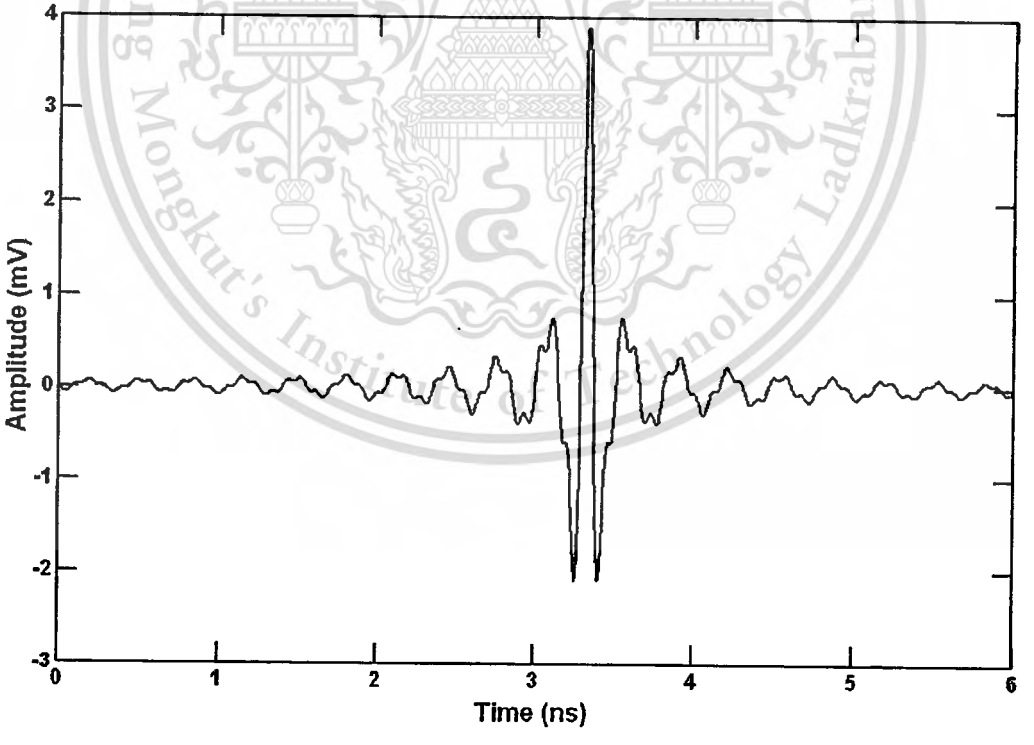

Figure 3.10 Received waveform with maximum bandwidth case for free space channel.

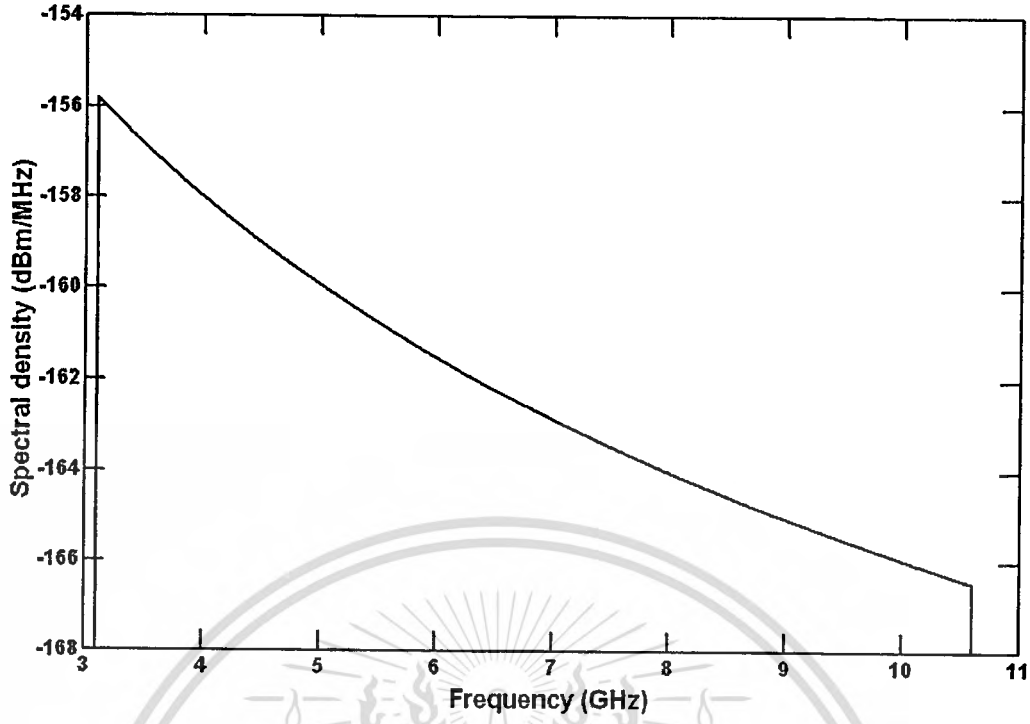

Figure 3.11 Spectral density of received waveform with maximum bandwidth case for fee space channel.

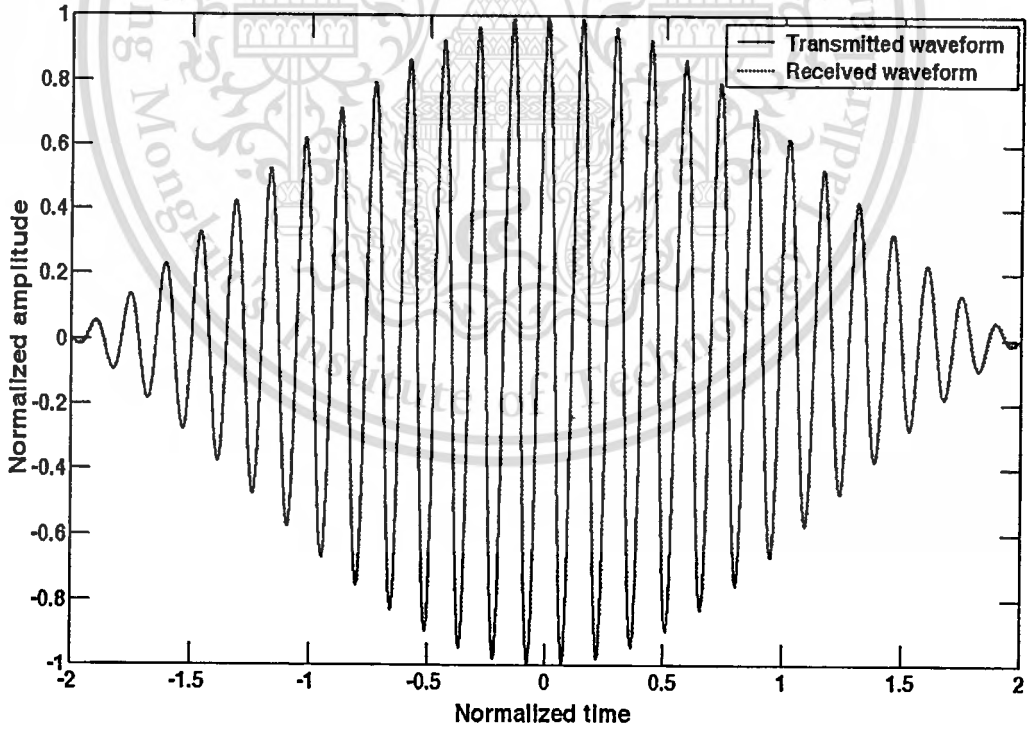

Figure 3.12 Normalized transmitted waveform compared with normalized received waveform for minimum bandwidth case.

For studying waveform distortion, Figures 3.12 and 3.13 show the normalized transmitted waveforms compared with normalized received waveforms for minimum and maximum bandwidths, respectively. From the figures, the waveform with minimum bandwidth is almost no distortion, but the waveform distortion can be clearly investigated for maximum bandwidth case.

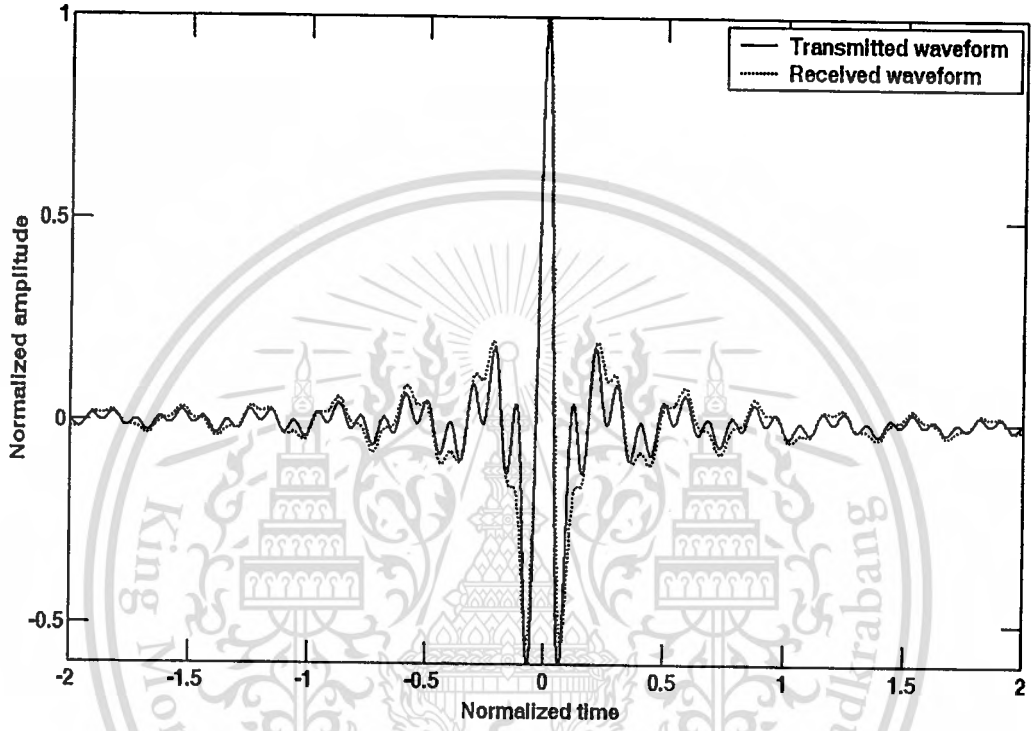

Figure 3.13 Normalized transmitted waveform compared with normalized received waveform for maximum bandwidth case.

3.5 Path Loss

There are two definitions of path losses: based on average and peak power losses. The peak power loss and average power loss from transmitter and receiver are equal for the distortionless condition. However, the distortion of UWB-IR waveform due to frequency and time dispersion of channel causes the difference. Therefore, both path losses based on average and peak power losses are necessary to model. In this section, both path losses are mathematically modeled in the closed form formulas.

3.5.1 Based on Average Power Loss

UWB-IR free space path loss based on average power loss $PL_{f,a}$ in dB is defined as the ratio between the average power of transmitted and received waveform in frequency domain and it can be written as

$$PL_{f,a} = 10\log\left(\frac{\int_{-\infty}^{\infty}|V_t(f)|^2\,df}{\int_{-\infty}^{\infty}|V_{r,f}(f)|^2\,df}\right). \tag{3.12}$$

From spectral density of transmitted waveform in Equation (3.1), it obtains

$$\begin{aligned}\int_{-\infty}^{\infty}|V_t(f)|^2\,df &= \frac{A^2}{4f_b^2}\int_{-f_H}^{-f_L}df + \frac{A^2}{4f_b^2}\int_{f_L}^{f_H}df \\ &= \frac{A^2}{2f_b^2}\int_{f_L}^{f_H}df \\ &= \frac{A^2}{2f_b^2}f\Big|_{f=f_L}^{f_H} \\ &= \frac{A^2}{2f_b}.\end{aligned} \tag{3.13}$$

From spectral density of received waveform in Equation (3.6), it obtains

$$\begin{aligned}\int_{-\infty}^{\infty}|V_{r,f}(f)|^2\,df &= \frac{c^2A^2}{64\pi^2f_b^2d^2}\int_{-f_H}^{-f_L}\frac{1}{f^2}df + \frac{c^2A^2}{64\pi^2f_b^2d^2}\int_{f_L}^{f_H}\frac{1}{f^2}df \\ &= \frac{c^2A^2}{32\pi^2f_b^2d^2}\int_{f_L}^{f_H}\frac{1}{f^2}df \\ &= -\frac{c^2A^2}{32\pi^2f_b^2d^2}\frac{1}{f}\Big|_{f=f_L}^{f_H} \\ &= \frac{c^2A^2}{32\pi^2f_Lf_Hf_bd^2}.\end{aligned} \tag{3.14}$$

From Equations (3.12) to (3.14), the free space path loss based on average power loss is derived in the closed form formula and can be written as

$$PL_{f,a} = 10\log\left(\frac{16\pi^2 f_L f_H d^2}{c^2}\right) = 20\log\left(\frac{4\pi\sqrt{f_L f_H}\,d}{c}\right). \quad (3.15)$$

This free space path loss based on peak power loss is the same as proposed in [16].

3.5.2 Based on Peak Power Loss

UWB-IR free space path loss based on peak power loss $PL_{f,p}$ in dB is defined as the ratio between the peak power of transmitted and received waveforms in time domain and it can be written as

$$PL_{f,p} = 10\log\left(\frac{\max\left[v_t^2(t)\right]}{\max\left[v_{r,f}^2(t)\right]}\right). \quad (3.16)$$

From transmitted waveform in Equation (3.3), it obtains

$$\max\left[v_t^2(t)\right] = A^2. \quad (3.17)$$

From received waveform in Equation (3.11), it obtains

$$\max\left[v_{r,f}^2(t)\right] = \frac{c^2 A^2}{16\pi^2 f_b^2 d^2}\ln^2\left(\frac{f_H}{f_L}\right). \quad (3.18)$$

From Equations (3.16) to (3.18), the free space path loss based on peak power loss is derived in the closed form formula and can be written as

$$PL_{f,p} = 10\log\left[\frac{16\pi^2 f_b^2 d^2}{c^2\ln^2\left(\frac{f_H}{f_L}\right)}\right] = 20\log\left[\frac{4\pi f_b d}{c\ln\left(\frac{f_H}{f_L}\right)}\right]. \quad (3.19)$$

3.6 Peak to Average Loss Ratio

Study of waveform distortion is necessary for designing optimum UWB-IR systems because the distortion of waveform degrades the performance of correlation receiver. In this section, the novel quantitative parameter of waveform distortion, peak to average loss ratio, is proposed and derived in the closed form formula for free space channel.

The peak to average loss ratio is defined as the ratio between peak power loss and average power loss from transmitter to receiver antennas. The free space peak to average loss ratio PAR_f in dB can be written as [34]

$$PAR_f = 10\log\left\{\frac{\max\left[v_t^2(t)\right]}{\max\left[v_{r,f}^2(t)\right]}\cdot\frac{\int_{-\infty}^{\infty}\left|V_{r,f}(f)\right|^2 df}{\int_{-\infty}^{\infty}\left|V_t(f)\right|^2 df}\right\}. \tag{3.20}$$

From Equations (3.13), (3.14), (3.17), (3.18) and (3.20), the free space peak to average loss ratio is derived in the closed form formula and can be written as

$$PAR_f = 20\log\left\{\frac{f_b}{\sqrt{f_L f_H}\ln\left(\frac{f_H}{f_L}\right)}\right\}. \tag{3.21}$$

3.7 Correlation Coefficient

For UWB-IR correlation receiver with transmitted template signal, the correlation coefficient is used to identify the receiver efficiency. The correlation coefficient is equal to 1 means the efficiency is 100%. In other words, that is the special case of correlation receiver, which is called as matched filter receiver. The transmitted template signal is identical with received signal. The correlation coefficient is decreased when the template signal is more differ. If the correlation coefficient is equal to 0, that means the template signal is orthogonal with received signal. There is no signal that can be detected from the receiver. The correlation coefficient is also applied to analyze the waveform distortion.

In this section, the closed form formula of correlation coefficient is derived for free space channel. The free space correlation coefficient C_f is defined as [35]

$$C_f = \frac{\max\left|\int_{-\infty}^{\infty} v_{r,f}^*(t)\cdot v_t(t+\tau)dt\right|}{\sqrt{\int_{-\infty}^{\infty}|v_{r,f}(t)|^2\,dt\cdot\int_{-\infty}^{\infty}|v_t(t)|^2\,dt}}, \tag{3.22}$$

where * is the complex conjugate operator. The closed form formula of free space correlation coefficient can be derived as

$$C_f = \frac{\sqrt{f_L f_H}}{f_b}\ln\left(\frac{f_H}{f_L}\right). \tag{3.23}$$

3.8 Results

In this section, the comparison between the proposed UWB-IR free space path loss models based on average and peak power losses are investigated to study the waveform distortion. After that, the peak to average loss ratio and correlation coefficient from proposed closed form formulas are shown.

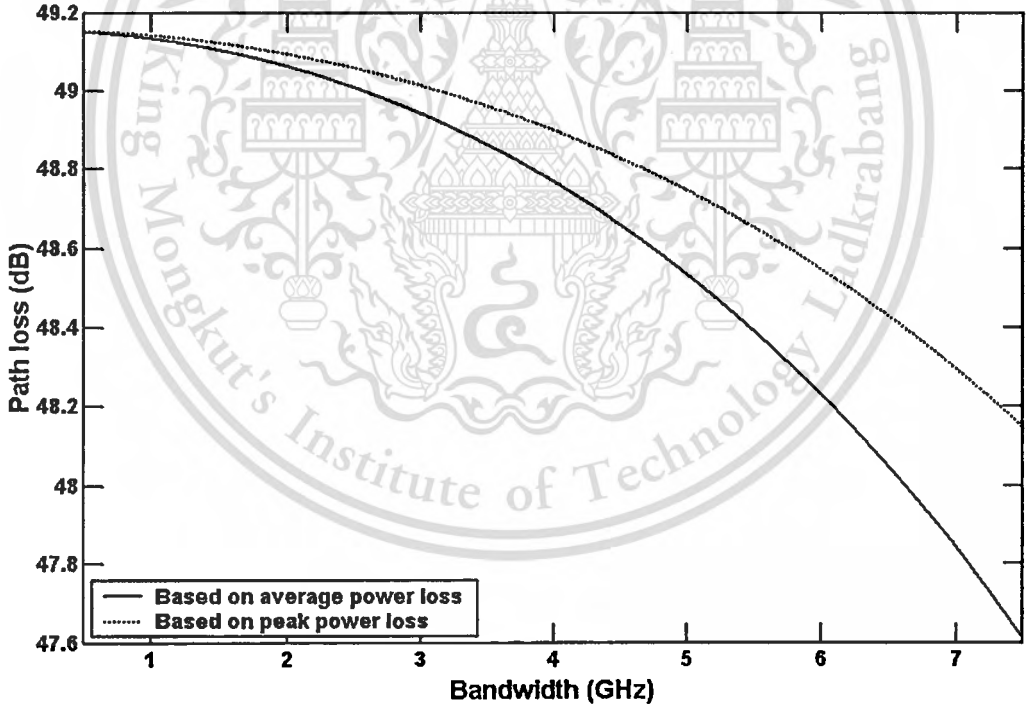

Figure 3.14 Comparison between free space path loss based on average and peak power losses.

For the analyzed parameters, center frequency f_c is fixed at 6.85 GHz, bandwidth f_b is varied from 500 MHz to 7.5 GHz and distance d is fixed at 1 m. These transmitted waveform parameters satisfy the UWB-IR signal defined by FCC [5].

3.8.1 Path Loss

The obtained UWB free space path losses are shown in Fig. 3.14. The UWB-IR free space path loss based on peak power loss is slightly higher than that based on average power loss. At narrow bandwidth, both path losses are almost the same. There is more difference when the bandwidth is wider. The maximum difference of path losses is at 7.5 GHz bandwidth. This difference is the same along an arbitrary distance d. This result reflects that there is almost no waveform distortion at narrow bandwidth. In addition, there is more waveform distortion when bandwidth is wider. Moreover, proposed free space path loss based on average power loss corresponds with path loss model that proposed in [16].

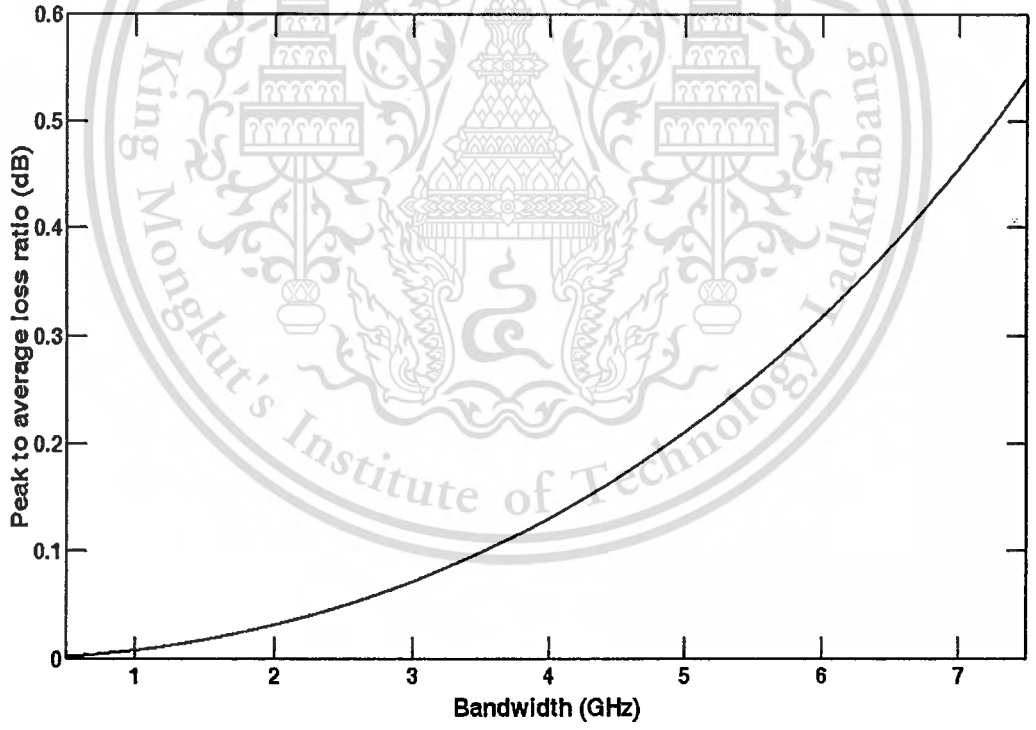

Figure 3.15 Free space peak to average loss ratio along bandwidth from 500 MHz to 7.5 GHz [34].

3.8.2 Peak to Average Loss Ratio

Figure 3.15 shows the peak to average loss ratio for free space channel. At narrow bandwidth, the peak to average loss ratio is approached to zero. In other words, there is slight distortion of narrow bandwidth waveform for free space channel. The maximum peak to average loss ratio is 0.54 dB at bandwidth of 7.5 GHz. The distortion of waveform is caused by frequency dispersion. In addition, the magnitude of frequency transfer function of free space channel is not constant along frequency [34].

3.8.3 Correlation Coefficient

The free space correlation coefficient is shown in Figure 3.16. At narrow bandwidth, the correlation coefficient is approached to 1. The efficiency of correlation receiver is almost to 100%. The minimum correlation coefficient is 0.94 at bandwidth of 7.5 GHz [35].

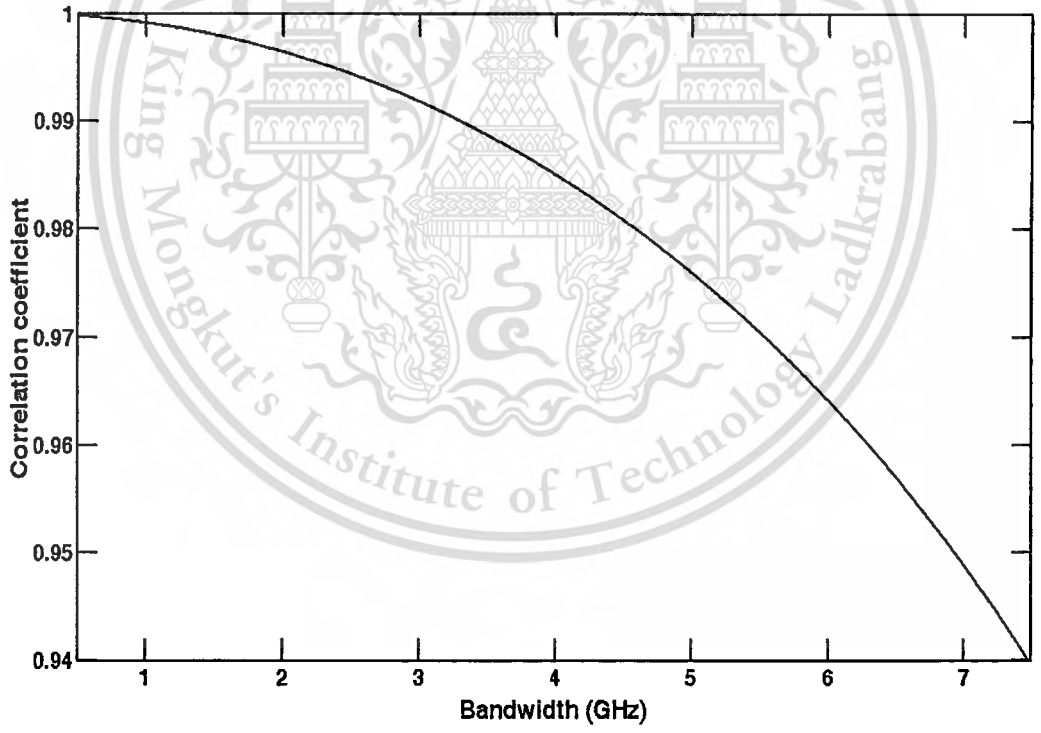

Figure 3.16 Free space correlation coefficient along bandwidth from 500 MHz to 7.5 GHz [35].

3.9 Conclusion

In this chapter, free space path loss, peak to average loss ratio and correlation coefficient are mathematically modeled in the closed form formulas. The novel method of derivation is proposed. The free space path losses based on average and peak power losses are almost the same at narrow bandwidth and have more difference when bandwidth is wider. The peak to average loss ratio is higher when bandwidth is increased. On the other hand, the correlation coefficient is lower when bandwidth is increased. These results mean there is more waveform distortion when the bandwidth is wider, due to frequency dependence of Friis' transmission formula. These proposed closed form formulas are useful to define the quantity of UWB-IR waveform distortion in free space channel.

CHAPTER 4
MATHEMATICAL MODELING OF GROUND REFLECTION CHANNEL

4.1 Introduction

In this chapter, the ground reflection channel is mathematically modeled for ultra wideband impulse radio (UWB-IR) systems. The novel method of derivation is proposed. The rectangular passband waveform [33] is used as transmitted waveform same as for free space channel and complex form of Friis' transmission formula [14]-[15] is applied to characterize ground reflection channel. Next, the received waveform is computed. In addition, the closed forms of path loss expressions are derived based on both average and peak power losses. After that, the novel quantitative parameter, peak to average loss ratio, is proposed and derived in the closed form formula [34]. Moreover, the closed form formulas of correlation coefficient using correlation receiver with transmitted waveform template are derived [35]. The results are shown and verified with measurement. Moreover, the ground reflection path loss based on average power loss is compared with the model in [20].

4.2 Transmitted Waveform

For ground reflection channel, UWB-IR transmitted waveform is rectangular passband waveform [33] same as for free space channel. The waveform in time domain and its spectral density function are in Equations (3.1) and (3.3), respectively.

4.3 Ground Reflection Channel

The ground reflection channel is considered in the terms of direct and reflection paths as is shown in Figure 4.1. The distance of direct and reflection paths, d' and d'', can be respectively calculated from [37]

$$d' = \sqrt{(h_t - h_r)^2 + d^2}, \tag{4.1}$$

$$d'' = \sqrt{(h_t + h_r)^2 + d^2}, \tag{4.2}$$

where h_t and h_r are the heights of transmitter and receiver antennas, respectively.

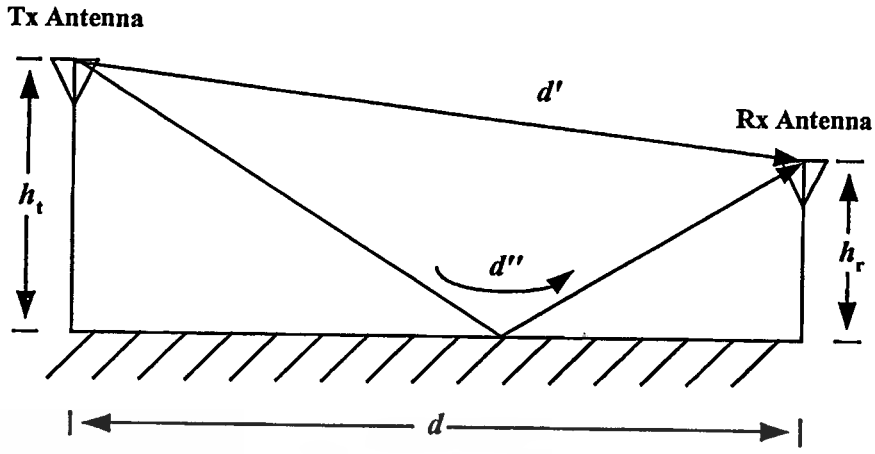

Figure 4.1 Ground reflection channel model.

Furthermore, the complex form Friis' transmission formula is applied for ground reflection channel [14]-[15]. The transmitter and receiver antennas are also considered to have one constant gains. Then, the frequency transfer function of ground reflection channel H_g is the addition between frequency transfer functions of direct and reflection paths and can be written as

$$H_g(f) = \frac{1}{4\pi |f| t'} e^{-j2\pi f t'} + \frac{\Gamma}{4\pi |f| t''} e^{-j2\pi f t''}, \tag{4.3}$$

where Γ is the reflection coefficient of ground, $t' = d'/c$ is the delay time of direct path and $t'' = d''/c$ is the delay time of reflection path. Equation (4.3) can be written in the term of real and imaginary parts as

$$\begin{aligned} H_g(f) &= \frac{1}{4\pi |f|} \left[\begin{array}{l} \frac{1}{t'}\cos(2\pi f t') - j\frac{1}{t'}\sin(2\pi f t') \\ + \frac{\Gamma}{t''}\cos(2\pi f t'') - j\frac{\Gamma}{t''}\sin(2\pi f t'') \end{array} \right] \\ &= \frac{1}{4\pi |f|} \left\{ \begin{array}{l} \left[\frac{1}{t'}\cos(2\pi f t') + \frac{\Gamma}{t''}\cos(2\pi f t'') \right] \\ - j\left[\frac{1}{t'}\sin(2\pi f t') + \frac{\Gamma}{t''}\sin(2\pi f t'') \right] \end{array} \right\}. \end{aligned} \tag{4.4}$$

From Equation (4.4), magnitude of ground reflection channel transfer function can be written as

$$
\begin{aligned}
|H_g(f)| &= \frac{1}{4\pi|f|}\sqrt{\left[\frac{1}{t'}\cos(2\pi ft')+\frac{\Gamma}{t''}\cos(2\pi ft'')\right]^2+\left[\frac{1}{t'}\sin(2\pi ft')+\frac{\Gamma}{t''}\sin(2\pi ft'')\right]^2} \\
&= \frac{1}{4\pi|f|}\sqrt{\begin{aligned}&\frac{1}{t'^2}\cos^2(2\pi ft')+\frac{2\Gamma}{t't''}\cos(2\pi ft')\cos(2\pi ft'')+\frac{\Gamma^2}{t''^2}\cos^2(2\pi ft'') \\ &+\frac{1}{t'^2}\sin^2(2\pi ft')+\frac{2\Gamma}{t't''}\sin(2\pi ft')\sin(2\pi ft'')+\frac{\Gamma^2}{t''^2}\sin^2(2\pi ft'')\end{aligned}} \\
&= \frac{1}{4\pi|f|}\sqrt{\begin{aligned}&\frac{1}{t'^2}\left[\cos^2(2\pi ft')+\sin^2(2\pi ft')\right]+\frac{\Gamma^2}{t''^2}\left[\cos^2(2\pi ft'')+\sin^2(2\pi ft'')\right] \\ &+\frac{2\Gamma}{t't''}\left[\cos(2\pi ft')\cos(2\pi ft'')+\sin(2\pi ft')\sin(2\pi ft'')\right]\end{aligned}} \\
&= \frac{1}{4\pi|f|}\sqrt{\frac{1}{t'^2}+\frac{\Gamma^2}{t''^2}+\frac{2\Gamma}{t't''}\cos(2\pi f\Delta t)}, \qquad (4.5)
\end{aligned}
$$

where $\Delta t = t'' - t'$ is time difference between time delay of direct and reflection paths.

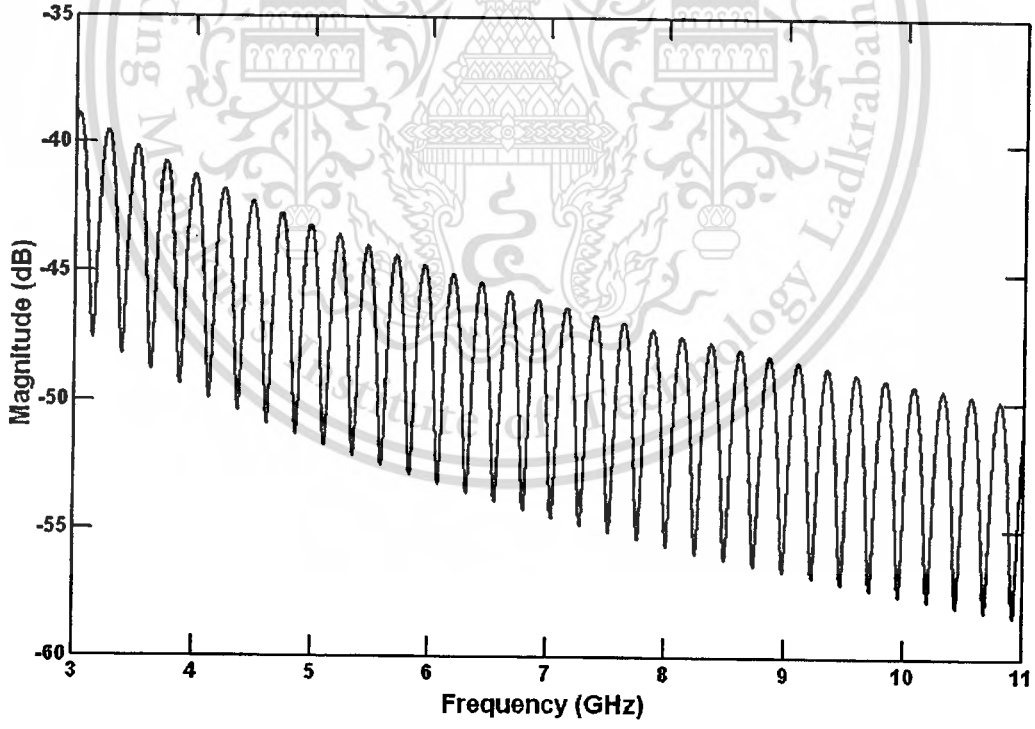

Figure 4.2 Magnitude of ground reflection channel transfer function with distance $d = 1$ m, the heights of transmitter and receiver antennas $h_t = h_r = 1$ m.

From Equation (4.4), phase of ground reflection channel transfer function can be written as

$$\angle H_g(f) = -\tan^{-1}\left[\frac{\frac{1}{t'}\sin(2\pi ft') + \frac{\Gamma}{t''}\sin(2\pi ft'')}{\frac{1}{t'}\cos(2\pi ft') + \frac{\Gamma}{t''}\cos(2\pi ft'')}\right], \tag{4.6}$$

The magnitude and phase of ground reflection channel transfer function with distance $d = 1$ m, the heights of transmitter and receiver antennas $h_t = h_r = 1$ m are shown in Figures 4.2 and 4.3, respectively. The fluctuation of magnitude and nonlinear phase caused from interference of ground reflection path can be investigated.

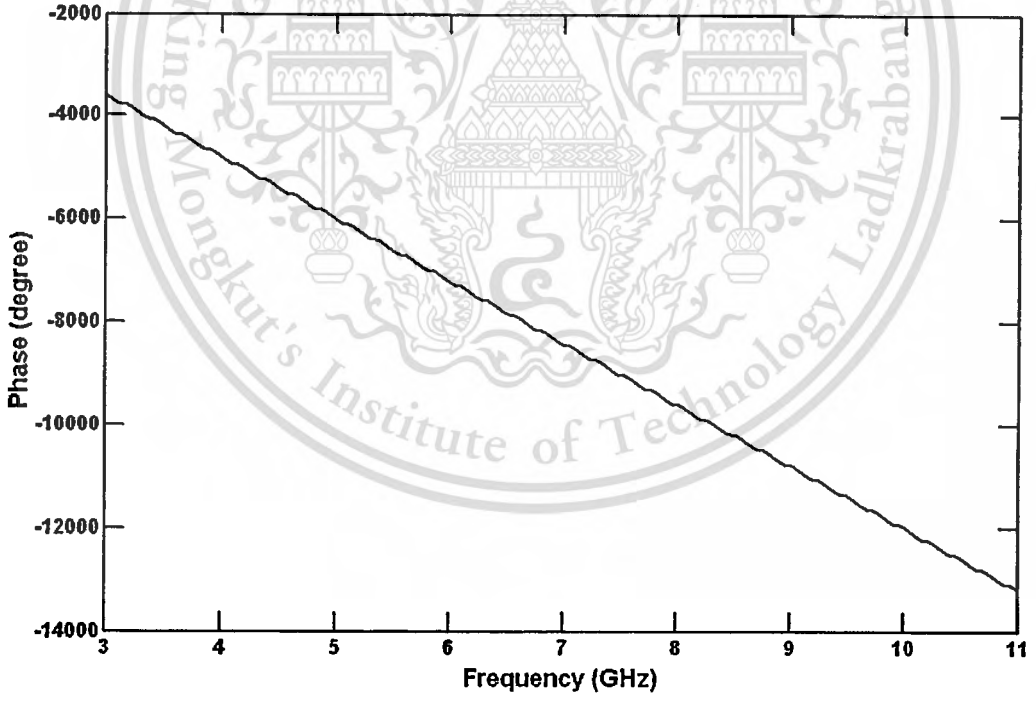

Figure 4.3 Phase of ground reflection channel transfer function with distance $d = 1$ m, the heights of transmitter and receiver antennas $h_t = h_r = 1$ m.

4.4 Received Waveform

The spectral density of received waveform for ground reflection channel $V_{r,g}$ is calculated by using the multiplication between ground reflection channel transfer function H_g and spectral density of transmitted waveform V_t. It obtains

$$V_{r,f}(f) = H_f(f) \cdot V_t(f). \tag{4.7}$$

From Equations (3.1), (4.5) and (4.7), the magnitude of spectral density of received waveform can be written as

$$|V_{r,g}(f)| = \begin{cases} \dfrac{A}{8\pi f_b |f|}\sqrt{\dfrac{1}{t'^2}+\dfrac{\Gamma^2}{t''^2}+\dfrac{2\Gamma}{t't''}\cos(2\pi f\Delta t)} & ||f|-f_c| \le \dfrac{f_b}{2} \\ 0 & ||f|-f_c| > \dfrac{f_b}{2} \end{cases}. \tag{4.8}$$

The received waveform in time domain is considered as the addition between free space received waveform with direct path distance $d = d'$ and free space received waveform with reflection path distance $d = d''$ multiplied by reflection coefficient Γ. Therefore, the received waveform in time domain for ground reflection channel $v_{r,g}$ can be written as

$$v_{r,g}(t) \tag{4.9}$$

$$= \begin{cases} \dfrac{A}{4\pi f_b t'}\ln\left(\dfrac{f_H}{f_L}\right)+\dfrac{\Gamma A}{4\pi f_b t''}\{C_i[2\pi f_H(t-t'')]-C_i[2\pi f_L(t-t'')]\} & t = t' \\ \dfrac{\Gamma A}{4\pi f_b t''}\ln\left(\dfrac{f_H}{f_L}\right)+\dfrac{A}{4\pi f_b t'}\{C_i[2\pi f_H(t-t')]-C_i[2\pi f_L(t-t')]\} & t = t'' \\ \dfrac{A}{4\pi f_b t'}\{C_i[2\pi f_H(t-t')]-C_i[2\pi f_L(t-t')]\} & \\ \quad +\dfrac{\Gamma A}{4\pi f_b t''}\{C_i[2\pi f_H(t-t'')]-C_i[2\pi f_L(t-t'')]\} & t \ne t',\ t \ne t'' \end{cases}$$

The received waveform in time domain and its spectral density for minimum bandwidth case are shown in Figures 4.4 and 4.5, respectively. For maximum bandwidth case, Figures 4.6 and 4.7 show the received waveform and its spectral density, respectively. The waveforms from direct and reflection paths can be investigated.

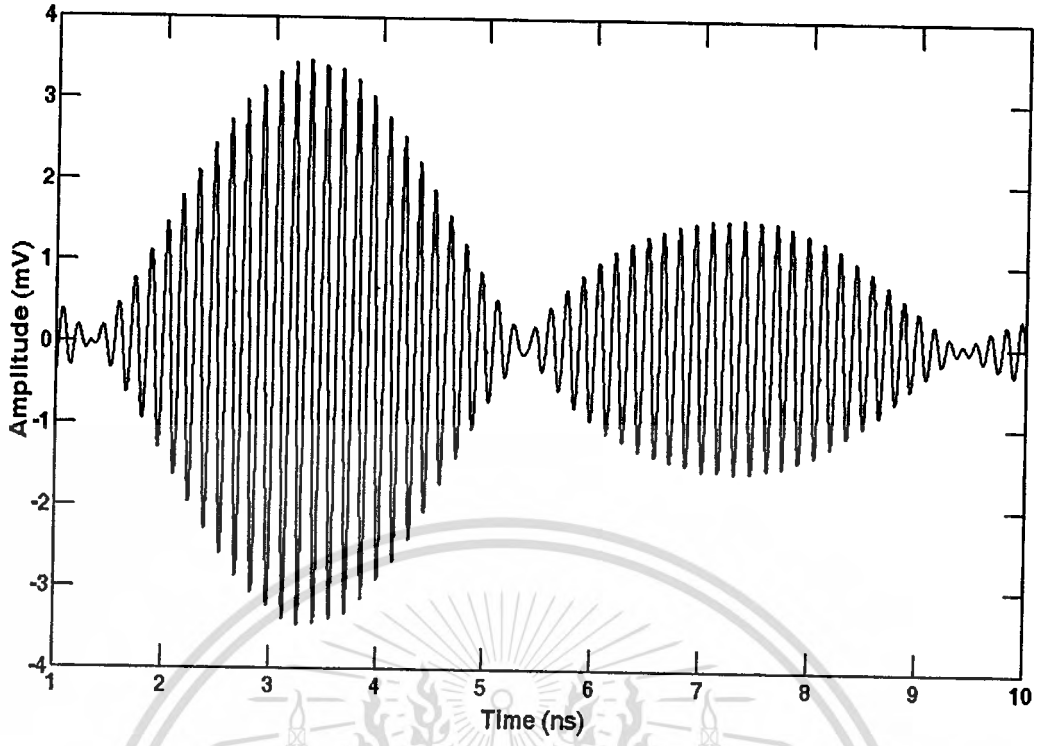

Figure 4.4 Received waveform with minimum bandwidth case for ground reflection channel.

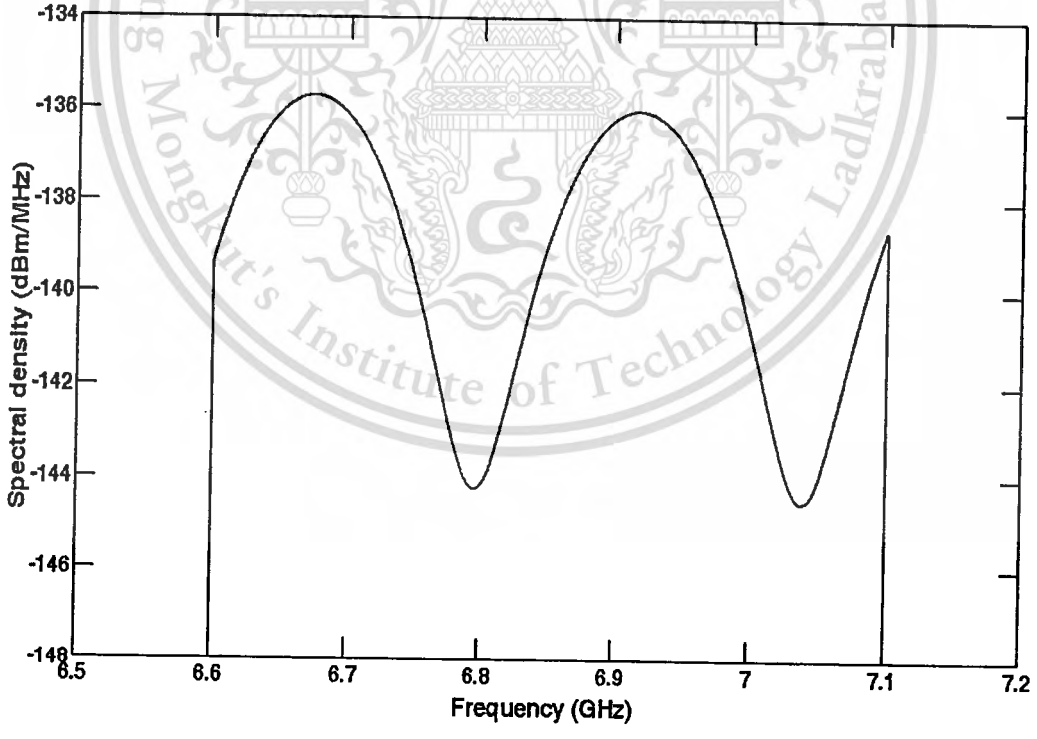

Figure 4.5 Spectral density of received waveform with minimum bandwidth case for ground reflection channel.

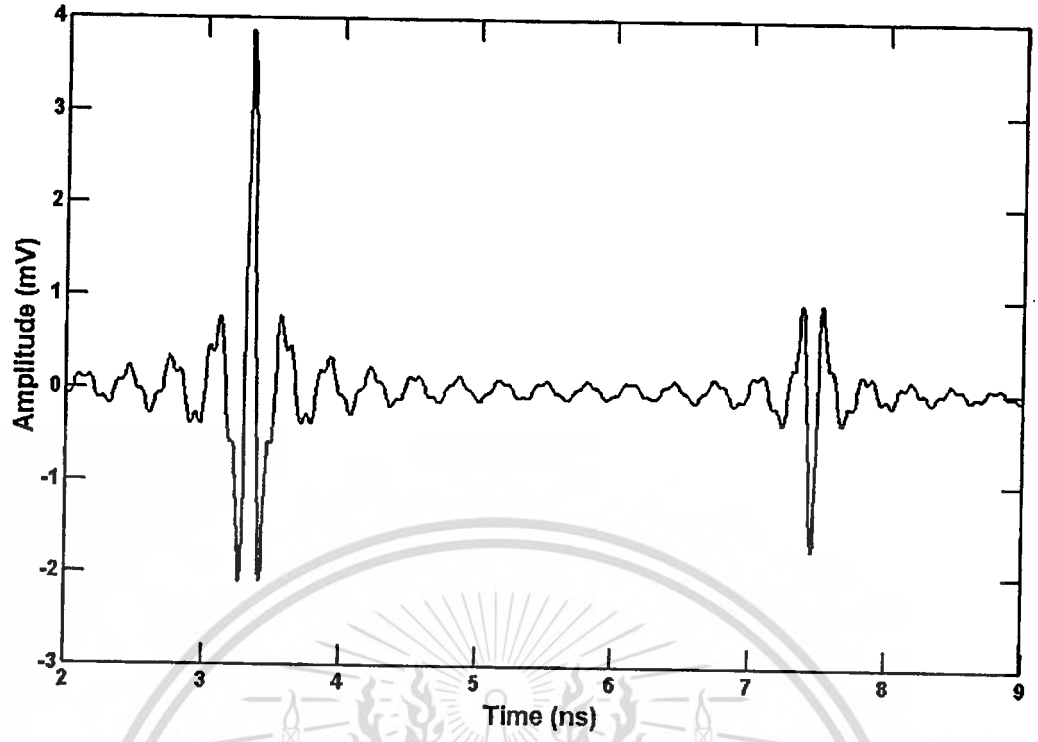

Figure 4.6 Received waveform with maximum bandwidth case for ground reflection channel.

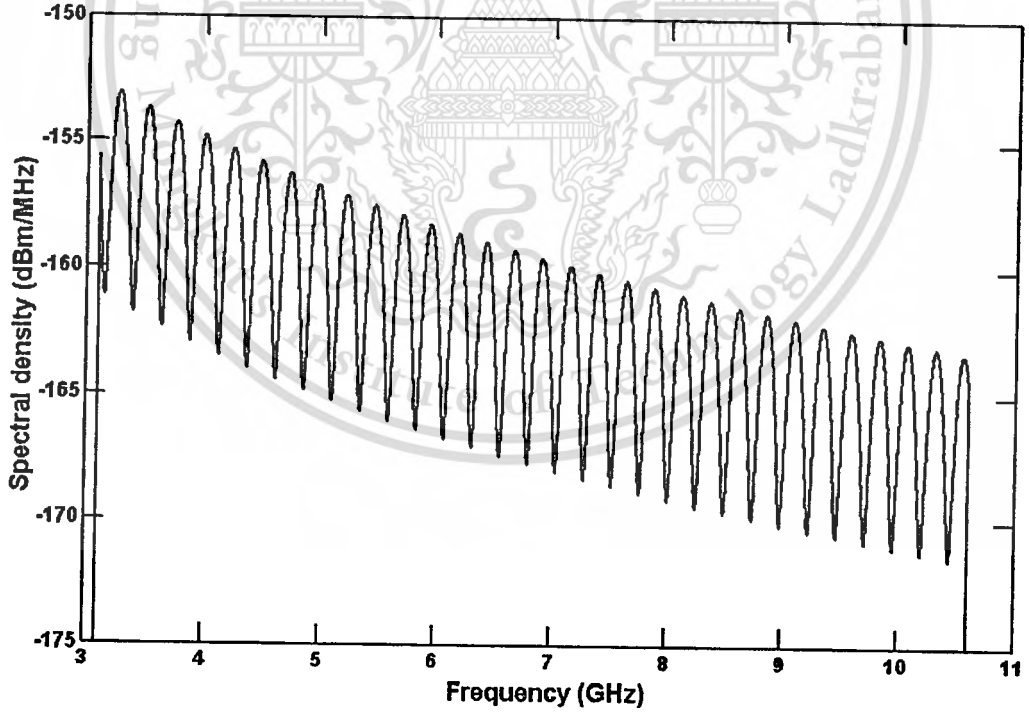

Figure 4.7 Spectral density of received waveform with maximum bandwidth case for ground reflection channel.

4.5 Path Loss

In this section, path losses based on average and peak power losses are mathematically modeled in the closed form formulas for ground reflection channel.

4.5.1 Based on Average Power Loss

UWB-IR ground reflection path loss based on average power loss $PL_{g,a}$ in dB is defined as the ratio between the average power of transmitted and received waveforms in frequency domain for ground reflection channel and it can be written as

$$PL_{g,a} = 10\log\left(\frac{\int_{-\infty}^{\infty}|V_t(f)|^2\,df}{\int_{-\infty}^{\infty}|V_{r,g}(f)|^2\,df}\right). \tag{4.10}$$

From spectral density of received waveform in Equation (4.8), it obtains

$$\begin{aligned}
\int_{-\infty}^{\infty}|V_{r,g}(f)|^2\,df &= \frac{A^2}{64\pi^2 f_b^2}\left\{\begin{aligned}&\int_{-f_H}^{-f_L}\frac{1}{f^2}\left[\frac{1}{t'^2}+\frac{\Gamma^2}{t''^2}+\frac{2\Gamma}{t't''}\cos(2\pi f\Delta t)\right]df\\&+\int_{f_L}^{f_H}\frac{1}{f^2}\left[\frac{1}{t'^2}+\frac{\Gamma^2}{t''^2}+\frac{2\Gamma}{t't''}\cos(2\pi f\Delta t)\right]df\end{aligned}\right\}\\
&= \frac{A^2}{32\pi^2 f_b^2}\left\{\int_{f_L}^{f_H}\frac{1}{f^2}\left[\frac{1}{t'^2}+\frac{\Gamma^2}{t''^2}+\frac{2\Gamma}{t't''}\cos(2\pi f\Delta t)\right]df\right\}\\
&= \frac{A^2}{32\pi^2 f_b^2}\left\{\left(\frac{1}{t'^2}+\frac{\Gamma^2}{t''^2}\right)\int_{f_L}^{f_H}\frac{1}{f^2}df+\frac{2\Gamma}{t't''}\int_{f_L}^{f_H}\left[\frac{1}{f^2}\cos(2\pi f\Delta t)\right]df\right\}\\
&= \frac{A^2}{32\pi^2 f_b^2}\left\{\begin{aligned}&-\left(\frac{1}{t'^2}+\frac{\Gamma^2}{t''^2}\right)\frac{1}{f}\Big|_{f=f_L}^{f_H}\\&-\frac{2\Gamma}{t't''}\left[\frac{1}{f}\cos(2\pi f\Delta t)+2\pi\Delta t\,\mathrm{S_i}(2\pi f\Delta t)\right]\Big|_{f=f_L}^{f_H}\end{aligned}\right\}\\
&= \frac{A^2}{32\pi^2 f_b^2}\left\{\begin{aligned}&\left(\frac{1}{t'^2}+\frac{\Gamma^2}{t''^2}\right)\frac{f_b}{f_L f_H}\\&+\frac{2\Gamma}{t't''}\left[\frac{1}{f_L}\cos(2\pi f_L\Delta t)-\frac{1}{f_H}\cos(2\pi f_H\Delta t)\right.\\&\left.+2\pi\Delta d\,\mathrm{S_i}(2\pi f_L\Delta t)-2\pi\Delta t\,\mathrm{S_i}(2\pi f_H\Delta t)\right]\end{aligned}\right\},
\end{aligned} \tag{4.11}$$

where $S_i(x)$ is sine integral function and defined as

$$S_i(x) = \int_0^x \frac{1}{\tau}\sin(\tau)d\tau .$$

From equations (3.13), (4.10) and (4.11), the ground reflection path loss based on average power loss is derived in the closed form formula and can be written as

$$PL_{g,a} = 10\log\left(\frac{16\pi^2 f_b}{\left(\frac{1}{t'^2}+\frac{\Gamma^2}{t''^2}\right)\frac{f_b}{f_L f_H}+\frac{2\Gamma}{t't''}\left[\begin{array}{l}\frac{1}{f_L}\cos(2\pi f_L\Delta t)-\frac{1}{f_H}\cos(2\pi f_H\Delta t)\\ +2\pi\Delta t S_i(2\pi f_L\Delta t)-2\pi\Delta t S_i(2\pi f_H\Delta t)\end{array}\right]}\right). \quad (4.12)$$

4.5.2 Based on Peak Power Loss

UWB-IR ground reflection path loss based on peak power loss $PL_{g,p}$ in dB is defined as the ratio between the peak power of transmitted and received waveforms in time domain for ground reflection channel and it can be written as

$$PL_{g,p} = 10\log\left(\frac{\max\left[v_i^2(t)\right]}{\max\left[v_{r,g}^2(t)\right]}\right). \quad (4.13)$$

From received waveform for ground reflection channel in Equation (4.9), it obtains

$$\max\left[v_{r,g}^2(t)\right] = \left(\frac{A}{4\pi f_b t'}\ln\left(\frac{f_H}{f_L}\right)+\frac{\Gamma A}{4\pi f_b t''}\left\{C_i\left[2\pi f_H(t-t'')\right]-C_i\left[2\pi f_L(t-t'')\right]\right\}\right)^2 . \quad (4.14)$$

From Equations (3.17), (4.13) and (4.14), the ground reflection path loss based on peak power loss is derived in the closed form formula and can be written as

$$PL_{g,p} = 10\log\left(\frac{A^2}{\left(\frac{A}{4\pi f_b t'}\ln\left(\frac{f_H}{f_L}\right)+\frac{\Gamma A}{4\pi f_b t''}\left\{C_i\left[2\pi f_H\left(t-t''\right)\right]-C_i\left[2\pi f_L\left(t-t''\right)\right]\right\}\right)^2}\right)$$

$$= 20\log\left(\frac{4\pi f_b}{\frac{1}{t'}\ln\left(\frac{f_H}{f_L}\right)+\frac{\Gamma}{t''}\left\{C_i\left[2\pi f_H\left(t-t''\right)\right]-C_i\left[2\pi f_L\left(t-t''\right)\right]\right\}}\right). \quad (4.15)$$

4.6 Peak to Average Loss Ratio

In this section, the novel quantitative parameter of waveform distortion, peak to average loss ratio, is proposed and derived in the closed form formula for ground reflection channel. The peak to average loss ratio is defined as the ratio between peak power loss and average power loss from transmitter to receiver antennas. The ground reflection peak to average loss ratio PAR_g in dB can be written as [34]

$$PAR_g = 10\log\left\{\frac{\max\left[v_t^2(t)\right]}{\max\left[v_{r,g}^2(t)\right]}\cdot\frac{\int_{-\infty}^{\infty}\left|V_{r,g}(f)\right|^2 df}{\int_{-\infty}^{\infty}\left|V_t(f)\right|^2 df}\right\}. \quad (4.16)$$

From Equations (3.13), (3.17), (4.11), (4.14) and (4.16), the ground reflection peak to average loss ratio is derived in the closed form formula and can be written as

$$PAR_g = 10\log\left\{\frac{f_b^2\left(t''^2+\Gamma^2 t'^2\right)-2\Gamma f_L f_H f_b t' t''\left[C_d\left(2\pi\Delta t\right)+2\pi\Delta t S_{id}\left(2\pi\Delta t\right)\right]}{f_L f_H\left[t''\ln\left(\frac{f_H}{f_L}\right)+\Gamma t' C_{id}\left(2\pi\Delta t\right)\right]^2}\right\}. \quad (4.17)$$

where

$$C_{id}(x) = C_i(xf_H)-C_i(xf_L),$$
$$S_{id}(x) = S_i(xf_H)-S_i(xf_L),$$
$$C_d(x) = \frac{1}{f_H}\cos(xf_H)-\frac{1}{f_L}\cos(xf_L).$$

4.7 Correlation Coefficient

In this section, the closed form formula of correlation coefficient is derived for ground reflection channel. The ground reflection correlation coefficient C_g is defined as [35]

$$C_g = \frac{\max\left|\int_{-\infty}^{\infty} v_{r,g}^*(t)\cdot v_t(t+\tau)\mathrm{d}t\right|}{\sqrt{\int_{-\infty}^{\infty}|v_{r,g}(t)|^2\,\mathrm{d}t\cdot\int_{-\infty}^{\infty}|v_t(t)|^2\,\mathrm{d}t}}, \tag{4.18}$$

The closed form formula of ground reflection correlation coefficient can be derived as

$$C_g = \frac{\frac{1}{f_b}\left[\frac{1}{t'}\ln\left(\frac{f_H}{f_L}\right)+\frac{\Gamma}{t''}\mathrm{C_{id}}(2\pi\Delta t)\right]}{\sqrt{\frac{1}{f_L f_H f_b t' t''}\left\{\frac{f_b\left(t''^2+\Gamma^2 t'^2\right)}{t' t''}-2\Gamma\mathrm{C_r}(2\pi\Delta t)-4\pi\Gamma f_L f_H \Delta t\,\mathrm{S_{id}}(2\pi\Delta t)\right\}}}, \tag{4.19}$$

where

$$\mathrm{C_r}(x) = f_L\cos(xf_H)-f_H\cos(xf_L).$$

4.8 Measurement

The measurement was done to verify proposed mathematical ground reflection model. The measurement equipment, setup and parameters are the same as in [38]. The frequency transfer function of ground reflection channel was measured using a vector network analyzer (VNA). The measurement was done in the open area, the soccer field of King Mongkut's Institute of Technology Ladkrabang (KMITL), Thailand. The metallic plate, zinc plate, was laid on the ground between transmitter and receiver antennas for the perfect reflection condition ($\Gamma = -1$). The measurement setup is shown in Figure 4.8.

The biconical antennas were used as transmitter and receiver antennas. Figure 4.9 shows the biconical antenna structure. The reflection loss of this antenna is shown in Figure 4.10. This antenna can be operated in the full band of UBW-IR that is frequency ranging from 3.1 to 10.6 GHz. Both transmitter and receiver antennas

were fixed at the height of $h_t = h_r = 0.75$ m with horizontal polarization for focusing the signal from direct and ground reflection paths. In other word, the main radiated and received paths by transmitter and receiver antennas are direct and ground reflection paths.

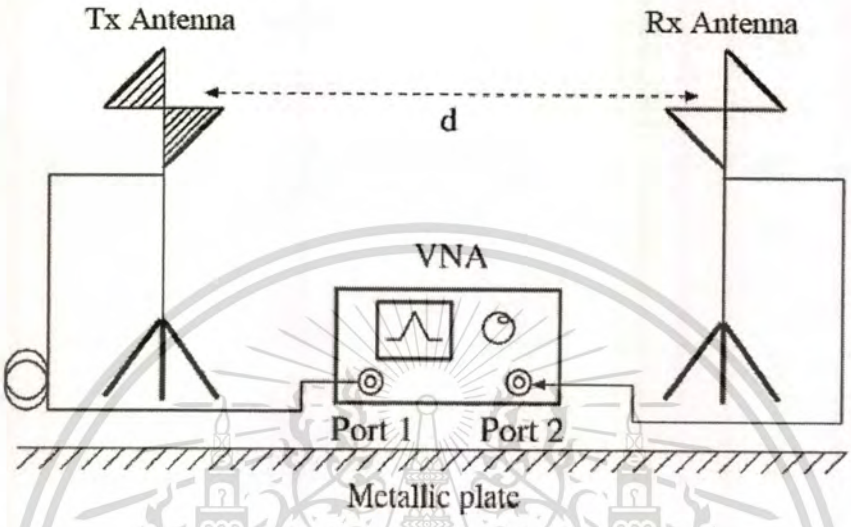

Figure 4.8 Measurement setup.

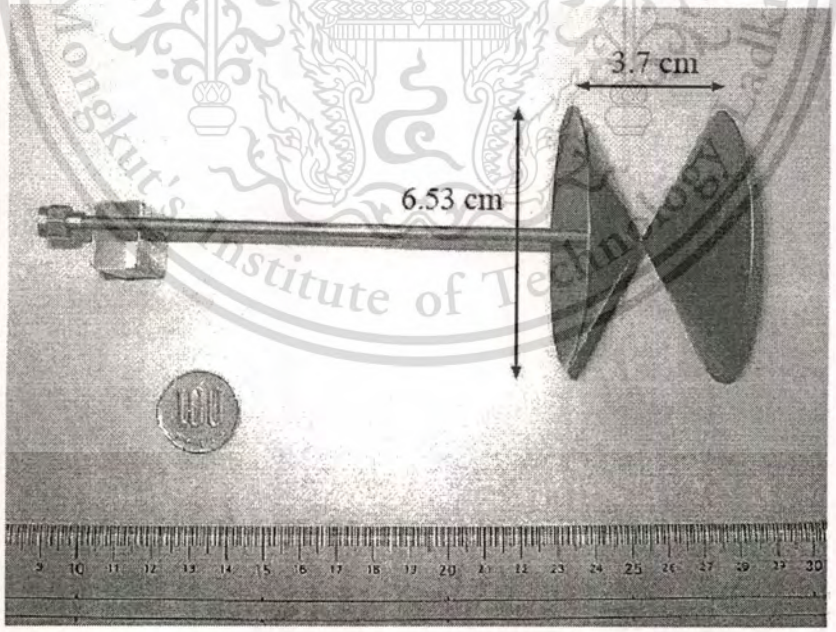

Figure 4.9 Biconical antenna structure.

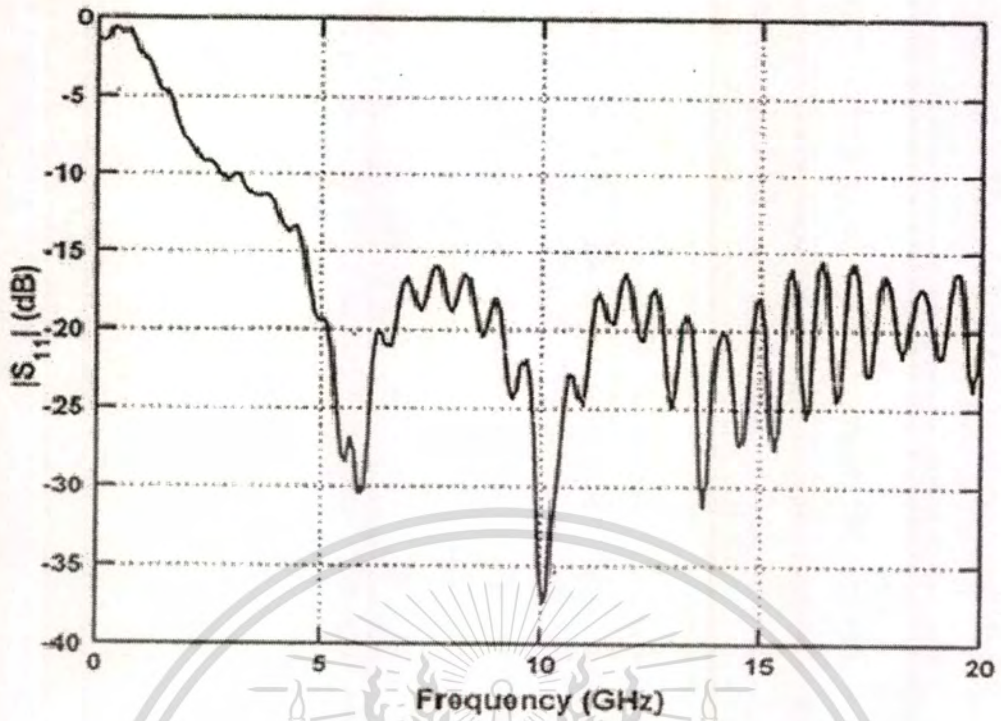

Figure 4.10 Reflection loss of biconical antenna.

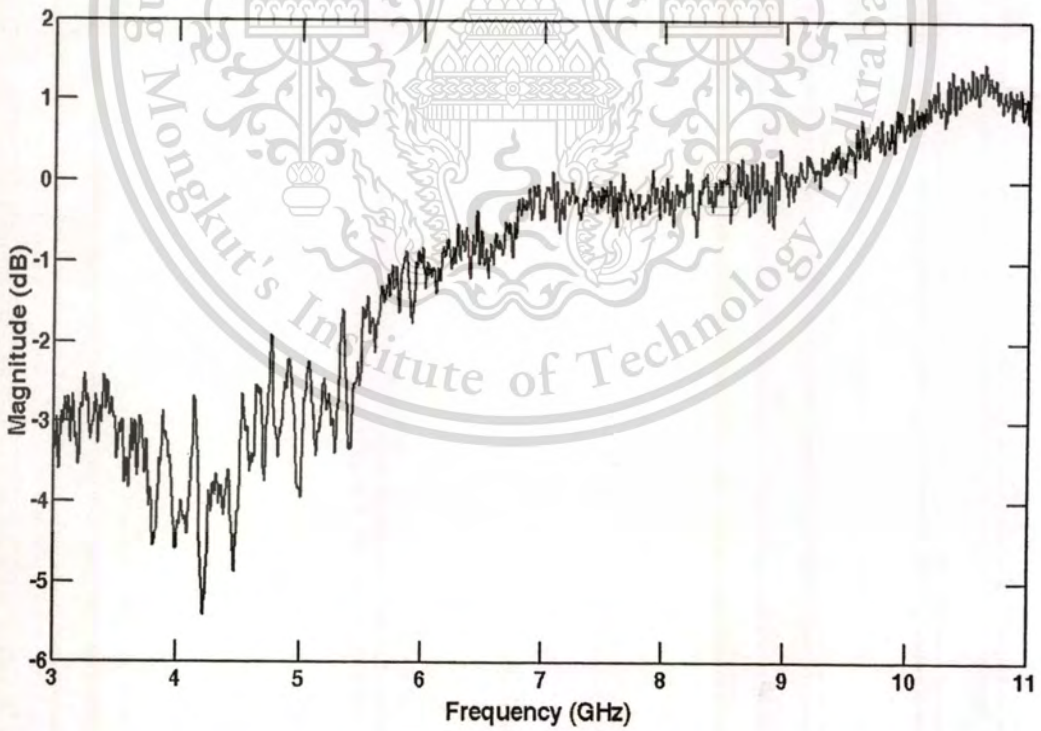

Figure 4.11 Magnitude of antenna transfer function.

The measurement distance d was ranged from 1 to 5 m with 0.25 m distance increment step. The frequency transfer functions of transmitter and receiver antennas were evaluated using method that proposed in [39]. The magnitude and phase of antenna transfer function of biconical antenna are shown in Figures 4.11 and 4.12, respectively. This antenna transfer function was used to remove the characteristics of transmitter and receiver antennas from measurement frequency transfer function for obtaining only frequency transfer function of ground reflection channel.

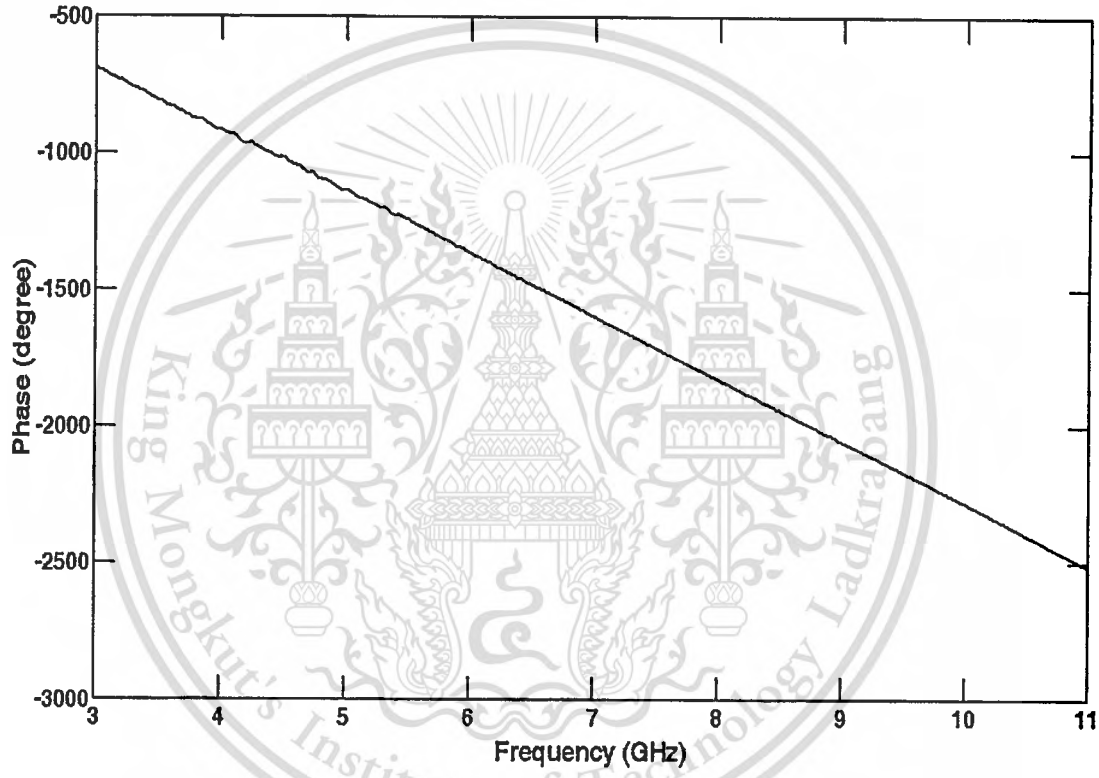

Figure 4.12 Phase of antenna transfer function.

4.9 Results

In this section, the proposed UWB-IR ground reflection path loss based on average and peak power losses, peak to average loss ratio and correlation coefficient are shown and verified with measurement.

For the analyzed parameters, the center frequency of waveform f_c is fixed at 4.1 GHz. The two cases of signal bandwidths, f_b = 0:5 and 1:4 GHz, are investigated. Therefore, the lowest frequencies f_L are equal to 3.85 and 3.40 GHz, while the highest frequencies f_H are equal to 4.35 and 4.80 GHz for fist and second cases, respectively. These signal bandwidths are in the lower band, which is specified by Ministry of Internal Affairs and Communications (MIC) of Japan [8].

4.9.1 Path Loss

Figures 4.13 and 4.14 show the proposed ground reflection path losses based on average power loss compared with model in [20] and measurement for 0.5 and 1.4 GHz signal bandwidths, respectively. From these figures, the proposed ground reflection path loss based on average power loss corresponds very well with measurement and has more accuracy than model in [20], especially at short distance.

The proposed ground reflection path losses based on peak power loss compared with measurement for 0.5 and 1.4 GHz signal bandwidths are shown in Figures 4.15 and 4.16, respectively. Similarly, the proposed ground reflection path loss base on peak power loss corresponds very well with measurement.

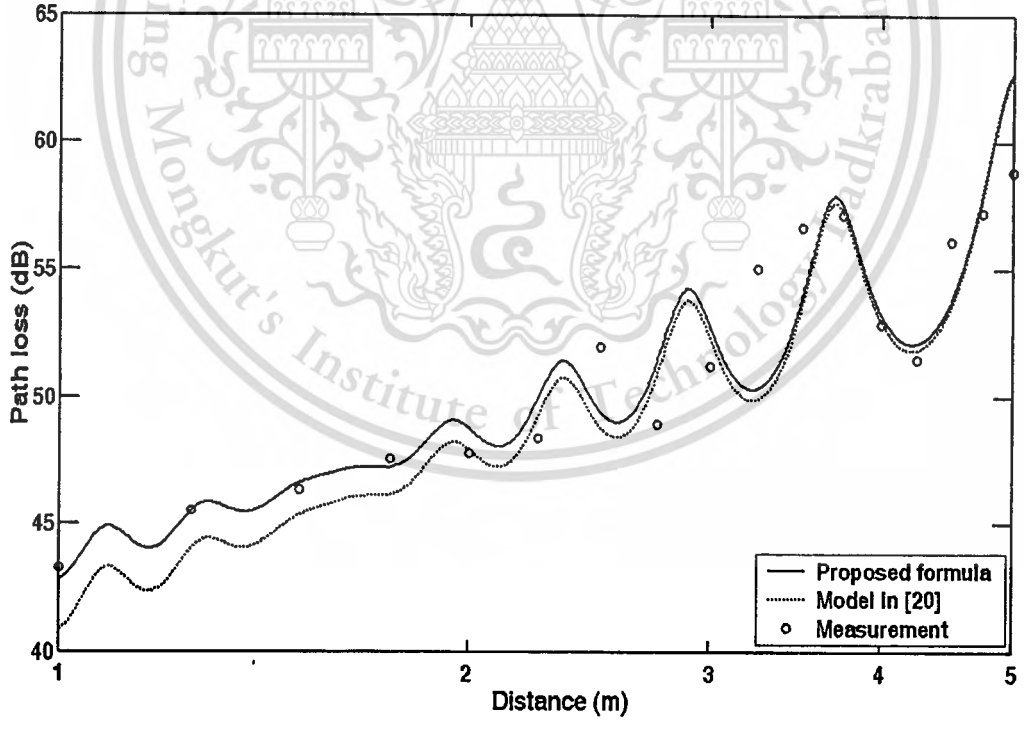

Figure 4.13 Proposed ground reflection path loss based on average power loss compared with model in [20] and measurement for bandwidth of 0.5 GHz.

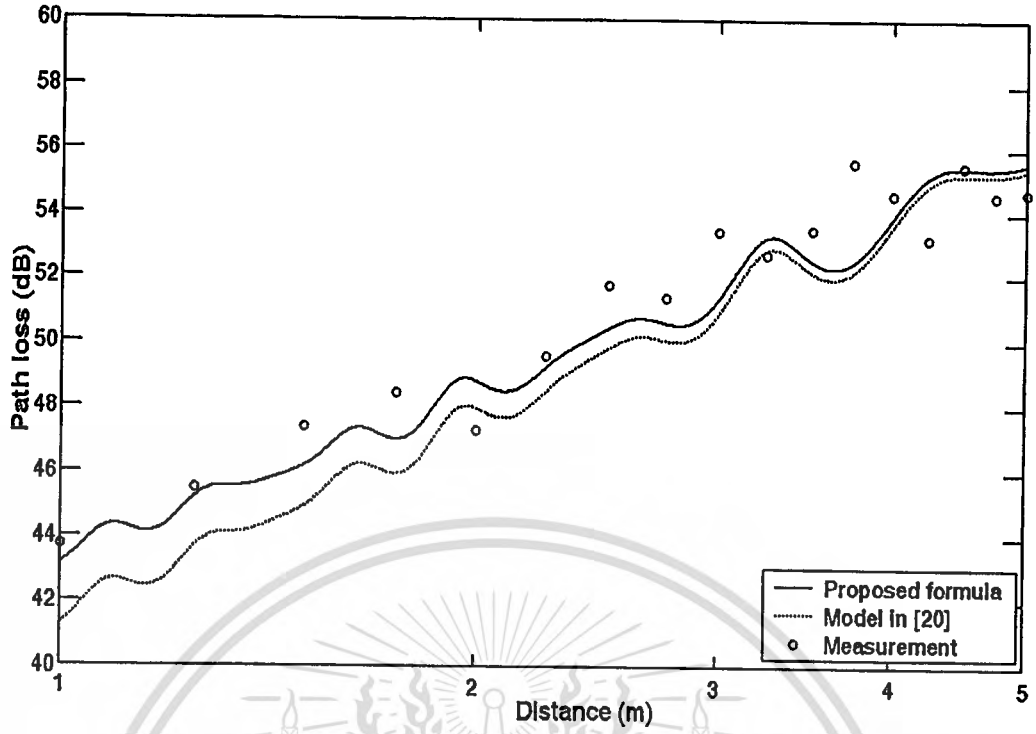

Figure 4.14 Proposed ground reflection path loss based on average power loss compared with model in [20] and measurement for bandwidth of 1.4 GHz.

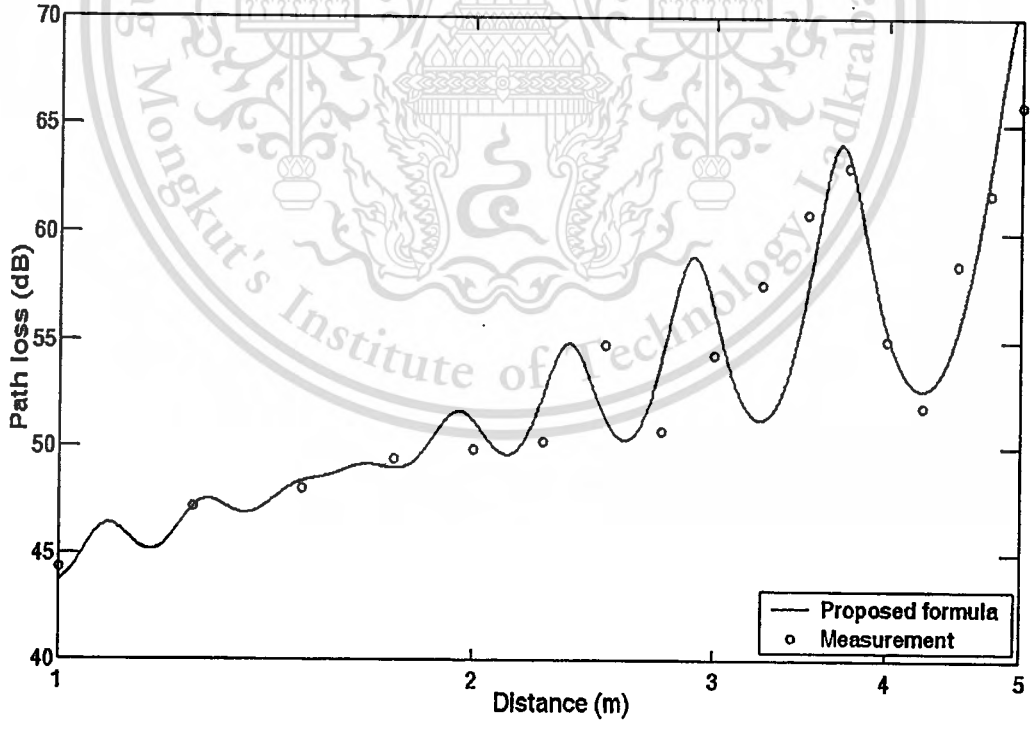

Figure 4.15 Proposed ground reflection path loss based on peak power loss compared with measurement for bandwidth of 0.5 GHz.

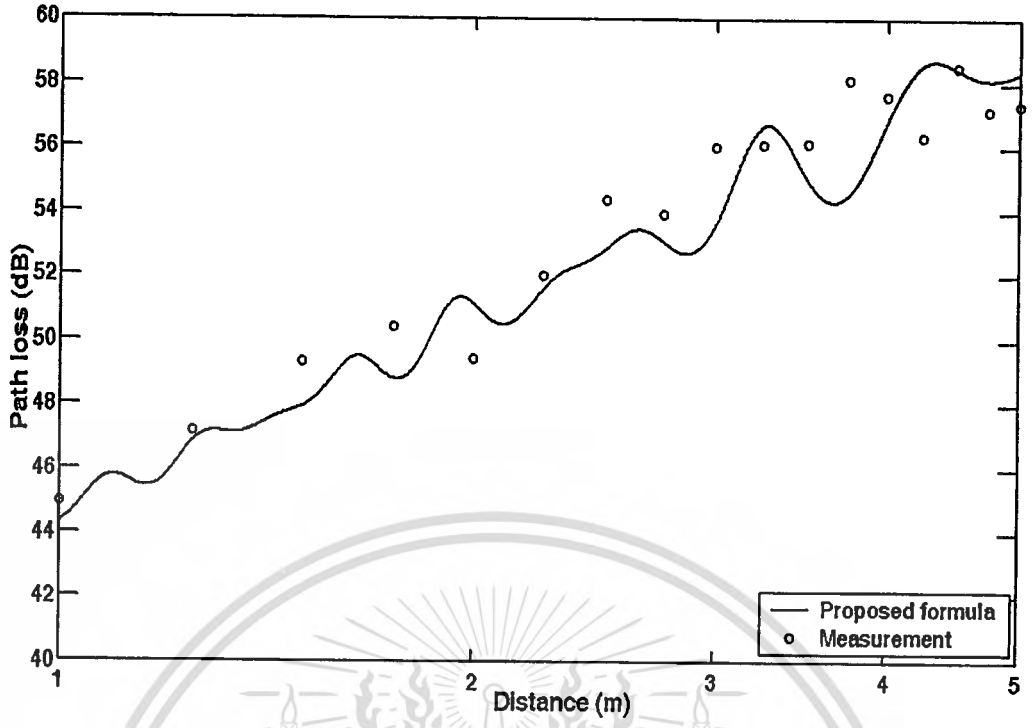

Figure 4.16 Proposed ground reflection path loss based on peak power loss compared with measurement for bandwidth of 1.4 GHz.

4.9.2 Peak to Average Loss Ratio

Figures 4.17 and 4.18 show the comparison between peak to average loss ratio from proposed formula and measurement with 500 MHz and 1.4 GHz bandwidths, respectively. Unlike with free space channel, the peak to average loss ratio of wide bandwidth is less than that of narrow bandwidth because the main waveform distortion causes from time dispersion or multi-path fading. Therefore, the UWB-IR systems are robust to multi-path fading more than narrowband systems. The distortion of waveform is also dependent on distance [34].

4.9.3 Correlation Coefficient

Figures 4.19 and 4.20 show the comparison between correlation coefficient from proposed formula and measurement with 500 MHz and 1.4 GHz bandwidths, respectively. The efficiency is significantly decreased compared with free space channel because of multi-path fading. The wide bandwidth has effect from multi-path fading along distance less than narrow bandwidth [35]. In addition, the narrow bandwidth with wide pulse has probability of overlap between direct and reflection pulses more than the wide bandwidth with short pulse.

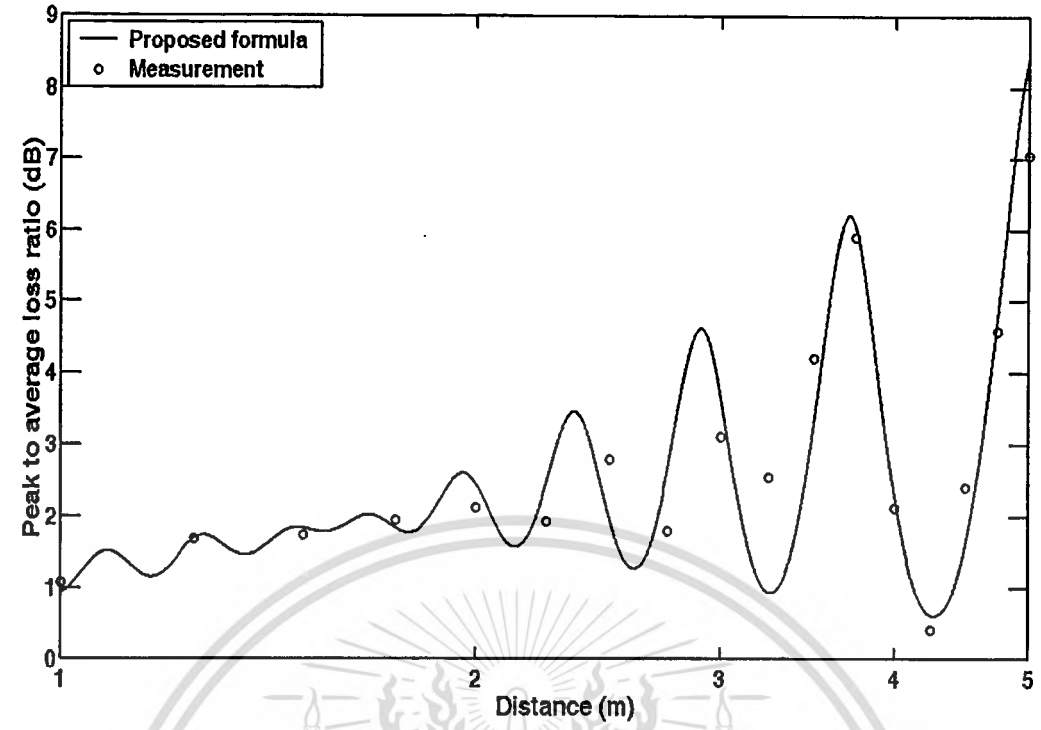

Figure 4.17 Comparison between ground reflection peak to average loss ratio from proposed formula and measurement with bandwidth of 500 MHz [34].

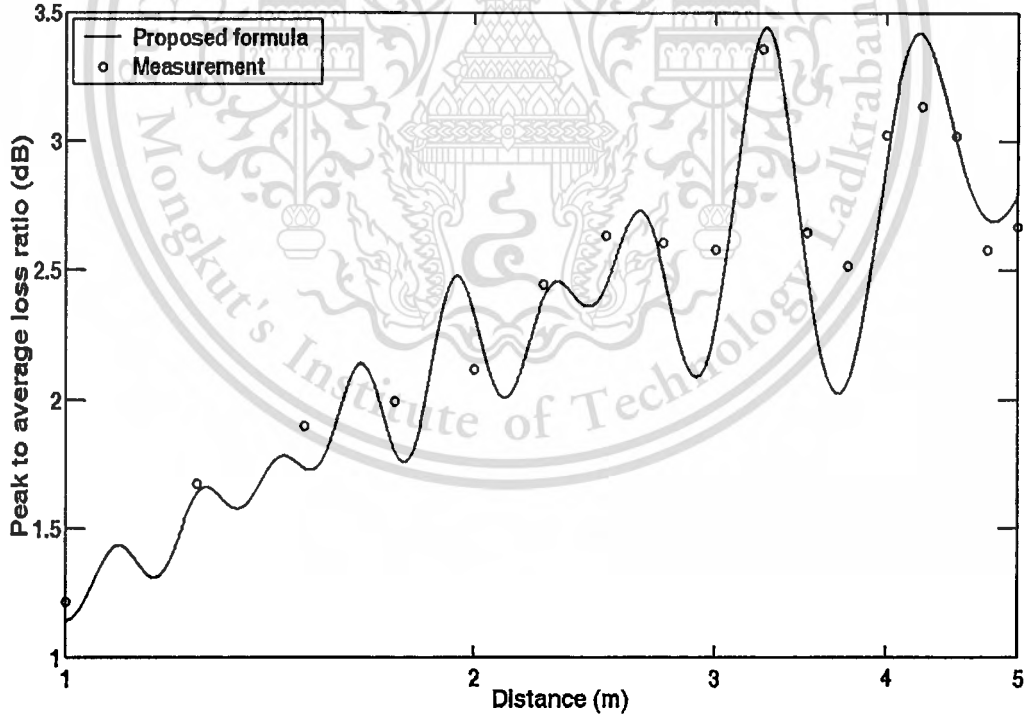

Figure 4.18 Comparison between ground reflection peak to average loss ratio from proposed formula and measurement with bandwidth of 1.4 GHz [34].

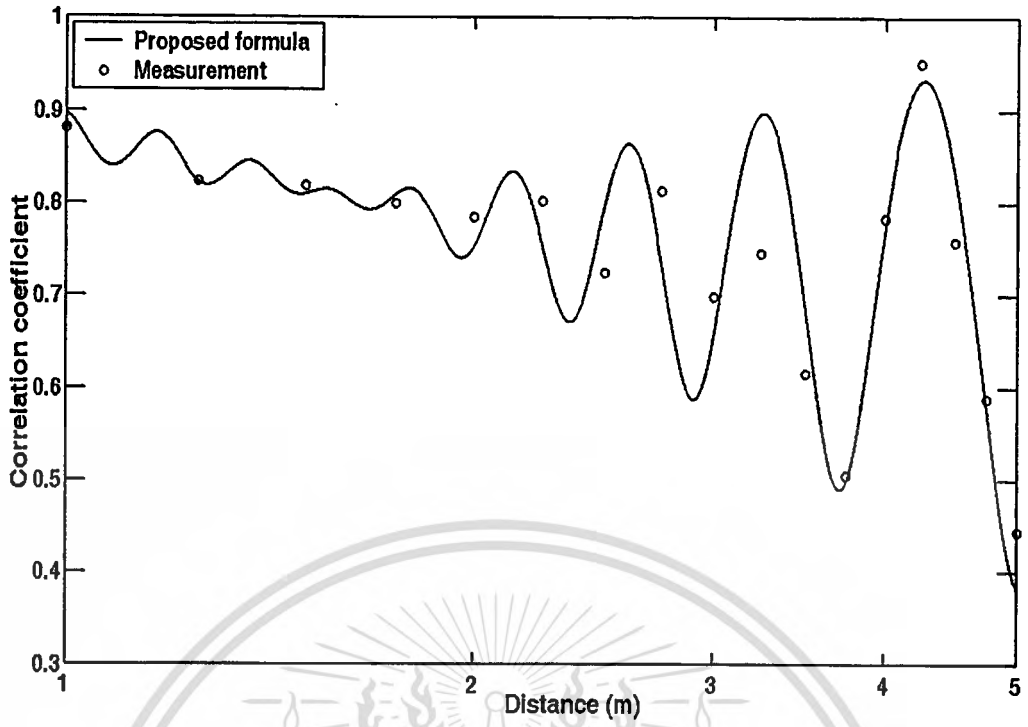

Figure 4.19 Comparison between ground reflection correlation coefficient from proposed formula and measurement with bandwidth of 500 MHz [35].

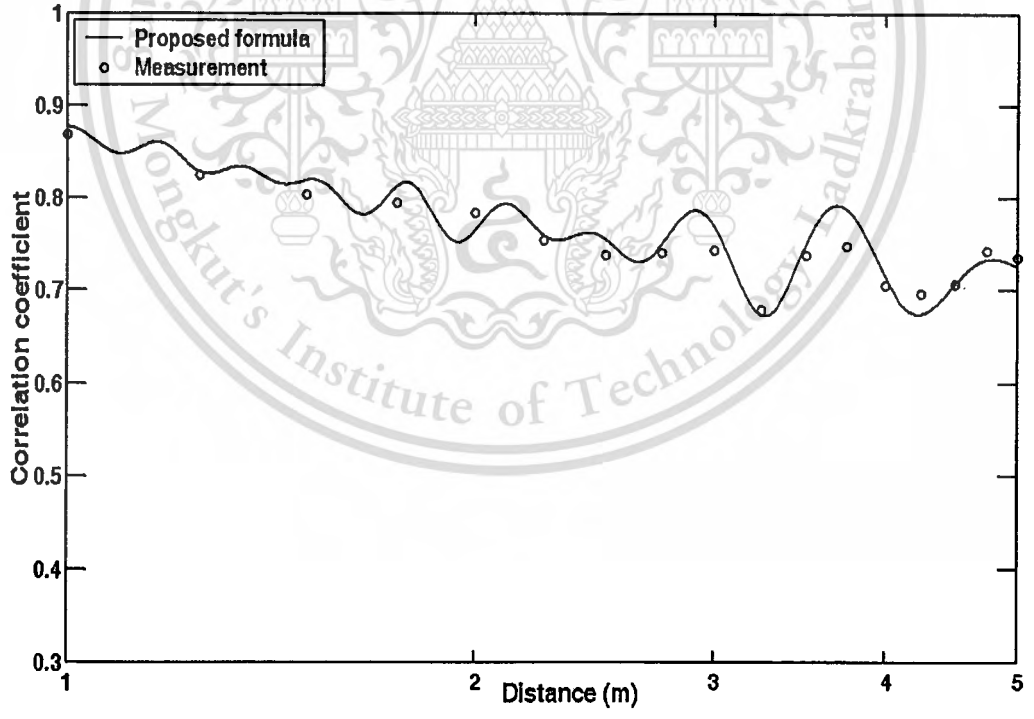

Figure 4.20 Comparison between ground reflection correlation coefficient from proposed formula and measurement with bandwidth of 1.4 GHz [35].

4.10 Conclusion

In this chapter, ground reflection path loss, peak to average loss ratio and correlation coefficient are mathematically modeled in the closed form formulas. The novel method of derivation is proposed. The measurement was done to verify the proposed model and compared with model in [20] for the path loss based on average power loss. The results reflect that the wider bandwidth has lower effect of multi-path fading. Therefore, the waveform distortion is reduced when bandwidth is wider. All of proposed formulas, path loss based on average and peak power loss, peak to average loss ratio, correlation coefficient, correspond very well with measurement. Therefore, the proposed model is accurate and can be a choice for modeling the ground reflection channel.

CHAPTER 5
LINK BUDGET

5.1 Introduction

In ultra wideband impulse radio (UWB-IR) systems, antennas usually act as significant pulse shaping filters and cause extreme waveform distortion. Moreover, low cost, geometrically small and still efficient antennas are required for the UWB-IR applications. Therefore, the link budget that considers the distortion due to antennas is important to design and improve the performance of UWB-IR systems.

In this chapter, a more generalized link budget model for studying the waveform distortion due to antenna on free space transmission is discussed. The free space link budget evaluation scheme in the term of frequency transfer function that takes into account the transmitted waveform, its distortion due to the antennas, the channel and the correlation receiver is developed. This model is based on Friis' transmission formula, adapted to the UWB-IR transmission systems [14]-[15]. The rectangular and root raised cosine passband waveforms are used as the transmitted waveform. The received waveform from receiver antenna and output waveform of correlation receiver for each case is evaluated. Experimental investigations are done for log-periodic dipole antenna (LPDA). The distortion quantities in the term of waveform distortion and transmission gain are defined and shown [36].

5.2 Model and Theory of Link Budget Evaluation

In this chapter, the short-range communication in line-of-sight (LOS) scenario is assumed, where other multi-path components are often less influential to the channel frequency transfer function. Therefore, the propagation channel is assumed to be free space, although it is rather straightforward to extend the discussion to double directional channel model [40]-[41].

5.2.1 Transmission System Model

The Friis' transmission formula [13] has been widely used to evaluate a link budget for narrowband LOS channels. The Friis' transmission gain G_{Friis} is defined as

$$G_{\text{Friis}}(f) = \frac{P_r(f)}{P_t(f)},$$
$$= G_f(f,d)G_t(f,\Omega_t)G_r(f,\Omega_r)\eta_p(f), \quad (5.1)$$

where P_t and P_r respectively are the input power to the transmitter antenna and the output power from the receiver antenna, G_t and G_r respectively are effective gains of transmitter and receiver antennas, G_f is the free space propagation gain and η_p is the polarization matching efficiency. The free space propagation gain can be written as

$$G_f(f,d) = \left(\frac{c}{4\pi df}\right)^2. \tag{5.2}$$

Figure 5.1(a) shows the block diagram of Equation (5.1). In Figure 5.1(a), $P_t^{e.i.r.p}$ is the effective isotropic radiation power from transmitter antenna toward $\mathbf{\Omega}_t$ direction and $P_r^{e.i.r.p}$ is the effective isotropic received power at receiver antenna.

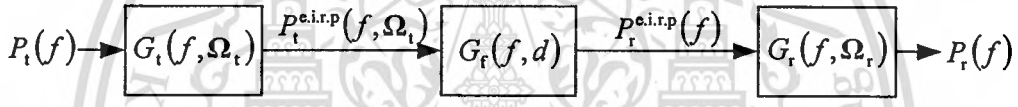

(a) Power representation in Equation (5.1)

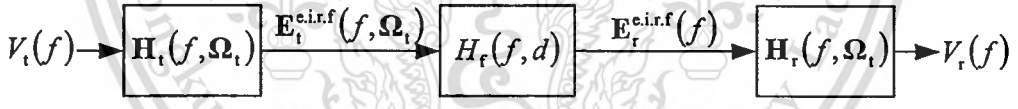

(b) Electric field representation in Equation (5.3)

Figure 5.1 Block diagram of Friis' transmission formula.

It is noted, however, that Equation (5.1) is satisfied only at some frequency, and is not directly applied to the UWB-IR transmission system. The formula shall be extended to take account the transmitted waveform, its distortion due to the antennas, the channel and the correlation receiver [14]-[15].

For UWB-IR systems, the free space link budget is formulated in the term of frequency transfer function that takes into account the transmitted waveform, its distortion due to the antennas, the channel and the correlation receiver. Free space channel transfer function H_c including the antennas is obtained by using the extension of Friis' transmission formula as [36]

$$H_c(f) = H_f(f,d)\mathbf{H}_t(f,\boldsymbol{\Omega}_t)\cdot\mathbf{H}_r(f,\boldsymbol{\Omega}_r), \tag{5.3}$$

where H_f is the free space channel transfer function and is defined in Equation (3.4), $\mathbf{H}_a$ ($a = t$ or r) is a complex transfer function vector of the antenna relative to the isotropic antenna towards the $\boldsymbol{\Omega}_a = (\theta_a, \varphi_a)$ direction, i.e.

$$\begin{aligned}\mathbf{H}_a(f,\boldsymbol{\Omega}_a) &= \mathbf{H}_a(f,\theta_a,\varphi_a)\\ &= \hat{\boldsymbol{\theta}}_a H_{a\theta}(f,\theta_a,\varphi_a) + \hat{\boldsymbol{\varphi}}_a H_{a\varphi}(f,\theta_a,\varphi_a),\end{aligned} \tag{5.4}$$

which has the relation as

$$\frac{1}{4\pi}\int_0^{2\pi}\int_0^{\pi}\left\|\mathbf{H}_a(f,\theta_a,\varphi_a)\right\|^2 \sin\theta \mathrm{d}\theta\mathrm{d}\varphi = \eta_a, \tag{5.5}$$

where η_a is the antenna efficiency, so the value is normalized by that for isotropic antenna.

It is noted that Equation (5.2) is often used in the free space link budget evaluation, although it is not correct in the electromagnetic theory [30]. The dependency of f is not really the propagation loss, but is due to the change of reception area of receiver antenna for the same gain. In other words, this is the compensation of the use of the relative gains of the antennas, i.e. $G_t(f,\boldsymbol{\Omega}_t) = G_r(f,\boldsymbol{\Omega}_r)$, when the same antennas are used as transmitter and receiver antennas.

Unit vectors $\hat{\boldsymbol{\theta}}_a$ and $\hat{\boldsymbol{\varphi}}_a$ express the polarizations and are defined with respect to the local polar coordinates of the antennas. The following relations can be easily derives as

$$\hat{\boldsymbol{\theta}}_t = \hat{\boldsymbol{\theta}}_r, \tag{5.6}$$

$$\hat{\boldsymbol{\varphi}}_t = -\hat{\boldsymbol{\varphi}}_r. \tag{5.7}$$

By introducing vector notation η_p in Equation (5.1), it is implicitly taken into account. For the identical transmitter and receiver antennas satisfying Equations (5.6) and (5.7), the complex transfer functions of transmitter and receiver antennas can be written as [36]

$$H_t(f) = H_r(f) = \sqrt{\frac{H_c(f)}{H_f(f,d)}}. \tag{5.8}$$

The factorization of channel transfer function H_c of Equation (5.3) and the complex transfer function of identical transmitter and receiver antennas of Equation (5.8) are mathematically corrected in the sense of identical transmitter and receiver antennas should have same gains. However, the factors H_t, H_f and H_r are not separated physically. In physical situation, H_t transfer the transmitting voltage (V) to the electric field (V/m) and H_r transfer the electric field (V/m) to received voltage (V). Physically, the factors H_t and H_r should have different units and forms.

Figure 5.1(b) shows the block diagram of Equation (5.3). In Figure 5.1(b), $\mathbf{E}_t^{e.i.r.f}$ is the effective isotropic radiated field vector from transmitter antenna toward $\boldsymbol{\Omega}_t$ direction and $\mathbf{E}_r^{e.i.r.f}$ is the effective isotropic received field vector of receiver antenna.

The received input waveform v_r is given by

$$v_r(t) = \int_{-\infty}^{\infty} H_c(f) V_t(f) e^{j2\pi ft} \mathrm{d}f. \tag{5.9}$$

5.2.2 Correlation Receiver

The block diagram of transmission model is shown in Figure 5.2. The output signal-to-noise ratio (SNR) is dependent of the choice of the template waveform. The correlator output v_o is therefore expressed as

$$v_o(\tau) = \int_{-\infty}^{\infty} v_r(t) h_w(t-\tau) \mathrm{d}\tau, \tag{5.10}$$

where h_w is the template waveform and τ corresponds to the timing of the template waveform. The optimum timing τ_o is chosen as

$$\tau_o = \arg\left[\max\left|v_o(\tau)\right|\right]. \tag{5.11}$$

Hereafter h_w is normalized as

$$\int_{-\infty}^{\infty} |h_w(t)|^2 \, dt = 2f_b. \tag{5.12}$$

Therefore, the output noise power is a constant as $N_0 f_b$, where $N_0/2$ is the power spectral density (PSD) of additive white Gaussian noise (AWGN).

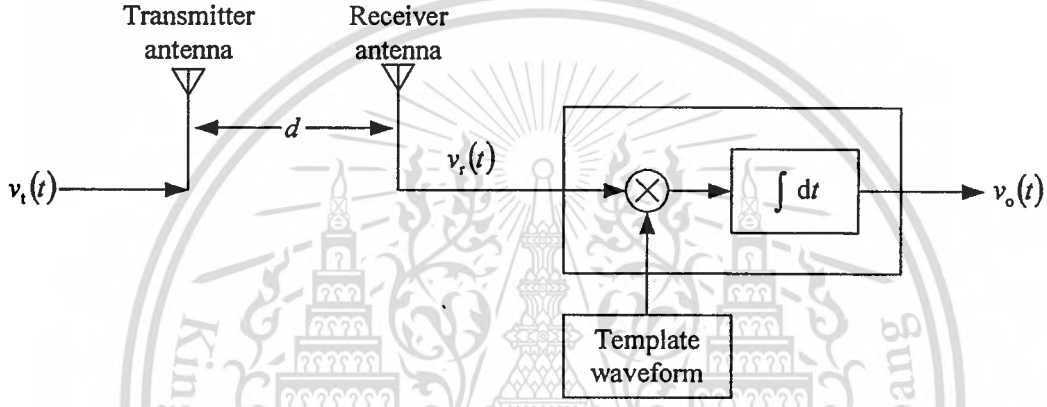

Figure 5.2 Block diagram of transmission model for UWB-IR signal.

Under the constraint of Equation (5.12), h_{wm} maximizes v_o when h_{wm} is a time-reversed and scaled version of v_r, i.e. [36]

$$h_{wm}(t) = \frac{\sqrt{2f_b}\, v_r(\tau_o - t)}{\sqrt{\int_{-\infty}^{\infty} |v_r(t)|^2 \, dt}}, \tag{5.13}$$

where τ_o is usually chosen so that $h_{wm} = 0$ for $t < 0$ to satisfy the causality. Hereafter, h_{wm} is called as the received signal template waveform. It is noted that the link budget evaluation is identical to that in [15] when h_{wm} is used as the received signal template waveform.

5.2.3 Feasibility of Optimum Correlation Receiver

It is obvious from Equation (5.13) that the received signal template waveform is not the simple time-reversed version of the transmitted waveform, but includes the frequency characteristics of the antennas and the free space propagation. Therefore, it is not always feasible to adapt the template waveform to the angular-dependent antenna characteristics, since the waveform shall be generated at the clock rate at least twice as high as the highest frequency of the signal. Therefore, a canonical template waveform h_{wc} is considered. In this section, h_{wc} is chosen that is optimum for the isotropic and the constant gain antennas, i.e. [36]

$$h_{wc}(t) = \frac{\sqrt{2f_b}\, v_{r\text{-}iso}(\tau_o - t)}{\sqrt{\int_{-\infty}^{\infty} | v_{r\text{-}iso}(t) |^2 \, dt}}, \tag{5.14}$$

where the receiver input voltage for the case of isotropic antennas used in both sides $v_{r\text{-}iso}$ can be written as

$$v_{r\text{-}iso}(t) = \int_{-\infty}^{\infty} H_f(f,d) V_t(f) e^{j2\pi ft} df. \tag{5.15}$$

5.2.4 Waveform Distortion

The waveform distortion is considered in the term of distortion between received waveform and received waveform for the case of isotropic antennas used in both sides and it can be written as [36]

$$W = 1 - \frac{\max \left| \int_{-\infty}^{\infty} v_r^*(t) v_{r-iso}(t+\tau) d\tau \right|}{\sqrt{\int_{-\infty}^{\infty} | v_r(t) |^2 dt \cdot \int_{-\infty}^{\infty} | v_{r\text{-}iso}(t) |^2 dt}}. \tag{5.16}$$

This quantity is equal to 0 when two waveforms are identical and it is increased when the waveform is more differ from another.

5.2.5 Transmission Gain

The transmission gain in this section is defined as the peak amplitude of the correlator output with the considered antennas normalized by that with the pair of isotropic antennas. Due to the normalization of template waveforms in Equations (5.13) and (5.14), this gain value represents the gain of SNR ratio. Therefore, the transmission gain of the received signal template case G_{wm} in dBi can be written as [36]

$$G_{wm} = 20\log\left[\frac{\max\left|\int_{-\infty}^{\infty} v_r(t)h_{wm}(t-\tau)\mathrm{d}t\right|}{\max\left|\int_{-\infty}^{\infty} v_{r\text{-iso}}(t)h_{wc}(t-\tau)\mathrm{d}t\right|}\right]. \tag{5.17}$$

Similarly, the transmission gain of the isotropic template case G_{wc} in dBi can be written as [36]

$$G_{wc} = 20\log\left[\frac{\max\left|\int_{-\infty}^{\infty} v_r(t)h_{wc}(t-\tau)\mathrm{d}t\right|}{\max\left|\int_{-\infty}^{\infty} v_{r\text{-iso}}(t)h_{wc}(t-\tau)\mathrm{d}t\right|}\right]. \tag{5.18}$$

The difference between the transmission gain of the received signal and the isotropic template cases also indicates the distortion quantity of the waveform. Different from the original Friis' transmission formula, the optimum transmission gain of UWB-IR signal cannot be simply expressed by the product of antenna indices.

5.3 Experimental Evaluation of Example UWB-IR Antenna Link

In this section, LOS link with the LPDA is evaluated based on the previous section.

5.3.1 Transmitted Waveforms

The effect of the waveform distortion is more obvious when the bandwidth is wider. The transmitted waveforms that fully cover Federal Communications Commission (FCC) frequency band, i.e., 3.1 to 10.6 GHz [5] and common frequency band available among the FCC of USA, European Telecommunications Standard Institute (ETSI) in Europe and Ministry of Internal Affairs and Communications (MIC) of Japan, i.e., 7.25 to 8.5 GHz [9] are considered.

In this section, the rectangular passband waveform is used as the transmitted waveform same as Chapters 2 and 3, but the waveform is in the simpler equation. The spectral density of rectangular passband waveform $V_{t,re}$ is defined as

$$V_{t,re}(f)=\begin{cases}1 & \| f|-f_c|\le \frac{f_b}{2}\\ 0 & \text{otherwise}\end{cases}. \quad (5.19)$$

For satisfying the FCC spectral masks for indoor and outdoor limits, the center frequency f_c and bandwidth f_b are set to 6.85 and 7.50 GHz, respectively. For satisfying the common frequency band spectral mask, the center frequency f_c and bandwidth f_b are set to 7.875 and 1.250 GHz respectively.

For analysis of waveform distortion, the root raised cosine passband waveform is used to compare with rectangular passband waveform. The spectral density of root raised cosine passband waveform $V_{t,ro}$ is defined as

$$V_{t,ro}(f)=\begin{cases}1 & \| f|-f_c|\le \frac{1-\alpha}{2T}\\ \sqrt{\frac{1}{2}\left[1+\cos\left(\frac{\pi T}{\alpha}\left[\| f|-f_c|-\frac{1-\alpha}{2T}\right]\right)\right]} & \frac{1-\alpha}{2T}<\| f|-f_c|\le \frac{1+\alpha}{2T}\\ 0 & \text{otherwise}\end{cases}, \quad (5.20)$$

where $T=1/f_b$ is the reciprocal of the symbol rate and $\alpha=0.3$ is the roll-off factor. For satisfying the FCC spectral mask, the center frequency f_c is set to 6.85 GHz. The bandwidths f_b are set to 6.37 and 5.94 GHz for satisfying FCC spectral masks for indoor and outdoor limits. For satisfying the common frequency band spectral mask, center frequency f_c and bandwidth f_b are set to 7.877 and 0.975 GHz, respectively.

5.3.2 Experimental Setup and Measurement Model

The UWB-IR radio channel transfer function was measured using vector network analyzer (VNA) in an anechoic chamber. Ports 1 and 2 of VNA were transmitter and receiver ports, respectively. Both transmitter and receiver antennas were fixed at the height of 1.75 m and separated by 3 m.

The experimental parameters are listed in Table 5.1. It is noted that the calibration of VNA is done at the connectors of the cables to be connected to the antennas. Therefore, all the impairments of the antenna characteristics are included in the measurement results. The experimental setup is shown in Figure 5.3.

Table 5.1 Experimental setup parameters

Parameter	Value
Frequency range	3 GHz to 11 GHz
Number of frequency points	1601
Dynamic range	80 dB
Transmitter antenna height	1.75 m
Receiver antenna height	1.75 m
Distance	3 m
Rotation range	0° to 360°
Rotation step	5°
Rotation cut	E-plane

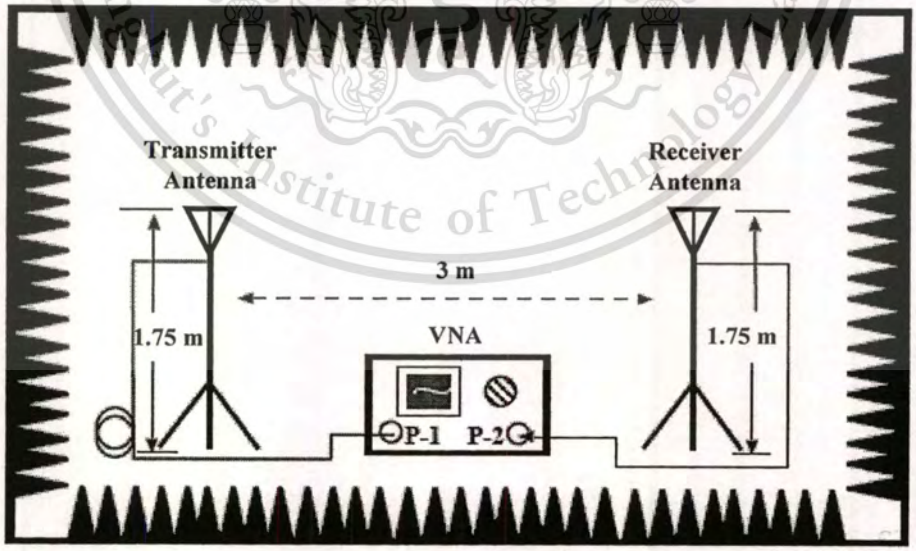

Figure 5.3 Experimental setup.

Experimental investigations are done for LPDA. A LPDA is also used at broadband with frequency-independent gain. The dispersion characteristic of the LPDA is rather big, since the phase center changes with frequency due to the resonance of the dipole elements [42]. A commercial LPDA, Watkins-Johnson's AR7-15A, is used and shown in Figure 5.4. The antenna has been designed to operate in the range of 1 to 12.4 GHz.

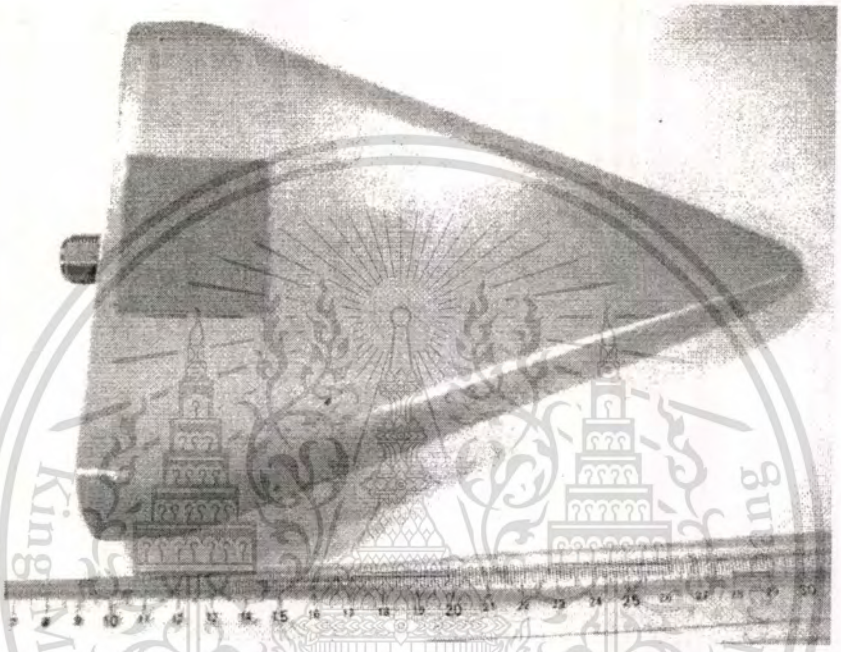

Figure 5.4 Log-periodic dipole antenna (Watkins-Johnson AR7-15A) [42].

5.3.3 Data Processing

The transmitted waveforms are simulated by using waveforms, $V_{t,re}$ and $V_{t,ro}$, defined in Section 5.3.1, channel frequency transfer function H_c measured in Section 5.3.2 and the correlation receivers presented in Sections 5.2.2 and 5.2.3. The received waveforms for the case of considered antennas used in the both sides v_r and received waveforms for the case of isotropic antennas used in both sides $v_{r\text{-}iso}$ are evaluated using Equations (5.9) and (5.15) to consider the received signal template waveform h_{wm} and isotropic template waveform h_{wc}. The output waveform of correlation receiver of each case is computed using Equation (5.10). The UWB-IR waveform distortion and transmission gain respectively defined in Sections 5.2.4 and 5.2.5 are evaluated.

5.4 Results

In this section, the example results of link budget evaluation with rectangular and root raised cosine passband waveforms satisfy FCC spectral masks for indoor and outdoor limits and common frequency band spectral mask are illustrated. The transmitted waveforms, received waveforms, waveform distortions and transmission gains for all case are shown in Appendix.

5.4.1 Transmitted Waveform

The normalized rectangular and root raised cosine passband waveforms satisfying the FCC spectral masks for indoor and outdoor limits are shown in Figures 5.5. Figure 5.6 shows the normalized rectangular and root raised cosine passband waveforms satisfying the common frequency band spectral mask. From the results, the correlation coefficients between rectangular and root raised cosine passband waveforms are 0.98, 0.96 and 0.96 for FCC indoor, FCC outdoor and common frequency band spectral masks, respectively. This means that the rectangular passband waveform, which is ideal signal and simple formula, are almost same as root raised cosine passband waveform, which is causal signal and complex formula.

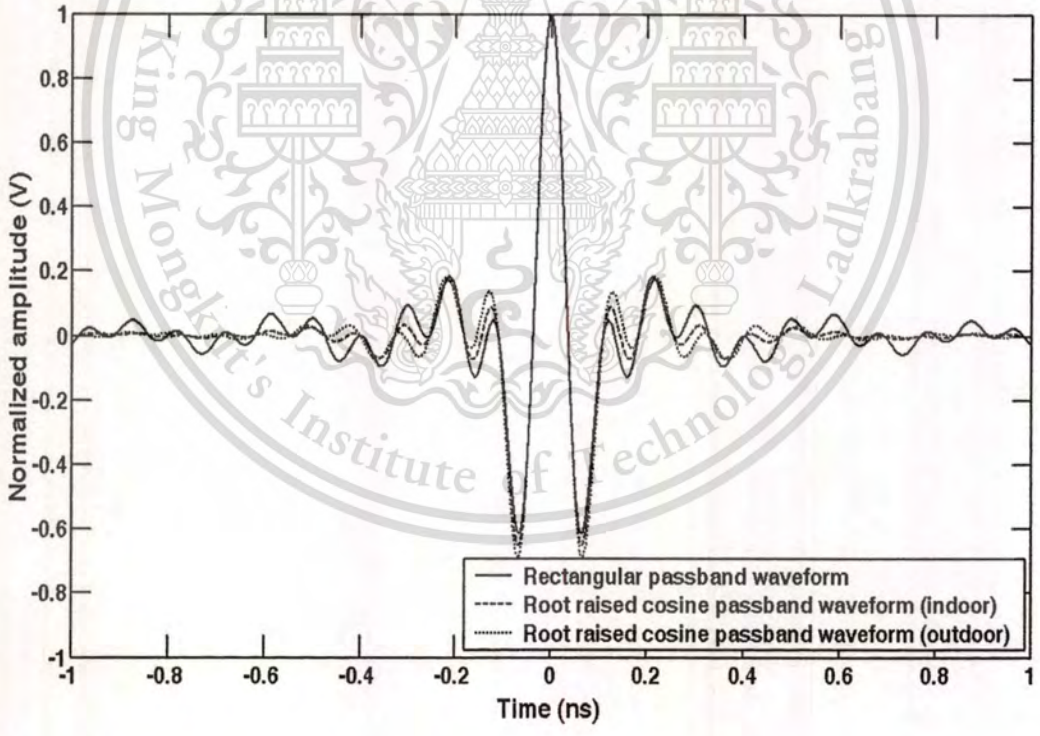

Figure 5.5 Normalized rectangular and root raised cosine passband waveforms satisfying FCC spectral masks for indoor and outdoor limits.

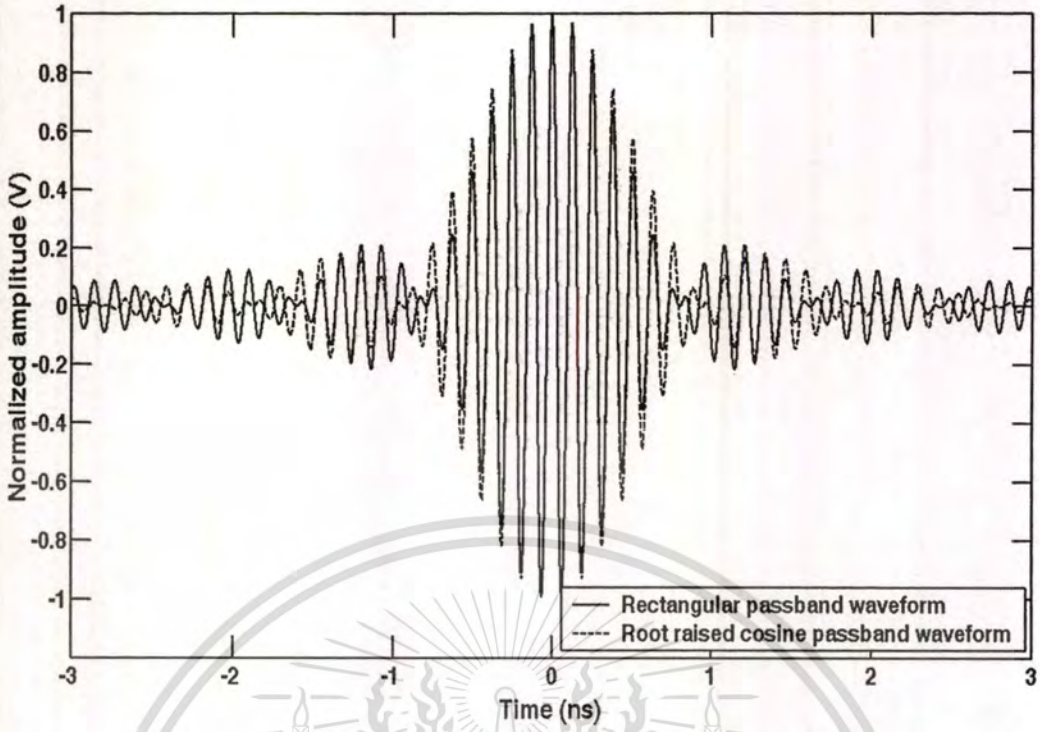

Figure 5.6 Normalized rectangular and root raised cosine passband waveforms satisfying common frequency band spectral mask.

5.4.2 Waveform Distortion

In this section, waveform distortion is evaluated using Equation (5.16) and shown. In other words, it is the comparison between received waveform with considered antennas at both sides and received waveform with isotropic antenna at both sides. Therefore, this quantity reflects the waveform distortion due to considered antennas.

The waveform distortion of rectangular and root raised cosine passband waveforms satisfying the FCC spectral masks for indoor and outdoor limits is shown in Figure 5.7. Figure 5.8 shows the waveform distortion of rectangular and root raised cosine passband waveforms satisfying the common frequency band spectral mask. The waveform distortion of rectangular passband waveform is almost same as that of root raised cosine passband waveform. The root mean square (RMS) difference between rectangular and root raised cosine passband waveform are only 0.03, 0.04 and 0.02 for FCC indoor, FCC outdoor and common frequency band spectral masks, respectively. This confirms that the rectangular passband waveform can be used instead of root raised cosine passband waveform to evaluate link budget for UWB-IR systems. Hereafter, only results from rectangular passband waveforms are discussed.

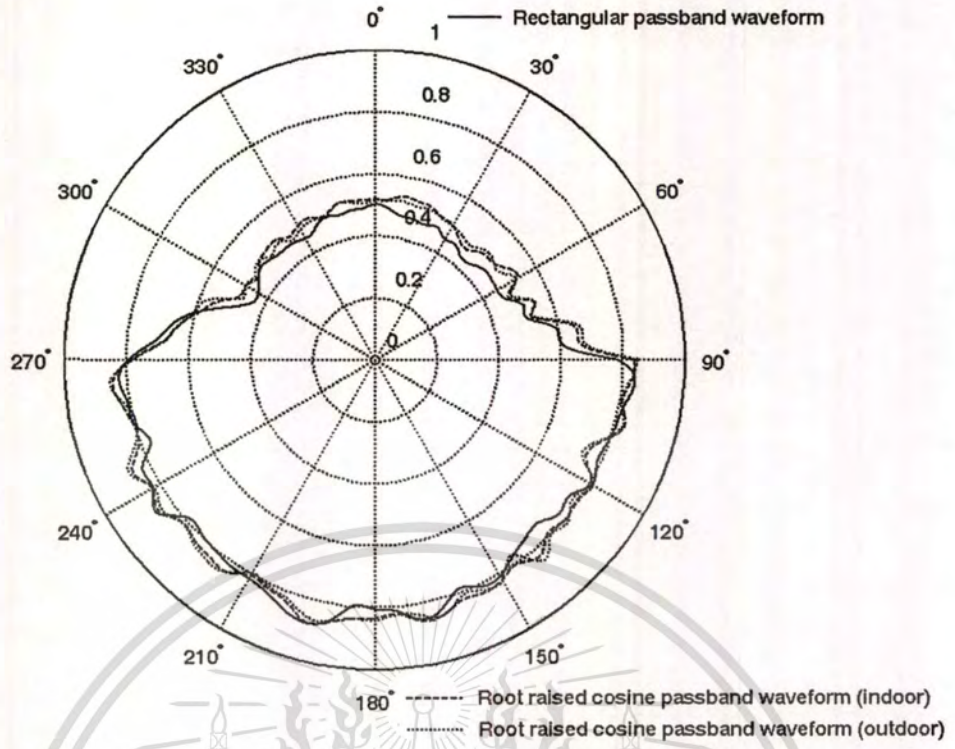

Figure 5.7 Waveform distortion of rectangular and root raised cosine passband waveforms satisfying FCC spectral masks for indoor and outdoor limits.

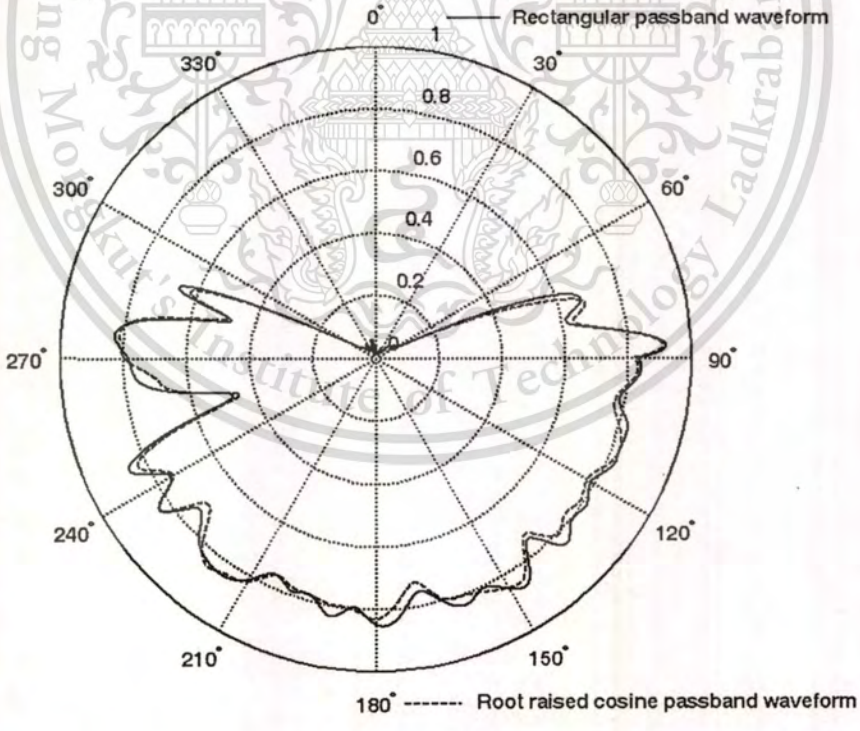

Figure 5.8 Waveform distortion of rectangular and root raised cosine passband waveforms satisfying common frequency band spectral mask.

The waveform distortion of LPDA-LPDA link is shown in Figure 5.9. Averagely, the waveform distortion of waveform satisfying FCC spectral mask is more than that satisfying common frequency band spectral mask, especially at 0° pointing angle. The values of waveform distortion of waveform satisfying FCC and common frequency band at 0° pointing angle are 0.50 and 0.04, respectively.

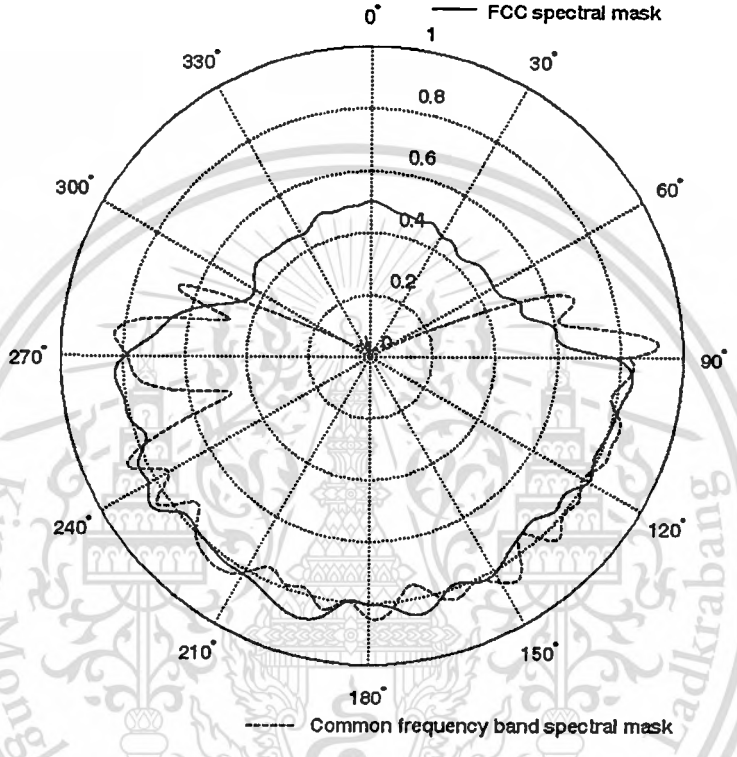

Figure 5.9 Waveform distortion of LPDA-LPDA link.

5.4.3 Transmission Gain

In this section, transmission gains of correlation receivers for both received signal and isotropic templates are considered. For correlation receiver with received signal template, the transmission gain is evaluated using Equation (5.17). This transmission gain reflects the maximum gain case of LPDA-LPDA link. The transmission gain of correlation receivers with isotropic template is evaluated using Equation (5.18). This transmission gain reflects the maximum gain case of isotropic antenna link. Therefore, the difference between transmission gains with received signal and isotropic templates can be used to consider the distortion caused from LPDA compare with isotropic antenna, which is ideal distortionless antenna.

Figures 5.10 and 5.11 show the transmission gains of waveforms satisfying FCC and common frequency band spectral masks, respectively. The difference between transmission gains of waveform satisfying FCC spectral mask is clearly more than that satisfying common frequency band spectral mask. The average difference of transmissions gains of waveform satisfying FCC and common frequency band spectral masks are 3.32 and 0.20 dB, respectively. This concludes that the waveform satisfying FCC spectral mask has more distortion than that satisfying common frequency band spectral mask. The waveform satisfying FCC spectral mask has significant distortion with waveform distortion of 0.50 and difference between transmission gains of 6.05 dB at 0° pointing angle. On the other hand, the waveform satisfying common frequency band spectral mask has low distortion with waveform distortion of 0.04 and difference between transmission gains of 0.32 dB at 0° pointing angle. This is because the frequency ranging from 3.1 to 10.6 GHz of FCC spectral mask is much wider than frequency ranging from 7.25 to 8.5 GHz of common frequency band spectral mask. In addition, the trend of frequency dispersion in FCC spectral mask is higher.

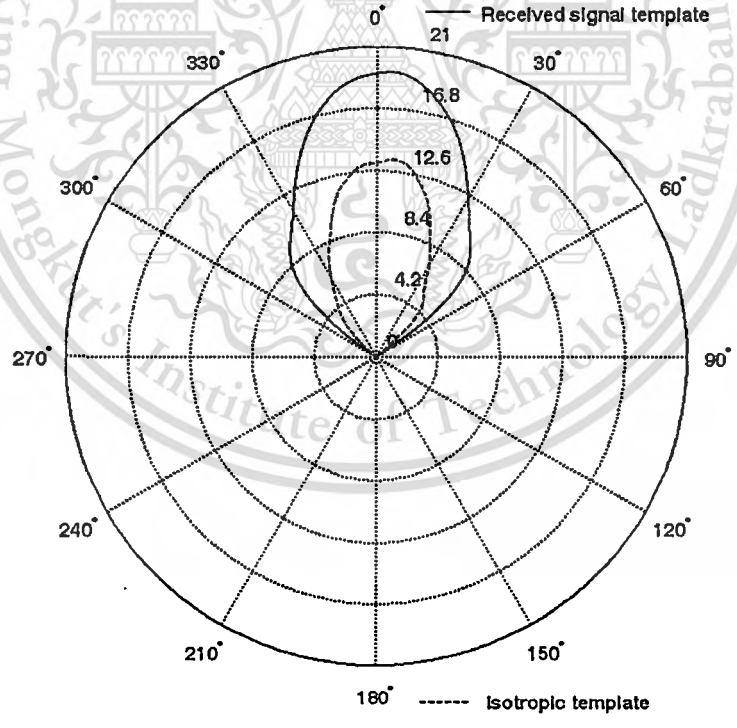

Figure 5.10 Transmission gain of LPDA-LPDA link for FCC spectral mask.

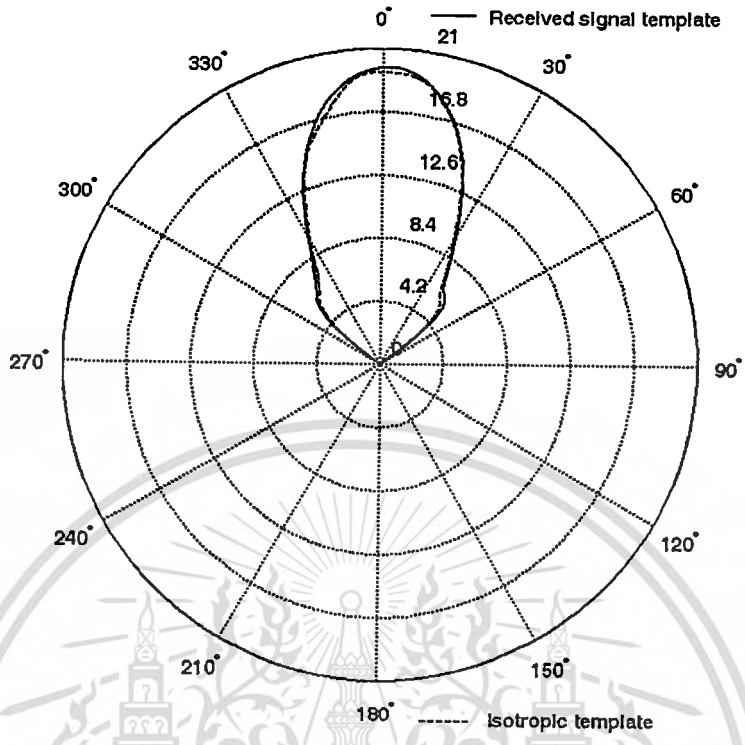

Figure 5.11 Transmission gain of LPDA-LPDA link for common frequency band spectral mask.

5.5 Conclusion

In this chapter, link budget model for studying the waveform distortion due to antenna on free space transmission is discussed. The rectangular and root raised cosine passband waveforms are considered as transmitted waveform. For the receiver, the correlation receivers with received signal and isotropic templates are investigated. Experimental investigations are done for LPDA link. The results of rectangular passband waveform, which is the ideal signal and easier analysis, are almost the same as that of root raised cosine passband waveform, which is the causal signal. Therefore, the rectangular passband waveform can be used as UWB-IR transmitted signal. Averagely, the waveform distortion and difference between transmission gains of waveform satisfying FCC spectral mask is more that that satisfying common frequency band spectral mask, especially at 0° pointing angle. This is because the bandwidth of FCC frequency band is much wider than that of common frequency band. The trend of frequency dispersion is higher.

CHAPTER 6
CONCLUSION AND FUTURE WORKS

6.1 Summary of Proceeding Chapters

This thesis presents a mathematical model of free space and ground reflection channels and evaluation of link budget for ultra wideband impulse radio (UWB-IR) systems. The closed form formulas and experimental link budget scheme are proposed.

Chapter 2 describes the basic principle of UWB-IR system. The advantages, definition and regulation of UWB-IR signal and standards of UWB-IR systems are presented.

Chapter 3 proposes the mathematical model of free space channel. The novel method of derivation is proposed. The path losses based on average and peak power losses, peak to average loss ratio and correlation coefficient are derived in the close form formulas. The free space path losses based on average and peak power losses are almost the same at narrow bandwidth and have more difference when bandwidth is wider. The peak to average loss ratio is higher when bandwidth is increased. On the other hand, the correlation coefficient is lower when bandwidth is increased. These results mean there is more waveform distortion when the bandwidth is wider, due to frequency dependence of Friis' transmission formula. These proposed closed form formulas are useful to study the path loss along different bandwidth of UWB-IR signal and define the quantity of UWB-IR waveform distortion in free space channel.

Chapter 4 proposes the mathematical model of ground reflection channel. The novel method of derivation is proposed. The path losses based on average and peak power losses, peak to average loss ratio and correlation coefficient are derived in the close form formulas. The measurement was done to verify the proposed ground reflection model. The results reflect that the wider bandwidth has lower effect of multi-path fading. Although the frequency dispersion of wider bandwidth is more than that of narrower bandwidth, the effect of multi-path fading on waveform distortion is more significant than that of frequency dispersion. Therefore, the waveform distortion is reduced when bandwidth is wider. All of proposed formulas, path loss based on average and peak power loss, peak to average loss ratio, correlation coefficient, correspond very well with measurement. Therefore, the proposed model is accurate and can be a choice for modeling the ground reflection channel.

Chapter 5 discusses experimental link budget evaluation scheme for UWB-IR systems. The more generalized link budget model for studying the waveform distortion due to antenna on free space transmission is discussed. The free space link budget evaluation scheme in the term of frequency transfer function that takes into account the transmitted waveform, its distortion due to the antennas, the channel and the correlation receiver is developed. The rectangular and root raised cosine passband waveforms are used as the transmitted waveform. The waveform satisfying FCC spectral masks for indoor and outdoor limits and common frequency band spectral mask are considered. The correlation receivers with received signal and isotropic templates are used. Experimental investigations are done for log-periodic dipole antenna (LPDA). The distortion quantities in the term of waveform distortion and transmission gain are defined and shown.

The results of rectangular passband waveform, which is the ideal signal and easier analysis, are almost the same as that of root raised cosine waveform, which is the causal signal. Therefore, the rectangular passband waveform can be used as UWB-IR transmitted signal. Averagely, the waveform distortion and difference between transmission gains of waveform satisfying FCC spectral mask is more than that satisfying common frequency band spectral mask, especially at 0° pointing angle. This is because the bandwidth of FCC frequency band is much wider than that of common frequency band. The trend of frequency dispersion is higher.

From these results, the UWB-IR transmission gain, using both received signal and isotropic template waveforms, gives the quantitative measurement of link budget. Sine the broadband antennas are chosen, the trend of the narrowband gain is reflected in the UWB-IR transmission gain. Another issue is the distortion due to the antennas. It is obvious that although LPDA has higher transmission gain, the distortion due to the LPDA is high. This scheme may be effective especially to evaluated the deployable antenna with non-ideal frequency characteristics of return loss and directivity, as the overall performances can be evaluate only by the term of UWB-IR transmission gain.

6.2 Recommendation for Future Works

This proposed free space and ground reflection models can be used as UWB-IR channel to analyze the performances of UWB-IR systems. Moreover, the same method of derivation can be extended to model the multi-path fading channel.

This proposed experimental link budget evaluation scheme can be easily extended to the multi-path environment as well. There are two key issues: one is the focus of this paper, i.e. the antenna transfer function is angular-dependent. The

other one is that the propagation channel is also angular dependent at both transmitter and receiver antennas. In the context of UWB-IR systems, just a few studies have been done with respect to the fist aspect, and almost none for the second. Although both antenna and multi-path channels are treated in [28], it only considered the impulse response of the whole channel. However, the impulse response itself is influenced by the antennas, the formulation for multi-path environment is not sufficient. The double-directional modeling of UWB-IR channel is studied in [40]-[41]. Due to this background, the multi-path environment can be treaded using this approach. The use of rake receiver may solve the antenna distortion and delay spread of propagation environment simultaneously.

REFERENCES

[1] K. Siwiak, "Ultra-Wide Band Radio: Introducing A New Technology," **2001 Spring IEEE Vehicular Technology Conference (VTC)**, vol. 2, pp. 1088-1093, May 2001.

[2] K. Siwiak, "Ultra-Wide Band Radio: The Emergence of An Important RF Technology," **2001 Spring IEEE Vehicular Technology Conference (VTC)**, vol. 2, pp. 1169-1172, May 2001.

[3] K. Siwiak, "Impact of Ultra Wide Band Transmissions on A Generic Receiver," **2001 Spring IEEE Vehicular Technology Conference (VTC)**, vol. 2, pp. 1181-1183, May 2001.

[4] I. Oppermann, M. Hamalainen and J. Iinatti, **UWB Theory and Applications**, John Wiley & Sons, Ltd., 2004.

[5] Federal Communications Commission, "Revision of Part 15 of The Commission's Rule Regarding UWB Transmission Systems," **First Report**, FCC 02-48, Apr. 2002.

[6] ETSI, "Harmonised Standards Covering Ultrawide Band (UWB) Applications," **Standisation Mandate: DG ENTR/G/3M/329**, Brussels, Feb. 2003.

[7] ETSI, "ECC Decision of 24 March 2006 on The Harmonised Conditions for Devices Using Ultra-Wideband (UWB) Technology in Bands below 10.6 GHz," **Doc. ECC/DEC/(06)04**, Mar. 2006.

[8] MIC, "Japan's UWB Emission Policy Advances," **EE Times**, Washington, 26 Aug. 2005.

[9] W. Hirt and M. Weisenhorn, "Overview and Implications of The Emerging Global UWB Radio Regulatory Frameworks," **2006 IEEE International Conference on Ultra-Wideband**, pp. 581-586, Sept. 2006.

[10] M. P. Wylie-Green, P. A. Ranta and J. Salokannel, "Multi-Band of OFDM UWB Solution for IEEE 802.15.3a WPANs," **Sarnoff Symposium on 2005 IEEE Advances in Wired and Wireless Communication**, pp. 102-105, 2005.

[11] L. D. Nardis and M. D. Benedetto, "Overview of The IEEE 802.15.4/4a Standards for Low Data Rate Wireless Personal Data Networks," **4th Workshop on Positioning, Navigation and Communication (WPNC)**, pp. 285-289, 2007.

[12] K. S. Kwak, S. Ullah and N. Ullah, "An Overview of IEEE 802.15.6 Standard," **2010 3rd International Symposium on Applied Sciences in Biomedical and Communication Technologies (ISABEL)**, pp. 1-6, 2010.

[13] Friis, H. T., "A Note on A Simple Transmission Formula," **Proceedings of IRE**, vol. 34, no. 5, pp. 254-256, May 1946.

[14] J. Takada, S. Promwong and W. Hachitani, "Extension of Friis' Transmission Formula for UWB Systems," **Technical Report of IEICE**, WBS2003-8/MW2003-20, May 2003.

[15] S. Promwong and J. Takada, "Free Space Link Budget Estimation Scheme for Ultra Wideband Impulse Radio with Imperfect Antennas," **IEICE Electronics Express**, vol. 1, no. 7, pp. 182-192, July 2004.

[16] J. Foerster, "Channel Modeling Sub-Committee Report Final," **IEEE P802.15.02/368r5-SG3a**, Nov. 2002.

[17] S. Promwong, J. Takada, P. Supanakoon and P. Tangtisanon, "Path Loss and Matched Filter Gain for UWB system," **International Symposium on Antenna and Propagation (ISAP)**, pp. 97-100, Aug. 2004.

[18] P. Supanakoon, S. Aroonpraparat, S. Promwong and J. Takada, "Free Space Path Loss of UWB Communications," **International Workshop on UWB Technologies (IWUWBT)**, pp. 134-138, 8-10 Dec. 2005.

[19] K. Siwiak, H. Bertoni and S. M. Yano, "Relation between Multipath and Wave Propagation attenuation," **Electronics Letters**, vol. 39, pp. 142-143, Jan. 2003.

[20] S. Sato and T. Kobayashi, "Path-Loss Exponents of Ultra Wideband Signals in Line-of-Sight Environments," **2004 IEEE Eighth International Symposium on Spread Spectrum Techniques and Applications**, pp. 488-492, Jan.-Sept. 2004.

[21] P. Supanakoon, S. Tanchotikul, S. Promwong and J. Takada, "Ground Reflection Path Loss Considering Waveform Polarization and Ground Characteristic for UWB Communication," **ECTI International Conference (ECTI-CON)**, pp. 630-633, May 2005.

[22] P. Supanakoon, A. Pokang, S. Promwong, S. Noppanakeepong and J. Takada, "Regression Models of Ultra Wideband Ground Reflection Path Loss Based on Peak Power Loss," **Asia-Pacific Conference on Communications (APCC)**, pp. 15-18, Oct. 2007.

[23] P. Supanakoon, S. Kaewsirisin, S. Promwong, S. Noppanakeepong and J. Takada, "Ground Reflection Path Loss Based on Average Power Loss for Ultra Wideband Communications," **Asia-Pacific Microwave Conference (APMC)**, vol. 4, pp. 2413-2416, Dec. 2007.

[24] H. F. Harmuth, **Antennas and Waveguides for Nonsinusoidal Waves**, Academic Press, Orlando, 1984.

[25] A. O. Boryessenko and D. H. Schaubert, "Antenna Link Transfer Function Factorization Applied to Optimized Channel Design," **IEEE Transactions on Antennas and Propagation**, vol. 54, no. 10, pp. 2878-2889, Oct. 2006.

[26] D. Lamensdorf and L. Susman, "Baseband-Pulse-Antenna Techniques," **IEEE Antennas and Propagation Magazine**, vol. 36, no. 1, pp. 20-30, Feb. 1994.

[27] A. H. Mohammadian, A. Rajkotia and S. S. Soliman, "Characterization of UWB Transmit-Receive Antenna System," **2003 IEEE Conference on Ultra Wideband system and Technologies (UWBST)**, pp. 157-161, Nov. 2003.

[28] A. Sibille, "A Framework for Analysis of Antenna Effect in UWB Communications," **2005 IEEE 61st Vehicular Technology Conference (VTC)**, vol. 1, pp. 48-52, June 2005.

[29] W. Sorgel and W. Wiesbeck, "Influence of The Antennas on The Ultra-Wideband Transmission," **EURASIP Journal on Applied Signal Processing**, pp. 296-305, 2005.

[30] J. Kunisch, "Implications of Lorentz Reciprocity for Ultra-Wideband Antennas," **2007 IEEE International Conference on Ultra-Wideband (ICUWB)**, pp. 214-219, Sept. 2007.

[31] Z. N. Chen, X. H. Wu, H. F. Li, N. Yang and M. Y. W. Chia, "Considerations for Source Pulses and Antennas in UWB Radio Systems," **IEEE Transactions on Antennas and Propagation**, vol. 52, no. 7, pp. 1739-1748, July 2004.

[32] Y. Duroc, A. Ghiotto, T. P. Vuong and S. Tedjini, "UWB Antenna: Systems with Transfer Function and Impulse Response," **IEEE Transactions on Antennas and Propagation**, vol. 55, no. 5, pp. 1449-1451, May 2007.

[33] P. Supanakoon, K. Wansiang, S. Promwong and J. Takada, "Simple Waveforms for UWB Communication," **ECTI International Conference (ETCI-CON)**, pp. 626-629, May 2005.

[34] P. Supanakoon, S. Promwong and J. Takada, "Novel Waveform Distortion Parameter for Ultra Wideband Impulse Radio Systems," **2011 International Symposium on Antennas and Propagation (ISAP)**, ThG3-4, 25-28 Oct. 2011.

[35] P. Supanakoon, S. Promwong and J. Takada, "Closed Form Formulas of Correlation Coefficient for Ultra Wideband Impulse Radio Systems," **2011 International Symposium on Antennas and Propagation (ISAP)**, ThG3-5, 25-28 Oct. 2011.

[36] S. Promwong, P. Supanakoon and J. Takada, "Waveform Distortion and Transmission Gain on Ultra Wideband Impulse Radio," **IEICE Transactions on Communications**, vol. E93-B, no. 10, Oct. 2010.

[37] T. S. Rappaport, **Wireless Communications: Principle and Practice**, Prentice Hall, 2002.

[38] S. Promwong, P. Supanakoon and J. Takada, "Ground Reflection Transmission Loss Evaluation Scheme for Ultra Wideband Impulse Radio," **ECTI-EEC Transaction on Electrical Engineering, Electronics, and Communications,** vol. 5, no. 1, pp. 18-24, Jan. 2007.

[39] S. Promwong, W. Hachitani and J. Takada, "Free Space Link Budget Evaluation of UWB-IR Systems," **2004 International Workshop on Ultra Wideband System Joint with Conference on Ultra Wideband Systems and Technologies (UWBST & IWUWBS)**, pp. 312-316, May 2004.

[40] J. Takada, K. Haneda and H. Tsuchiya, "Joint DOA/DOD/DTOA Estimation System for UWB Double Directional Channel Modeling," in ed. S. Changran, **Advance in Direction of Arrival Estimation**, pp. 345-362, Artech House, MA, USA, 2006.

[41] K. Haneda, J. Takada and T. Kobayashi, "Double Directional Ultra Wideband Channel Characterization in a Line-of-Sight Home Environment," **IEICE Transactions on Fundamentals**, vol. E88-A, no. 9, pp. 2264-2271, Sept. 2005.

[42] H. G. Schantz, "Dispersion and UWB Antennas," **2004 International Workshop on Ultra Wideband System Joint with Conference on Ultra Wideband Systems and Technologies (UWBST & IWUWBS)**, pp. 161-164, May 2004.

APPENDIX

A.1 Transmitted Waveforms

The normalized rectangular passband waveform and normalized spectral density satisfying the FCC spectral masks for indoor and outdoor limits are shown in Figures A.1 and A.2, respectively. The normalized rectangular passband waveform and normalized spectral density satisfying the common frequency band spectral mask are shown in Figures A.3 and A.4, respectively.

The normalized root raised cosine passband waveform and normalized spectral density satisfying the FCC spectral mask for indoor limit are shown in Figures A.5 and A.6, respectively. Figures A.7 and A.8 show the normalized root raised cosine passband waveform and normalized spectral density satisfying the FCC spectral mask for outdoor limit, respectively. The normalized root raised cosine passband waveform and normalized spectral density satisfying the common frequency band spectral mask are shown in Figures A.9 and A.10, respectively.

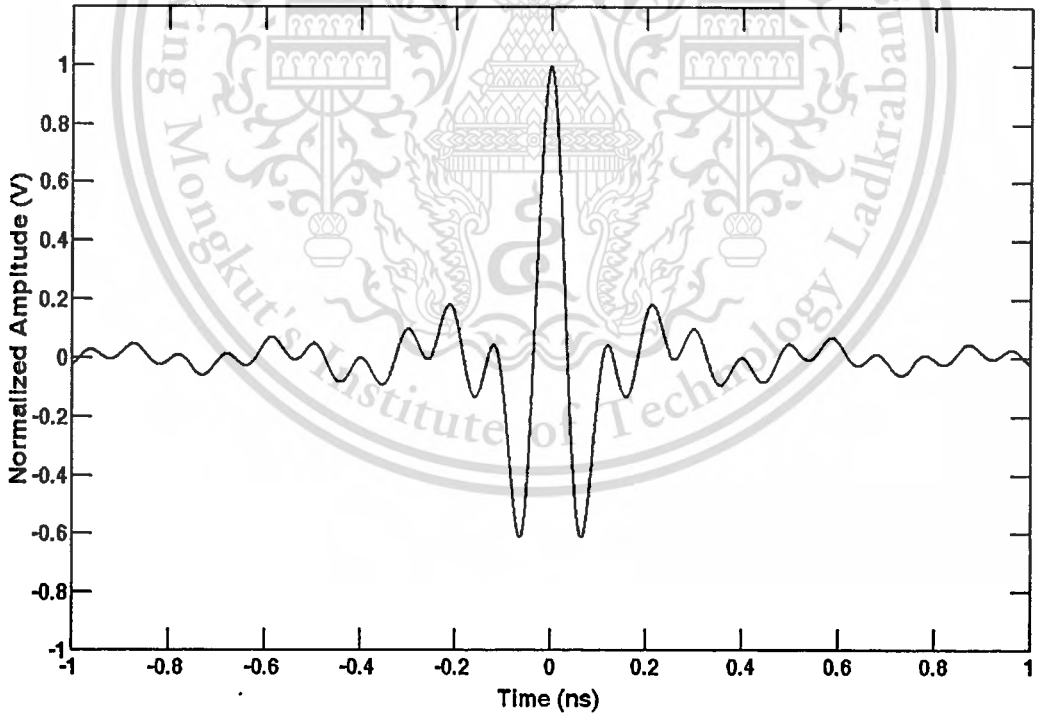

Figure A.1 Normalized rectangular passband waveform satisfying FCC spectral masks for indoor and outdoor limits.

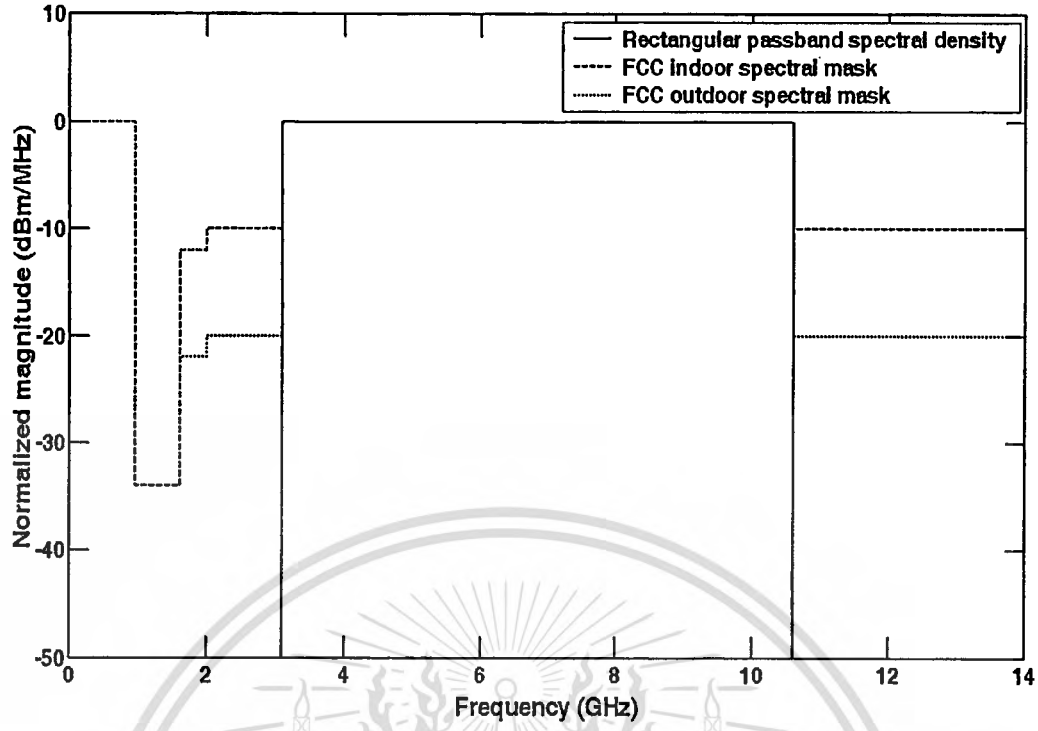

Figure A.2 Normalized magnitude power density of rectangular passband waveform satisfying FCC spectral masks for indoor and outdoor limits.

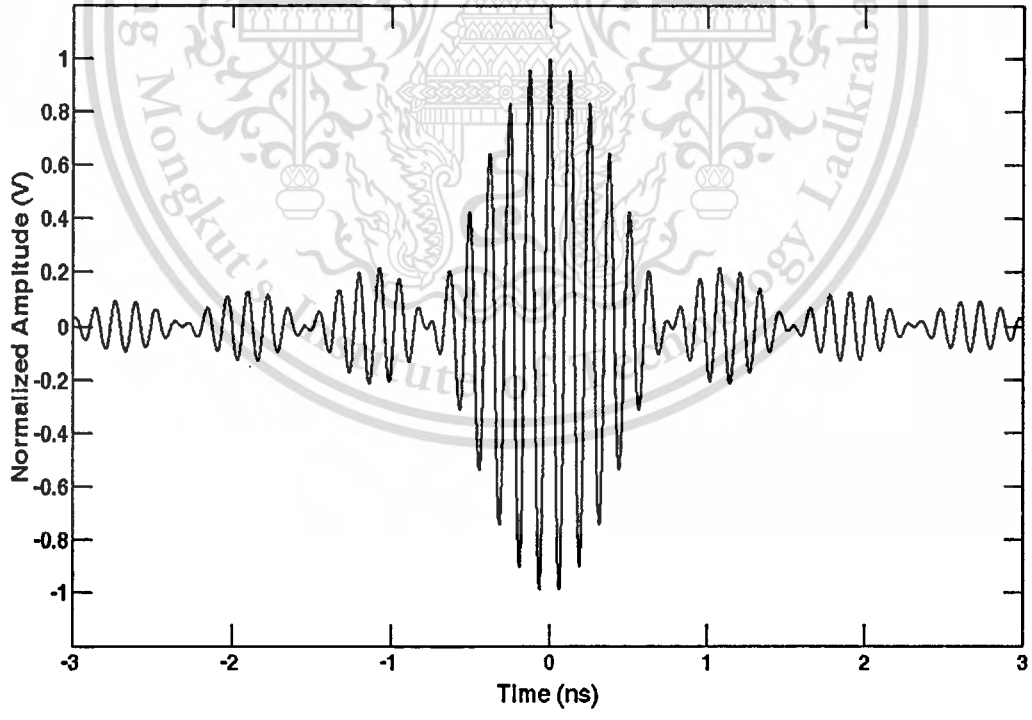

Figure A.3 Normalized rectangular passband waveform satisfying common frequency band spectral mask.

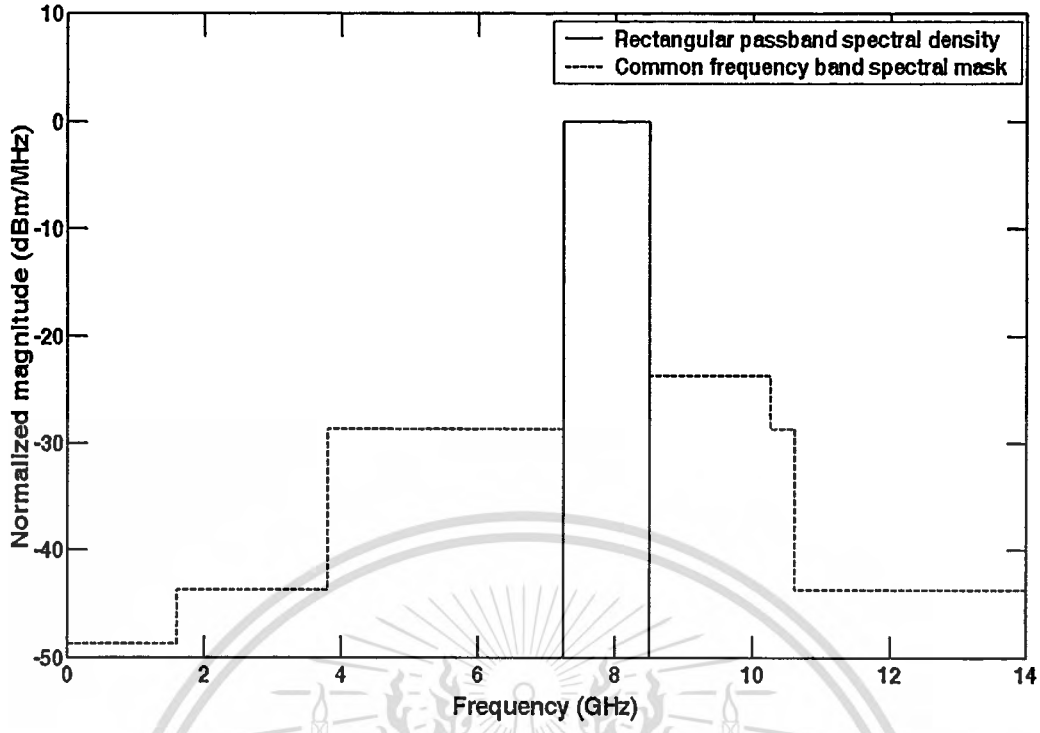

Figure A.4 Normalized magnitude power density of rectangular passband waveform satisfying common frequency band spectral mask.

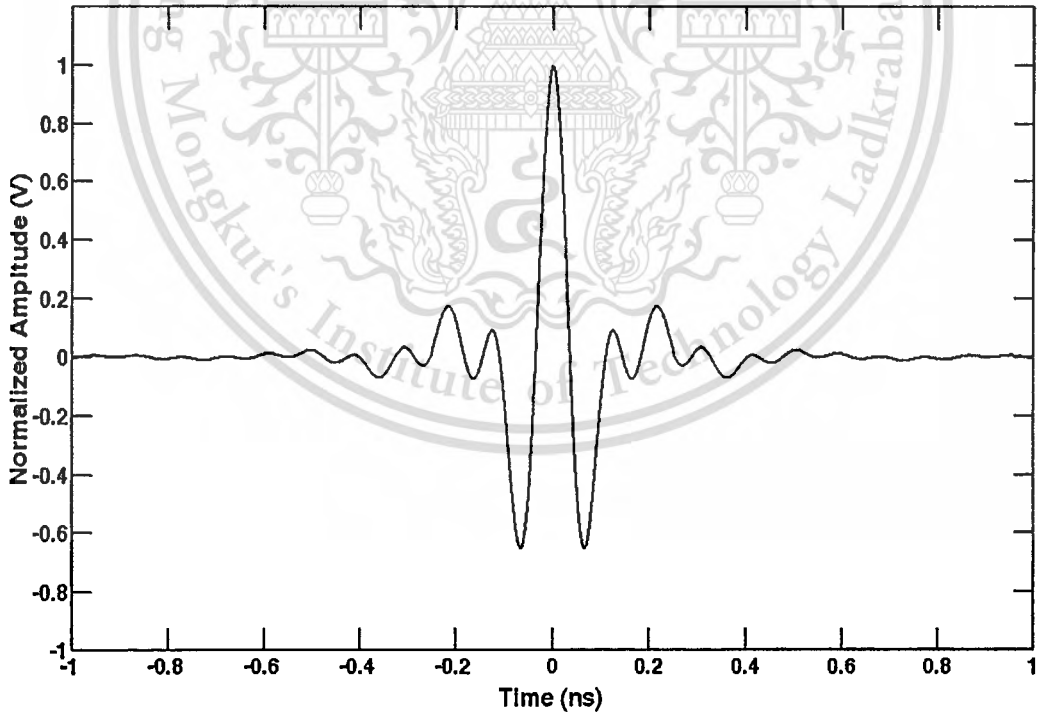

Figure A.5 Normalized root raised cosine passband waveform satisfying FCC spectral mask for indoor limit.

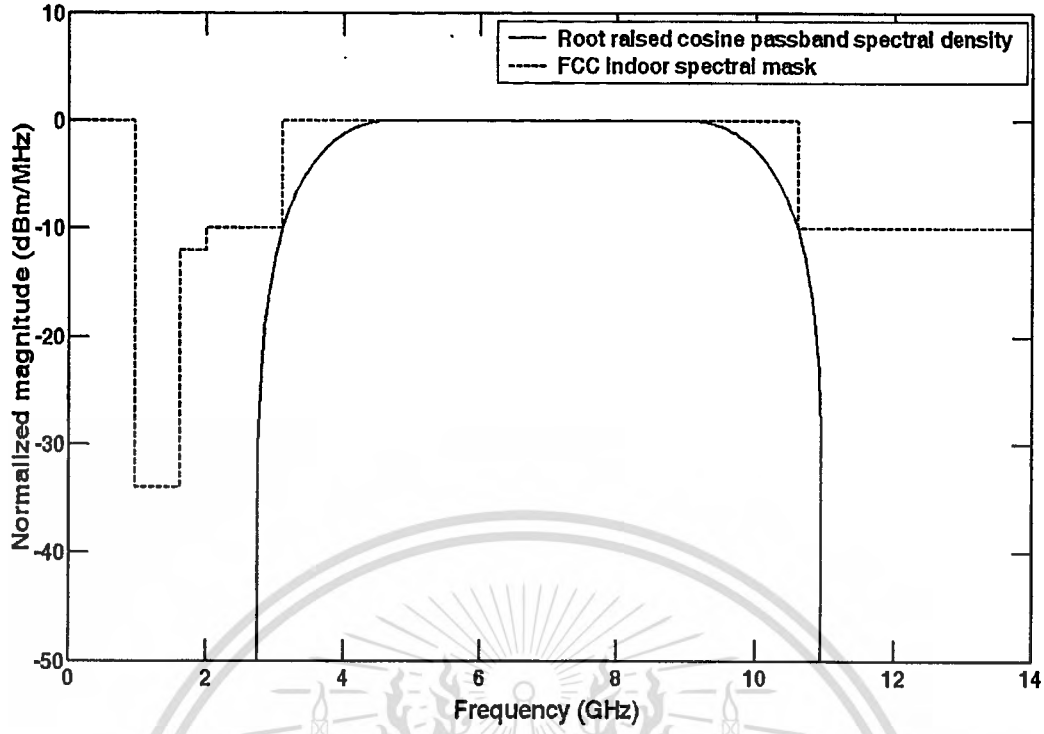

Figure A.6 Normalized magnitude power density of root raised cosine passband waveform satisfying FCC spectral mask for indoor limit.

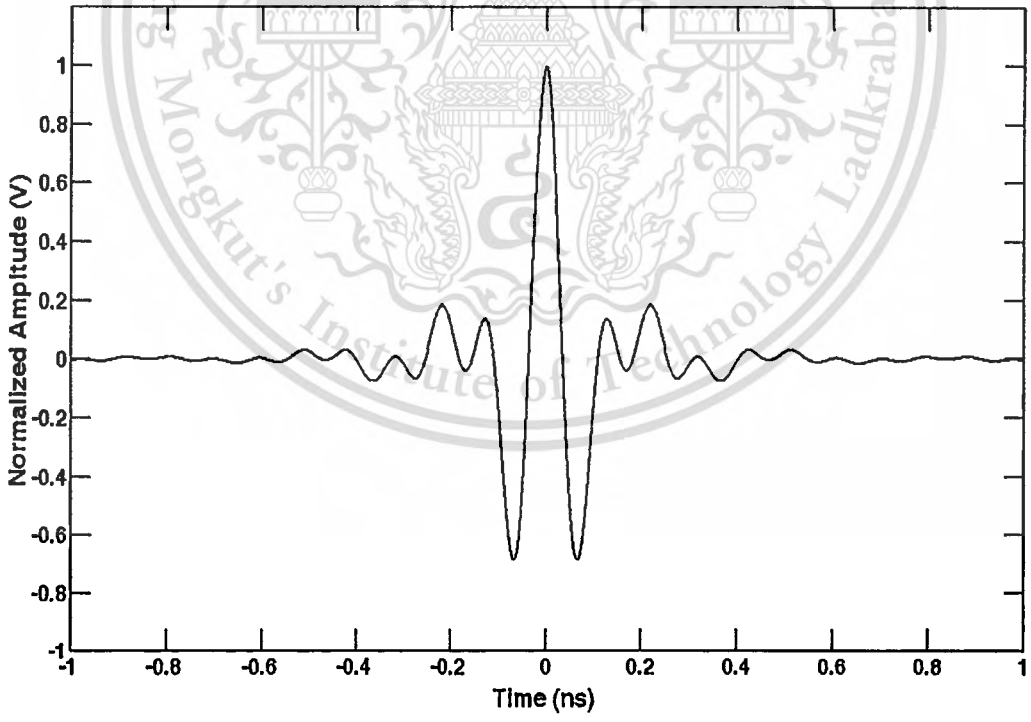

Figure A.7 Normalized root raised cosine passband waveform satisfying FCC spectral mask for outdoor limit.

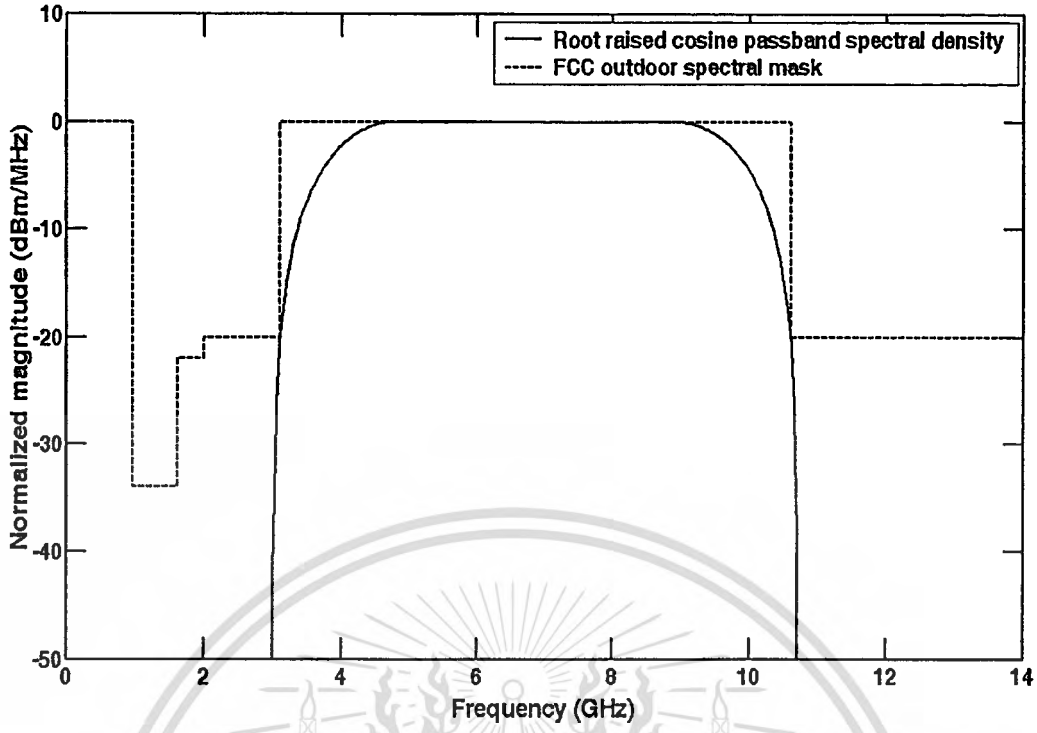

Figure A.8 Normalized magnitude power density of root raised cosine passband waveform satisfying FCC spectral mask for outdoor limit.

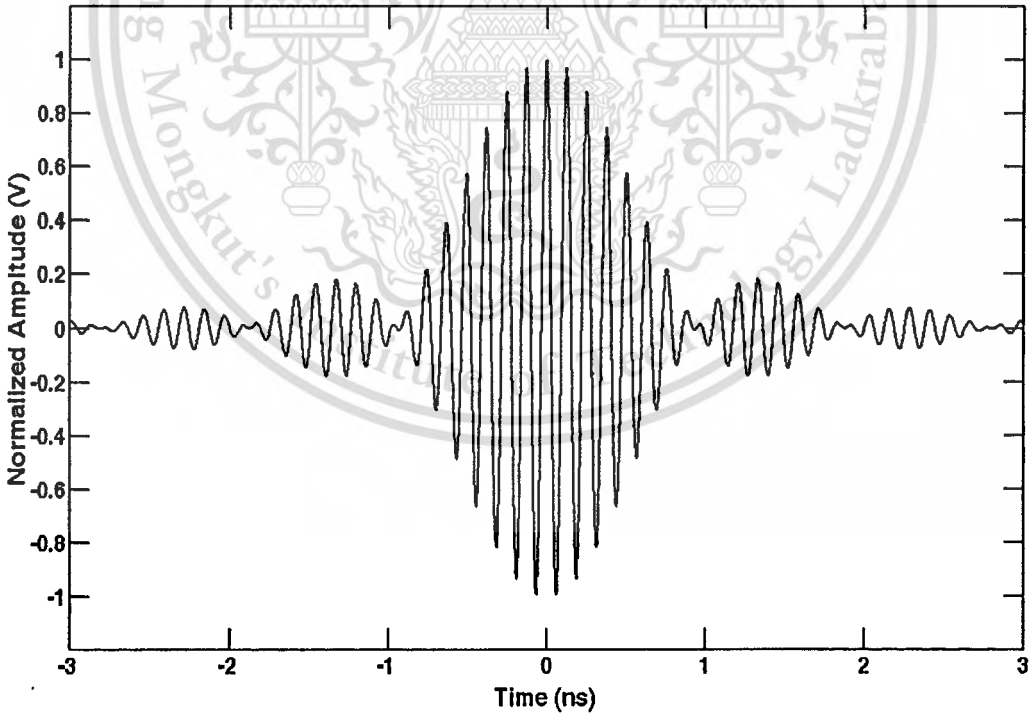

Figure A.9 Normalized root raised cosine passband waveform satisfying common frequency band spectral mask.

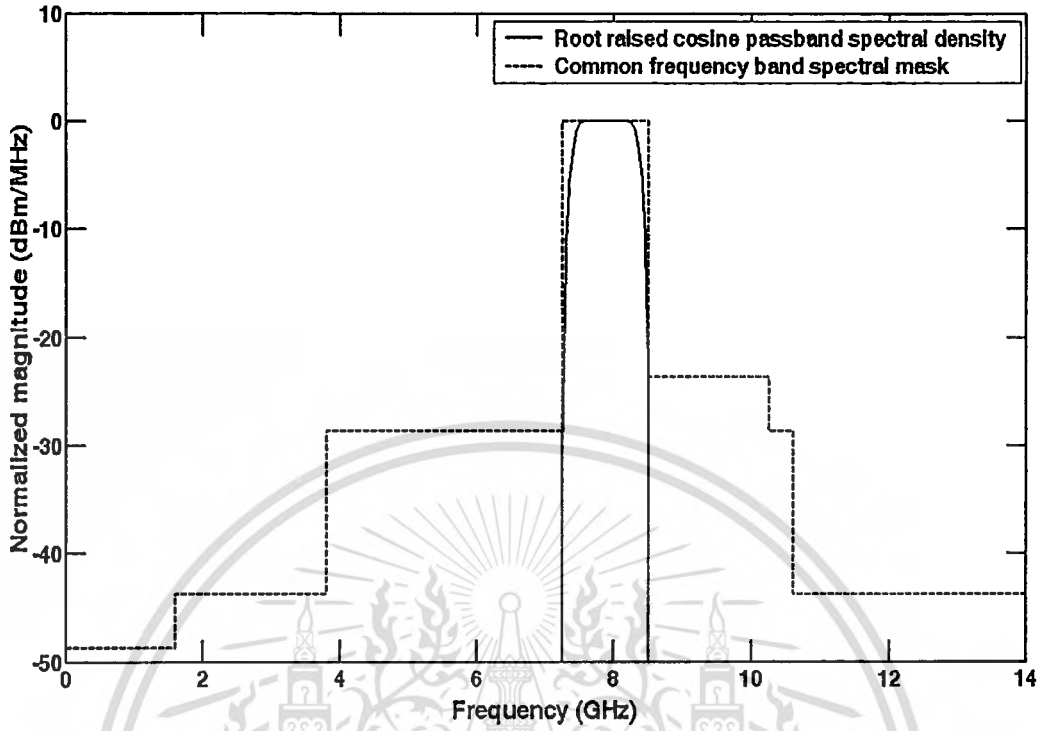

Figure A.10 Normalized magnitude power density of root raised cosine passband waveform satisfying common frequency band spectral mask.

A.2 Received Waveform from Receiver Antenna

In this section, received waveforms used to consider the received and isotropic signal templates at 0° pointing angle are evaluated and shown. For received signal template, the receive waveforms for the case of LPDA link are computed using Equation (5.9) The received waveform with rectangular passband transmitted waveform satisfying the FCC spectral masks for indoor and outdoor limits is shown in Figure A.11. Figure A.12 shows the received waveform with rectangular passband transmitted waveform satisfying the common frequency band spectral mask. For root raised cosine passband transmitted waveform, the received waveforms satisfying the FCC spectral masks for indoor and outdoor limits are shown in Figures A.13 and A.14, respectively. Figure A.15 shows the received waveform satisfying the common frequency band spectral mask.

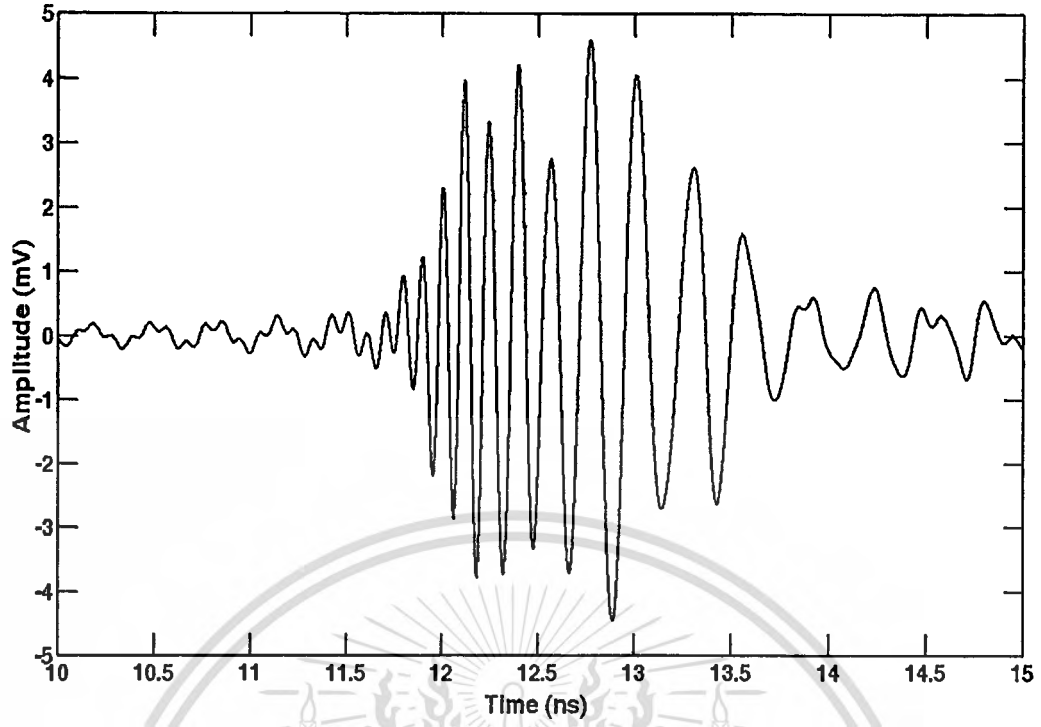

Figure A.11 Received waveform with rectangular passband transmitted waveform satisfying the FCC spectral masks for indoor and outdoor limits.

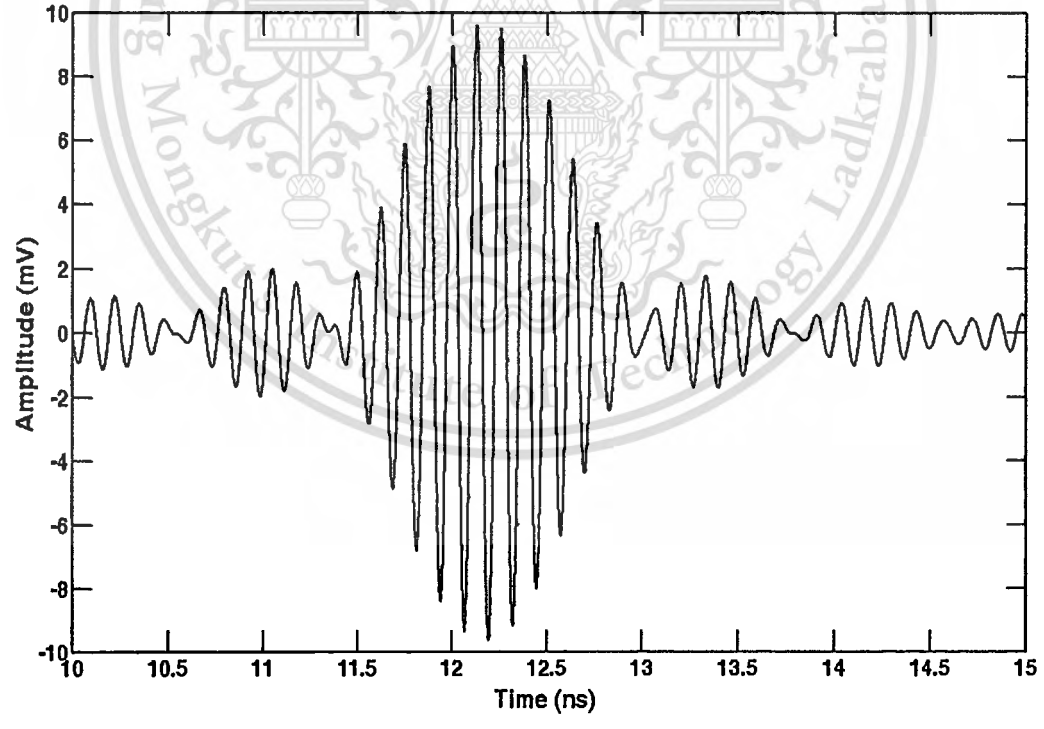

Figure A.12 Received waveform with rectangular passband transmitted waveform satisfying the common frequency band spectral mask.

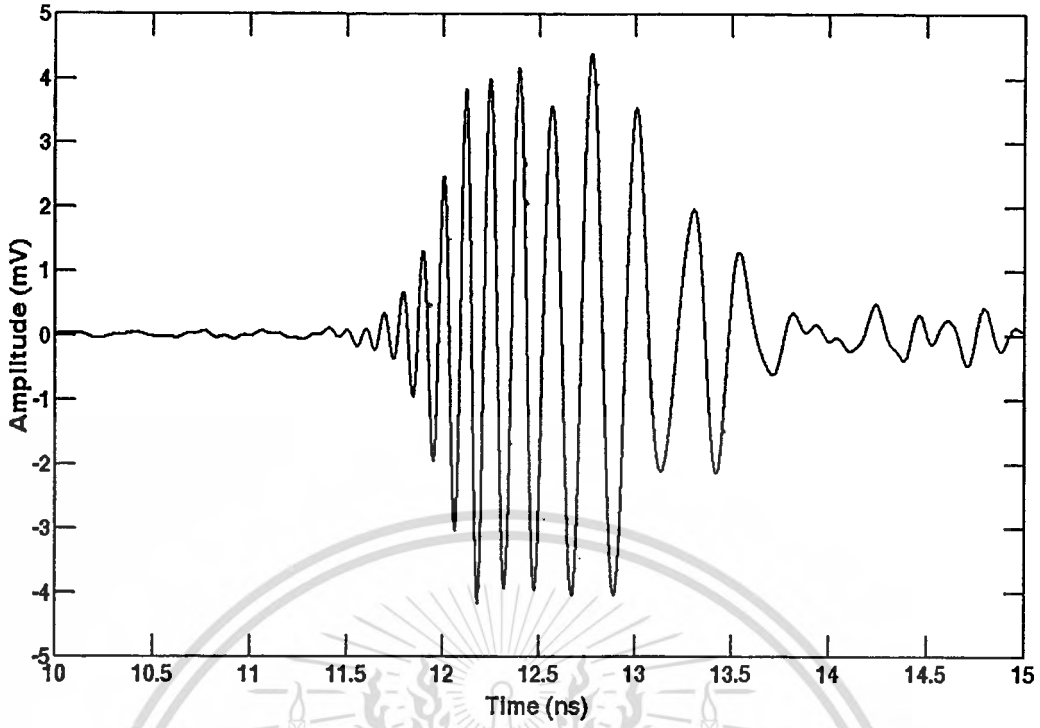

Figure A.13 Received waveform with root raised cosine passband transmitted waveform satisfying the FCC spectral mask for indoor limit.

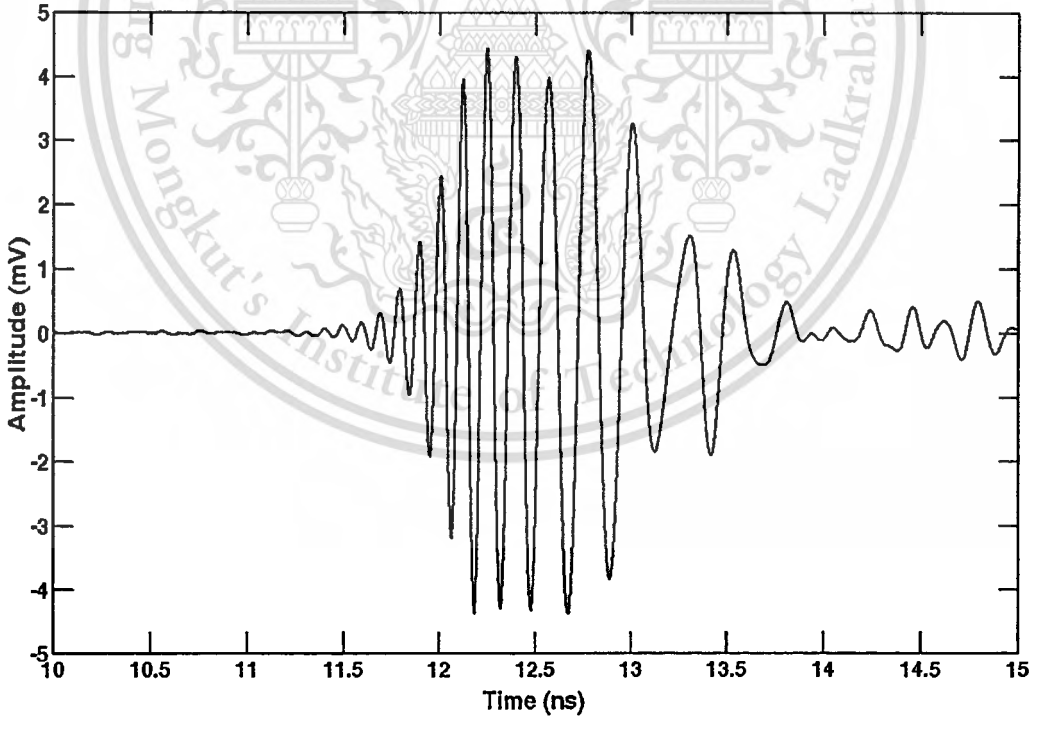

Figure A.14 Received waveform with root raised cosine passband transmitted waveform satisfying the FCC spectral mask for outdoor limit.

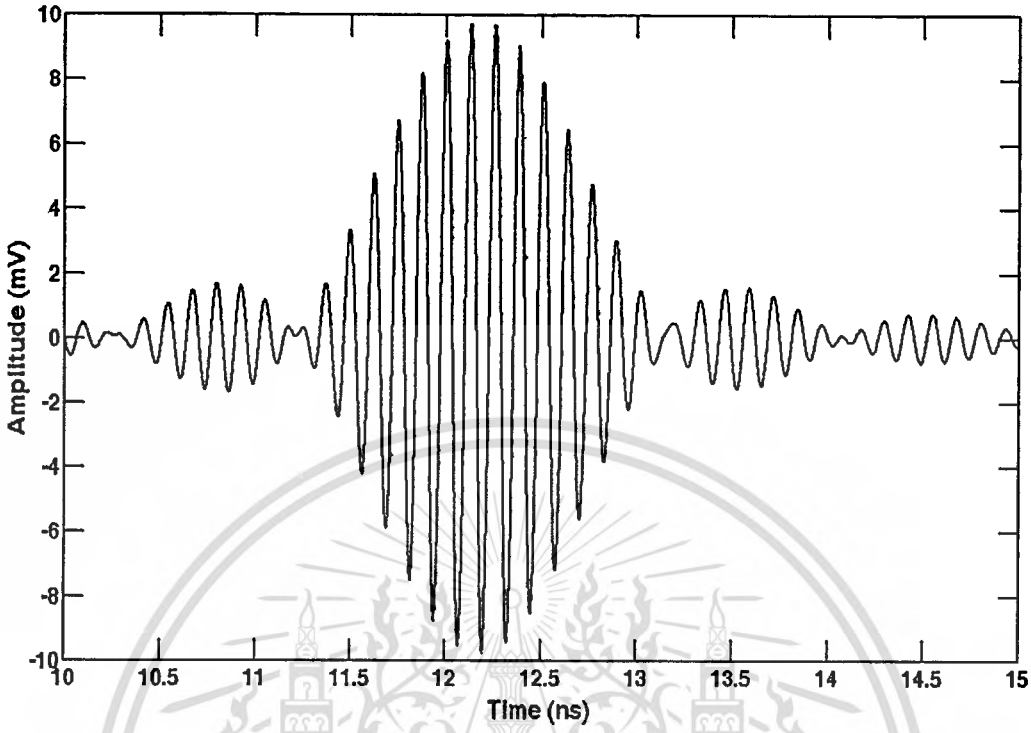

Figure A.15 Received waveform with root raised cosine passband transmitted waveform satisfying the common frequency band spectral mask.

For isotropic signal template, the receive waveforms for the case of isotropic antenna link, isotropic waveform, are computed using Equation (5.15) The isotropic waveform with rectangular passband transmitted waveform satisfying the FCC spectral masks for indoor and outdoor limits is shown in Figure A.16. Figure A.17 shows the isotropic waveform with rectangular passband transmitted waveform satisfying the common frequency band spectral mask. The isotropic waveforms with root raised cosine passband transmitted waveforms satisfying the FCC spectral masks for indoor and outdoor limits are shown in Figures A.18 and A.19, respectively. Figure A.20 shows the isotropic waveform with root raised cosine passband transmitted waveform satisfying the common frequency band spectral mask. From these Figures, the isotropic waveform has less distortion compared with received waveform because there is no effect of transmitter and receiver antennas. These waveforms are used to evaluate the waveform distortion.

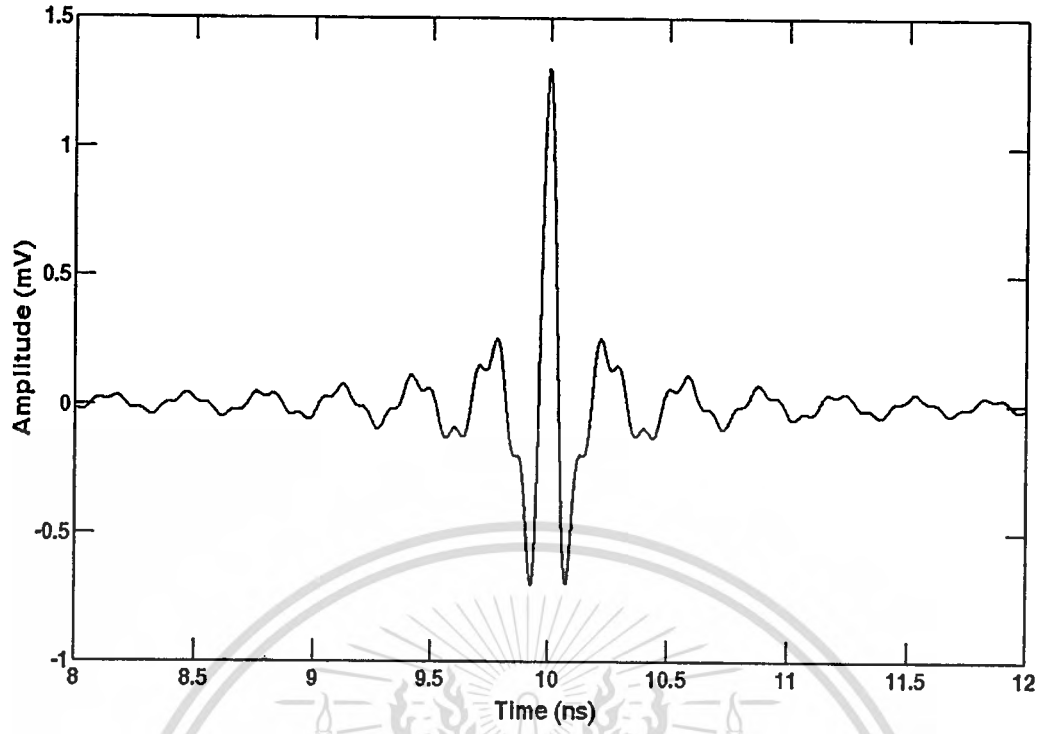

Figure A.16 Isotropic waveform with rectangular passband transmitted waveform satisfying the FCC spectral masks for indoor and outdoor limits.

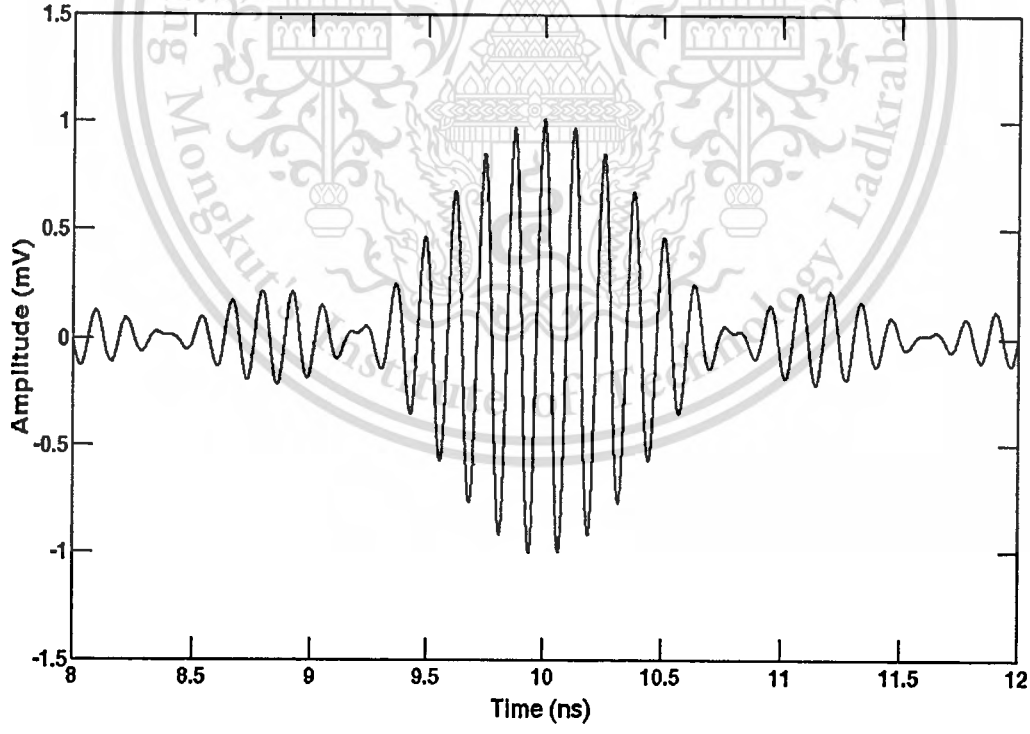

Figure A.17 Isotropic waveform with rectangular passband transmitted waveform satisfying the common frequency band spectral mask.

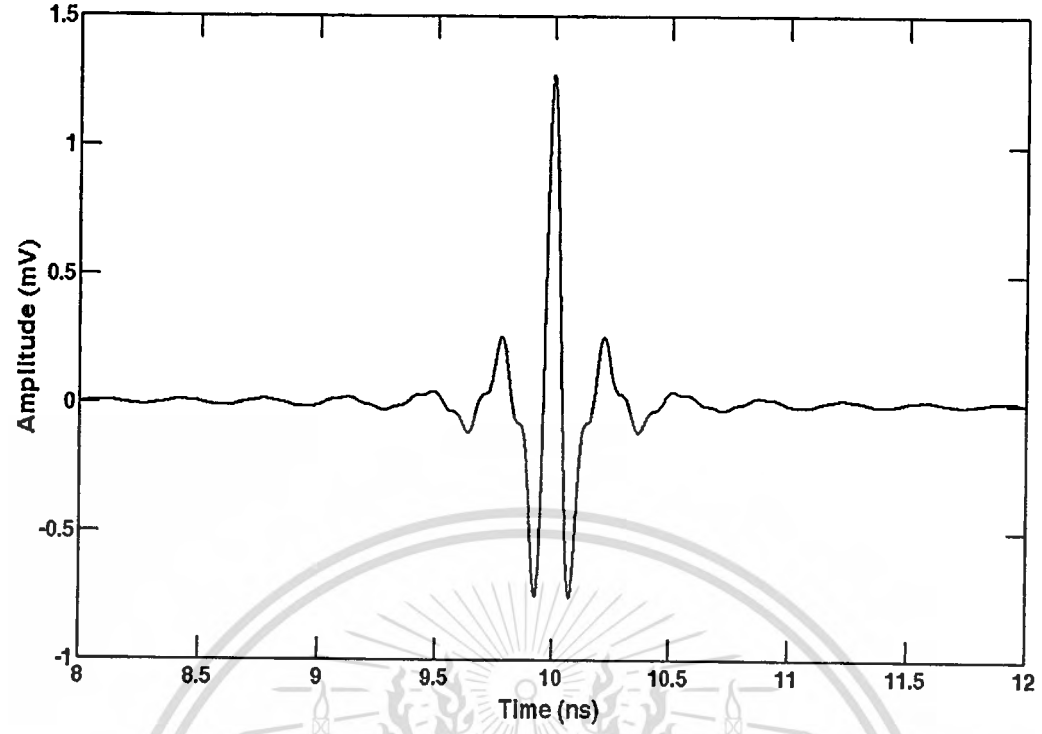

Figure A.18 Isotropic waveform with root raised cosine passband transmitted waveform satisfying the FCC spectral mask for indoor limit.

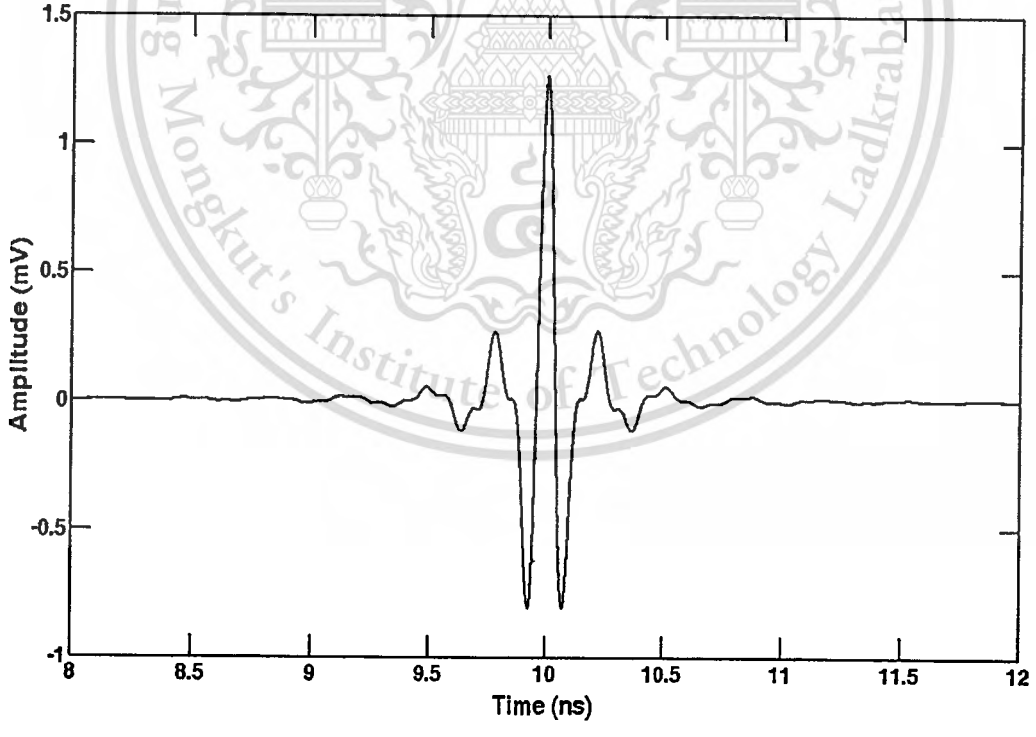

Figure A.19 Isotropic waveform with root raised cosine passband transmitted waveform satisfying the FCC spectral mask for outdoor limit.

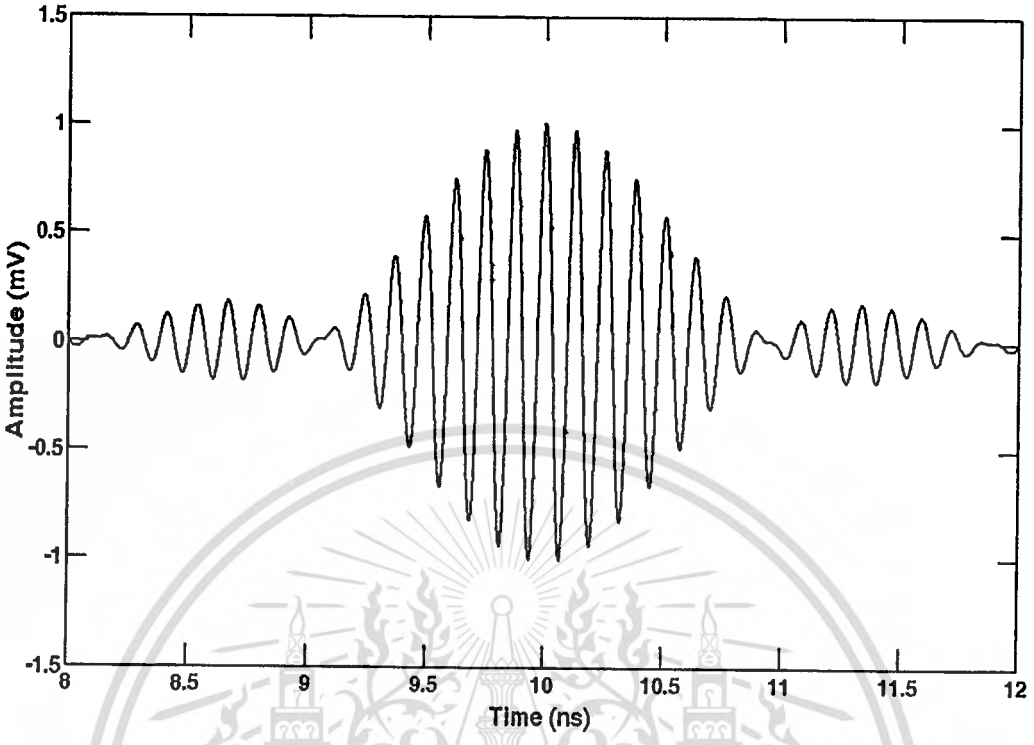

Figure A.20 Isotropic waveform with root raised cosine passband transmitted waveform satisfying the common frequency band spectral mask.

A.3 Output Waveform of Correlation Receiver

In this section, output waveforms of correlation receivers with received signal and isotropic templates at 0° pointing angle are evaluated and shown. For correlation receiver with received signal template, the output waveform with rectangular passband transmitted waveform satisfying the FCC spectral masks for indoor and outdoor limits is shown in Figure A.21. Figure A.22 shows the output waveform with rectangular passband transmitted waveform satisfying the common frequency band spectral mask. For root raised cosine passband transmitted waveform, the output waveforms satisfying the FCC spectral masks for indoor and outdoor limits are shown in Figures A.23 and A.24, respectively. Figure A.25 shows the output waveform satisfying the common frequency band spectral mask.

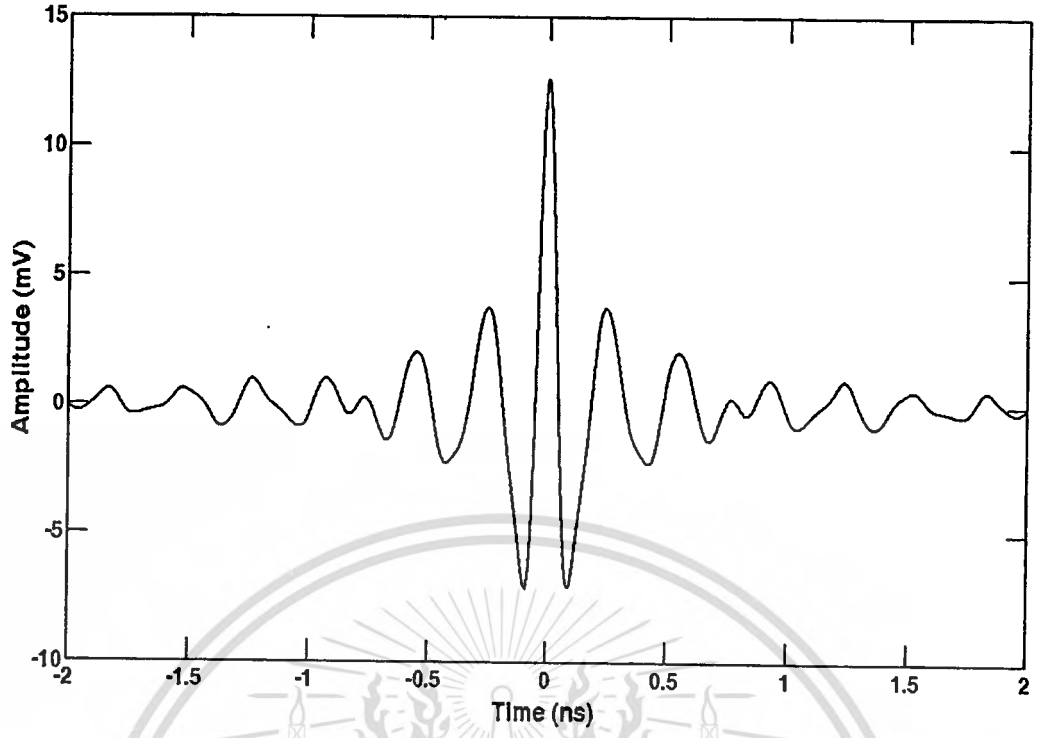

Figure A.21 Output waveform with rectangular passband transmitted waveform and received signal template satisfying the FCC spectral masks for indoor and outdoor limits.

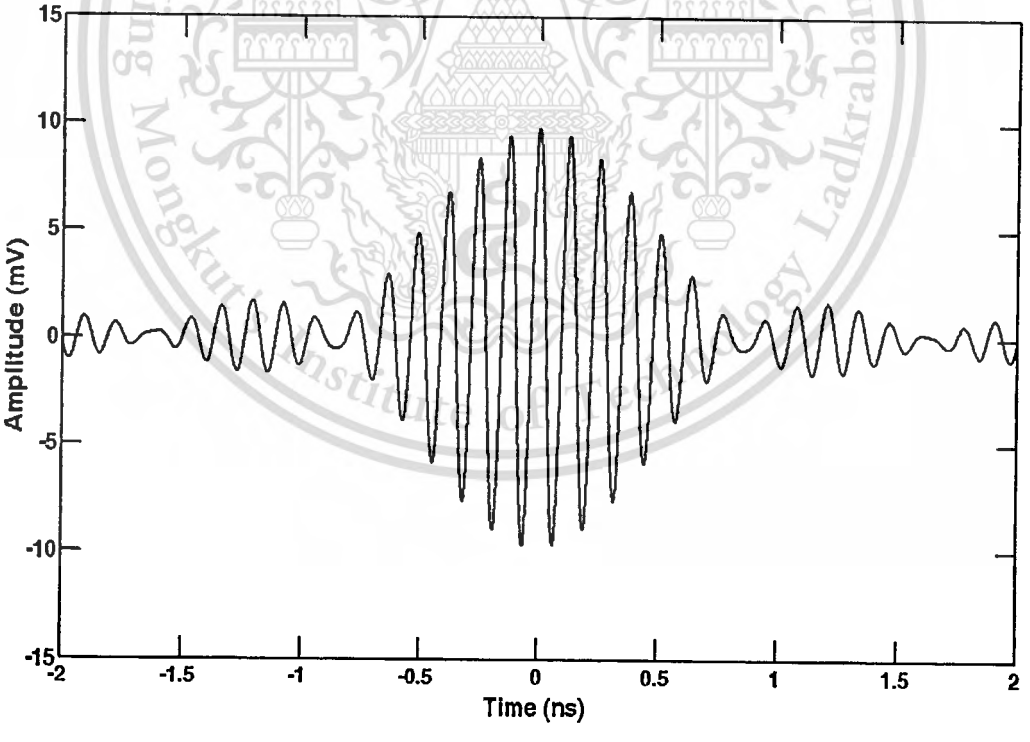

Figure A.22 Output waveform with rectangular passband transmitted waveform and received signal template satisfying the common frequency band spectral mask.

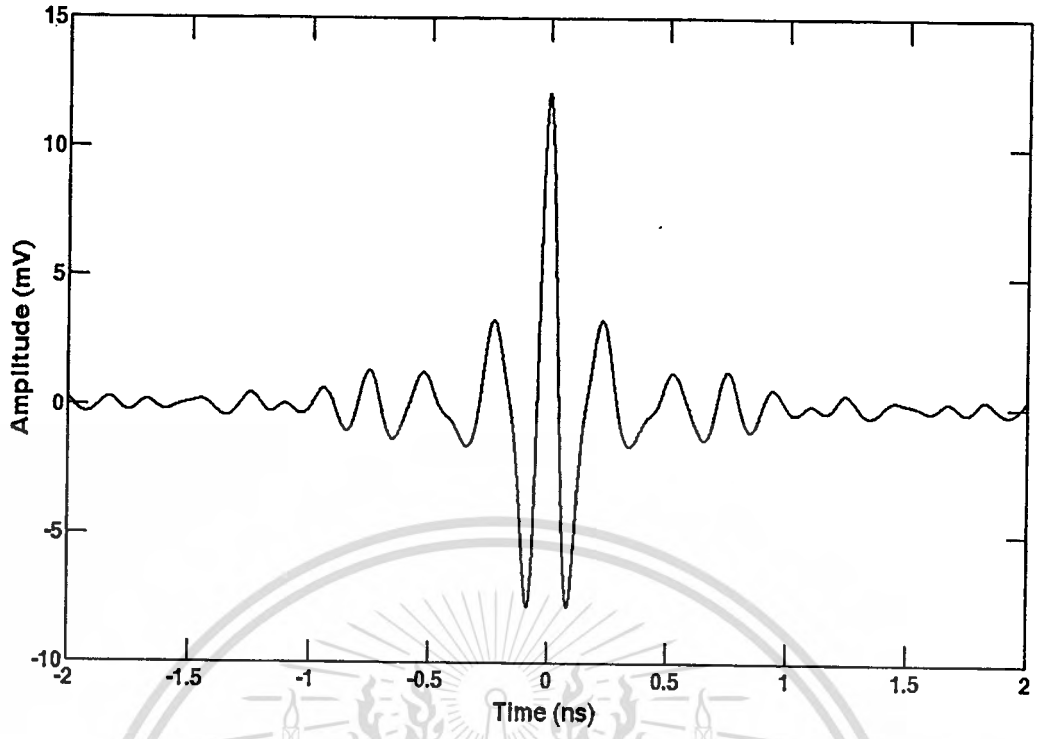

Figure A.23 Output waveform with root raised cosine passband transmitted waveform and received signal template satisfying the FCC spectral mask for indoor limit.

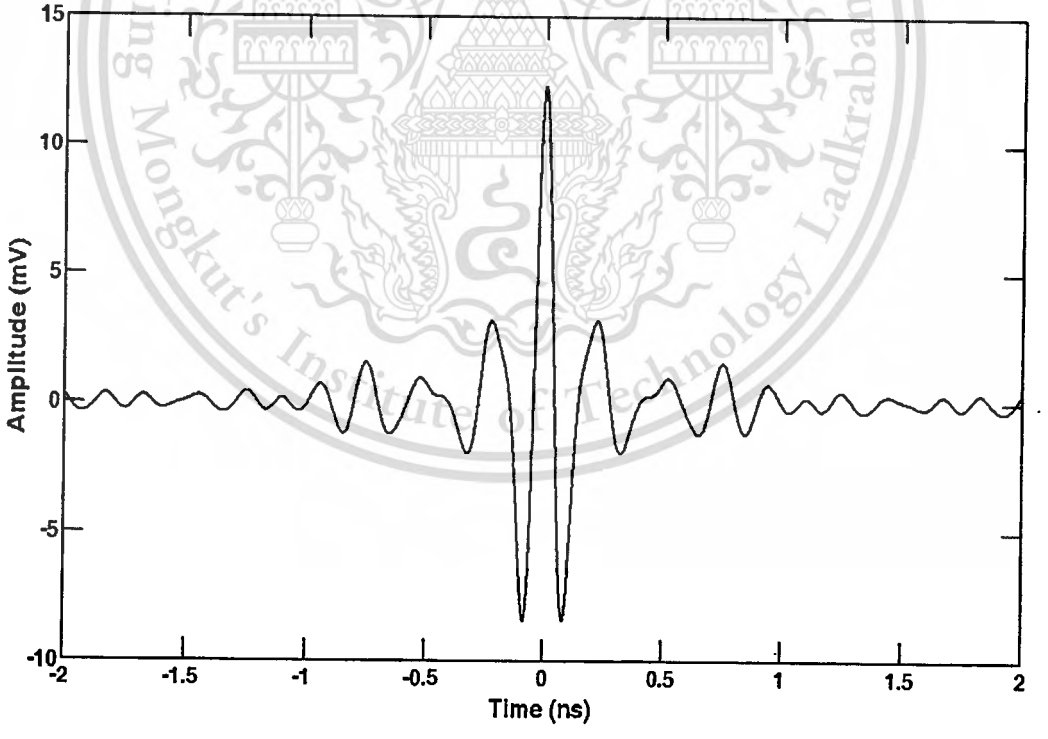

Figure A.24 Output waveform with root raised cosine passband transmitted waveform and received signal template satisfying the FCC spectral mask for outdoor limit.

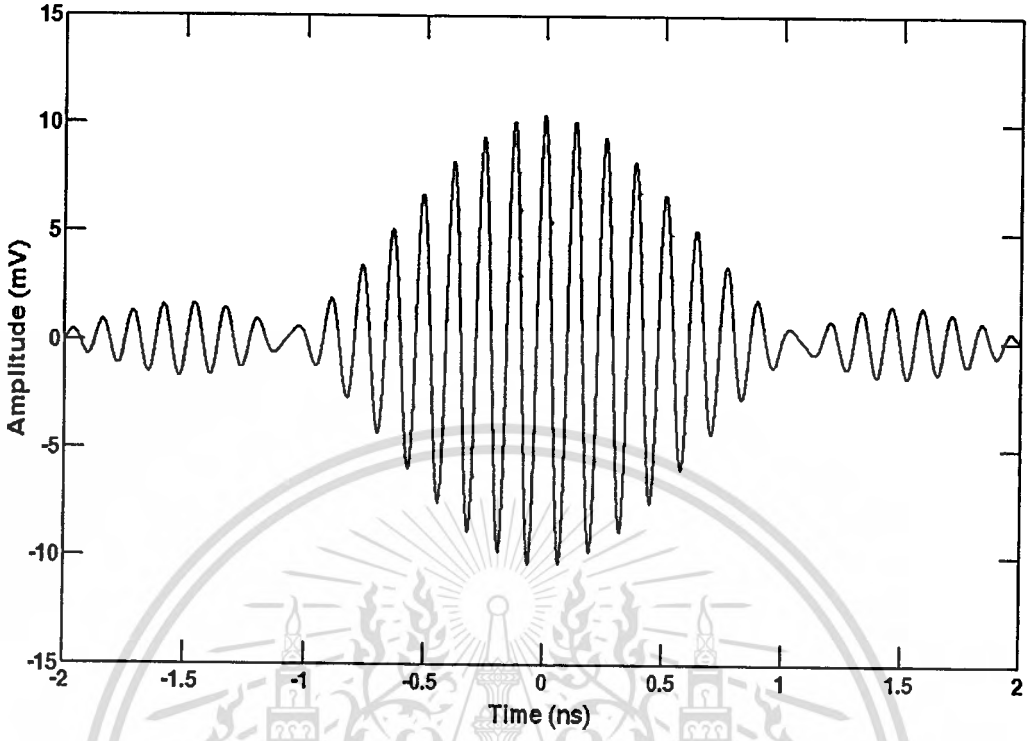

Figure A.25 Output waveform with root raised cosine passband transmitted waveform and received signal template satisfying the common frequency band spectral mask.

For correlation receiver with isotropic template, the output waveform with rectangular passband transmitted waveform satisfying the FCC spectral masks for indoor and outdoor limits is shown in Figure A.26. Figure A.27 shows the output waveform with rectangular passband transmitted waveform satisfying the common frequency band spectral mask. The output waveforms with root raised cosine passband transmitted waveforms satisfying the FCC spectral masks for indoor and outdoor limits are shown in Figures A.28 and A.29, respectively. Figure A.30 shows the output waveform with root raised cosine passband transmitted waveform satisfying the common frequency band spectral mask. From these Figures, the output waveforms of correlation receiver with received signal template have more peak amplitude than that of correlation receiver with isotropic template.

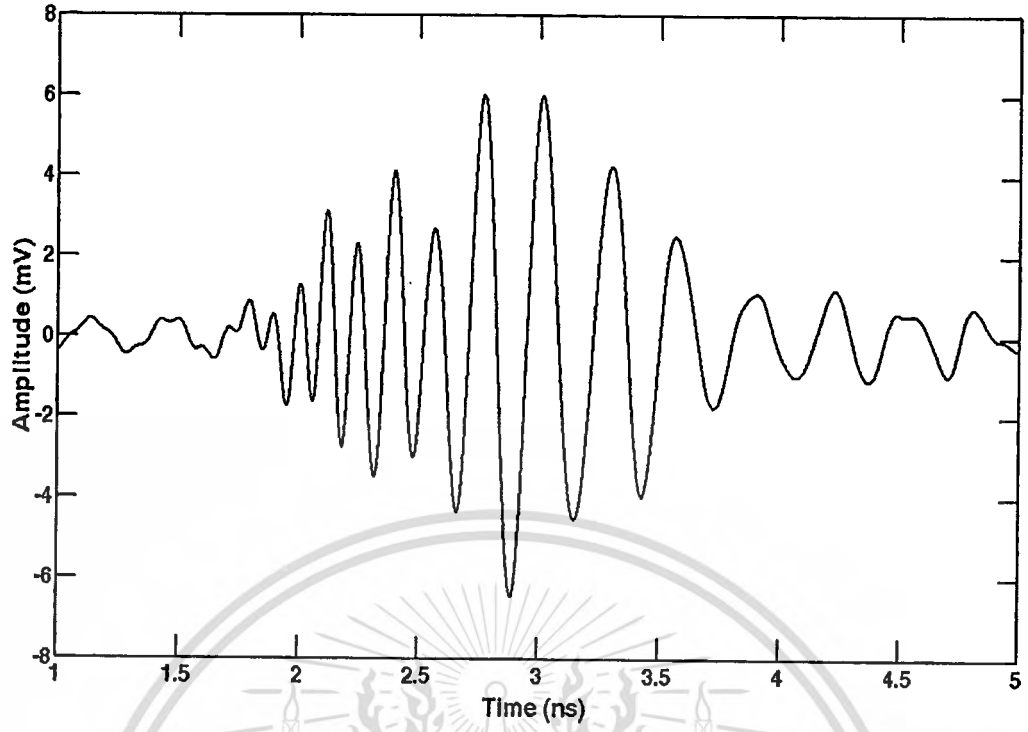

Figure A.26 Output waveform with rectangular passband transmitted waveform and isotropic template satisfying the FCC spectral masks for indoor and outdoor limits.

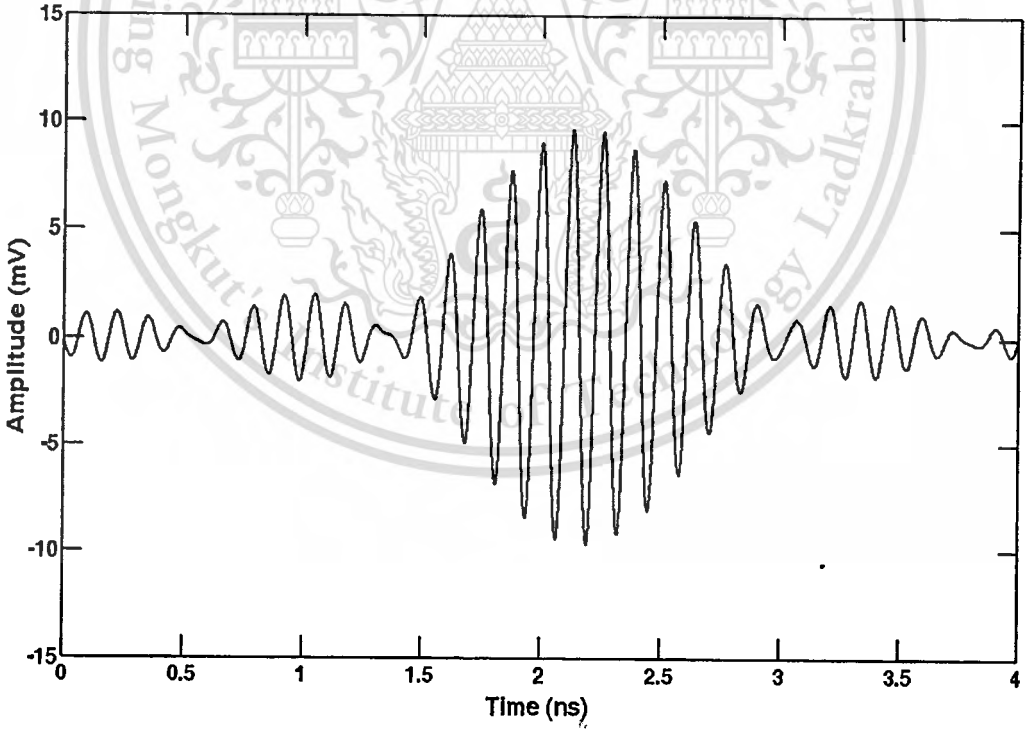

Figure A.27 Output waveform with rectangular passband transmitted waveform and isotropic template satisfying the common frequency band spectral mask.

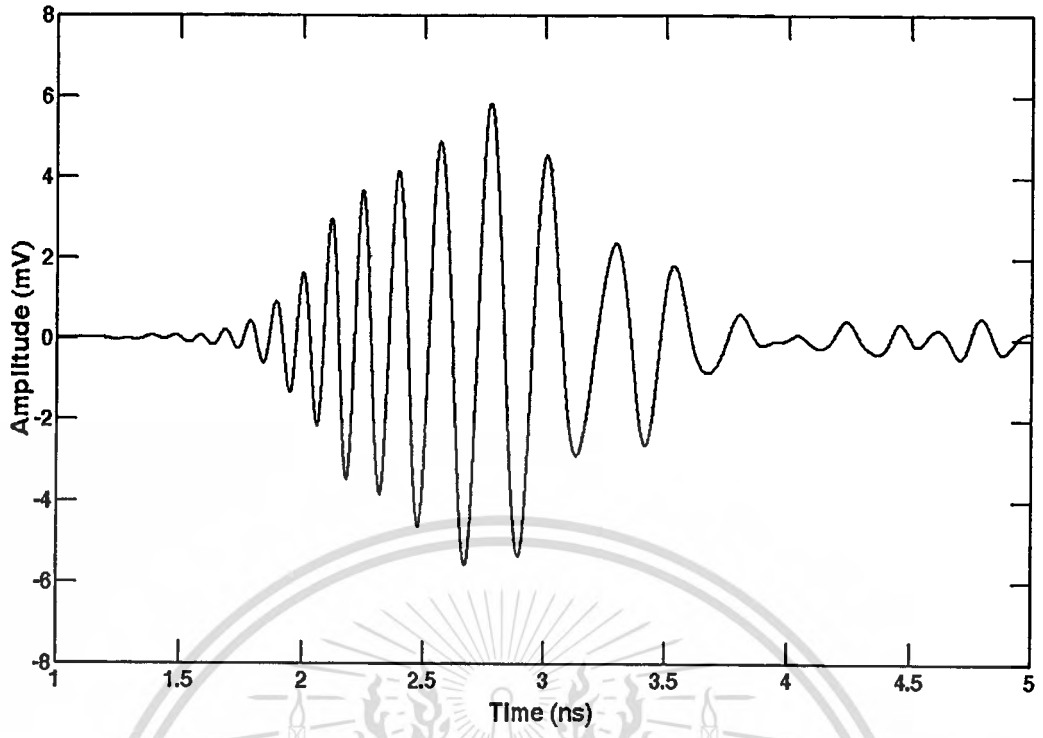

Figure A.28 Output waveform with root raised cosine passband transmitted waveform and isotropic template satisfying the FCC spectral mask for indoor limit.

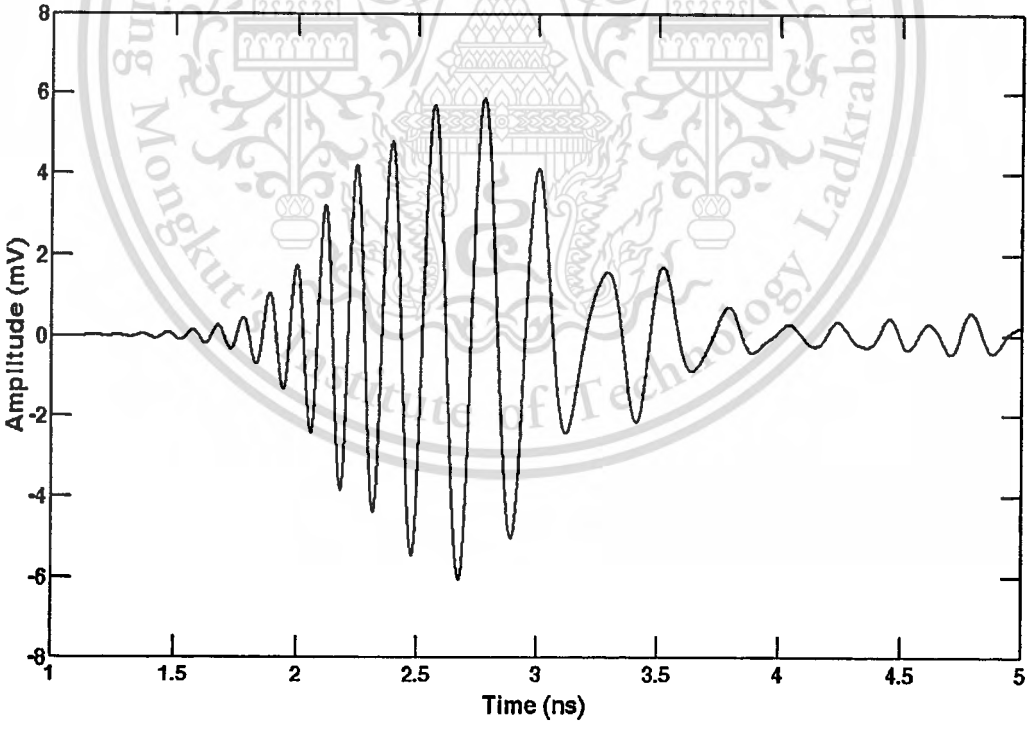

Figure A.29 Output waveform with root raised cosine passband transmitted waveform and isotropic template satisfying the FCC spectral mask for outdoor limit.

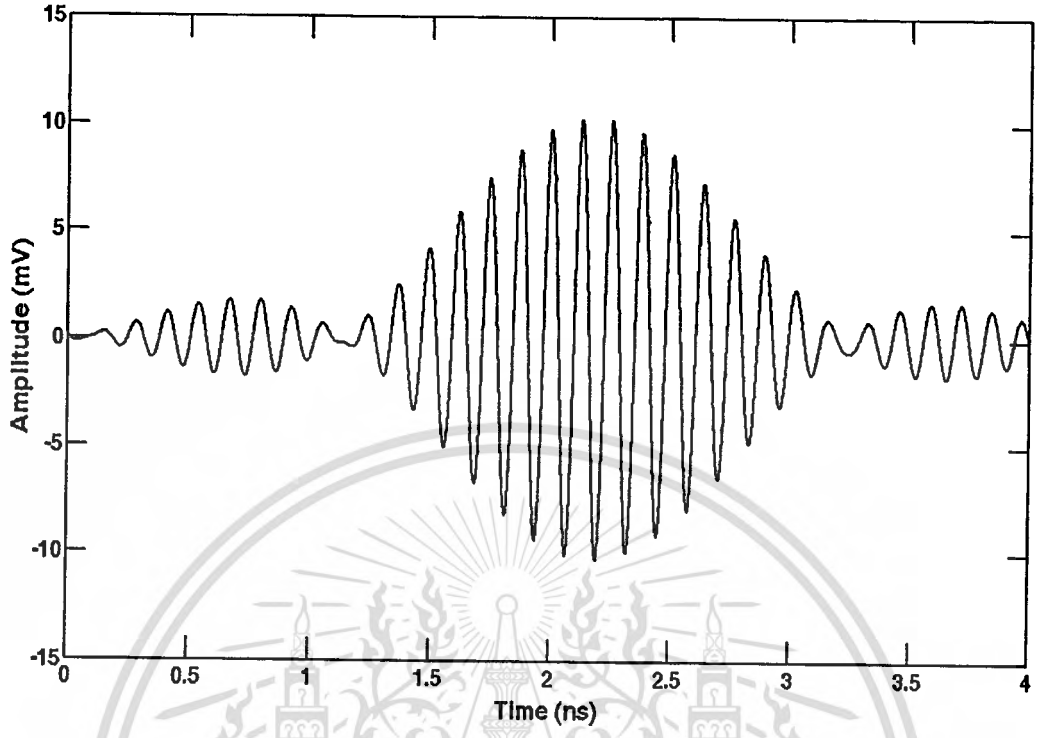

Figure A.30 Output waveform with root raised cosine passband transmitted waveform and isotropic template satisfying the common frequency band spectral mask.

For correlation receiver with isotropic template and receive waveforms for the case of isotropic antenna link, the output isotropic waveform with rectangular passband transmitted waveform satisfying the FCC spectral masks for indoor and outdoor limits is shown in Figure A.31. Figure A.32 shows the output isotropic waveform with rectangular passband transmitted waveform satisfying the common frequency band spectral mask. The output isotropic waveforms with root raised cosine passband transmitted waveforms satisfying the FCC spectral masks for indoor and outdoor limits are shown in Figures A.33 and A.34, respectively. Figure A.35 shows the output isotropic waveform with root raised cosine passband transmitted waveform satisfying the common frequency band spectral mask. These waveforms are used to normalize for evaluating transmission gain as defined in Section 5.2.5.

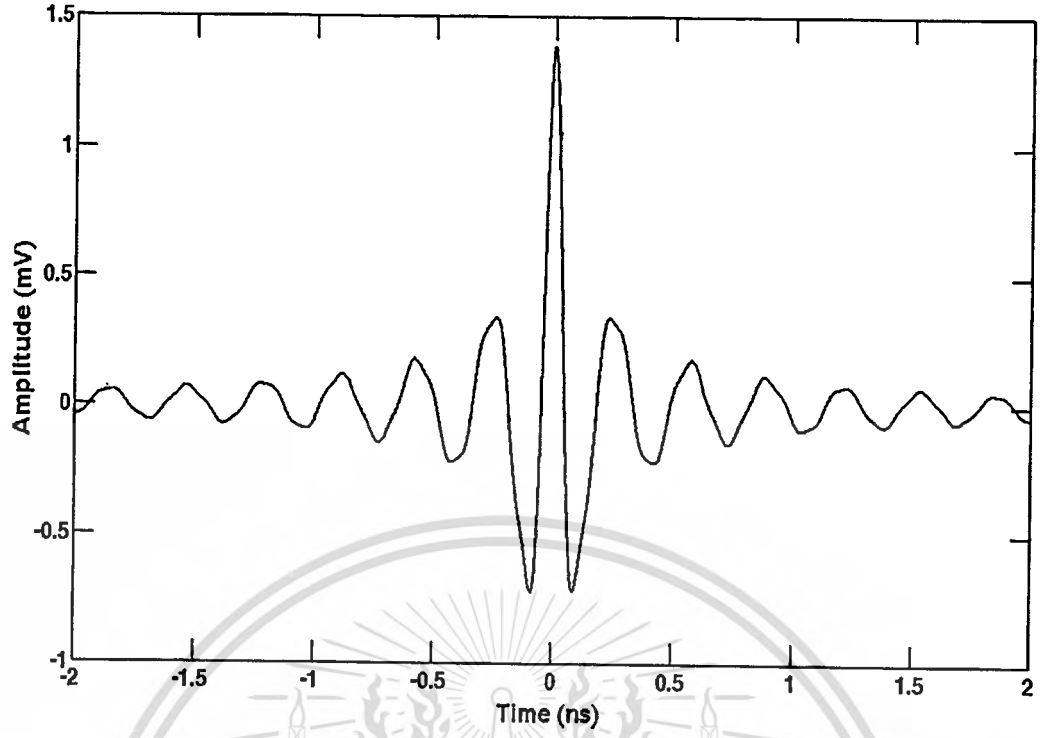

Figure A.31 Output waveform with rectangular passband transmitted waveform and isotropic template satisfying the FCC spectral masks for indoor and outdoor limits.

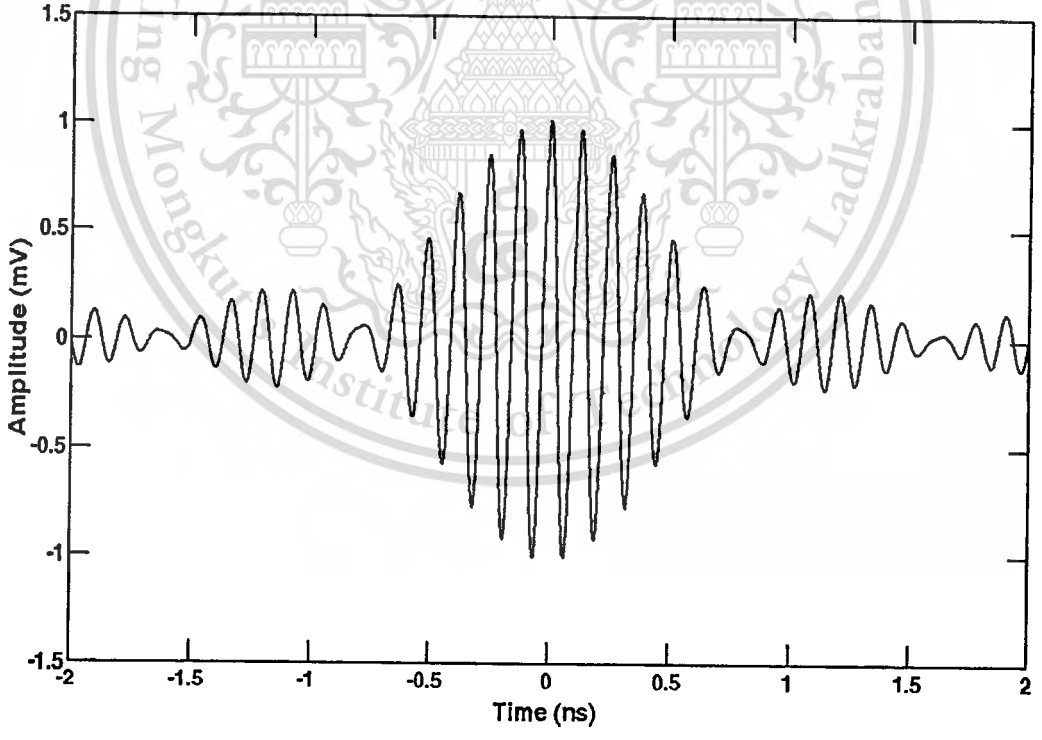

Figure A.32 Output waveform with rectangular passband transmitted waveform and isotropic template satisfying the common frequency band spectral mask.

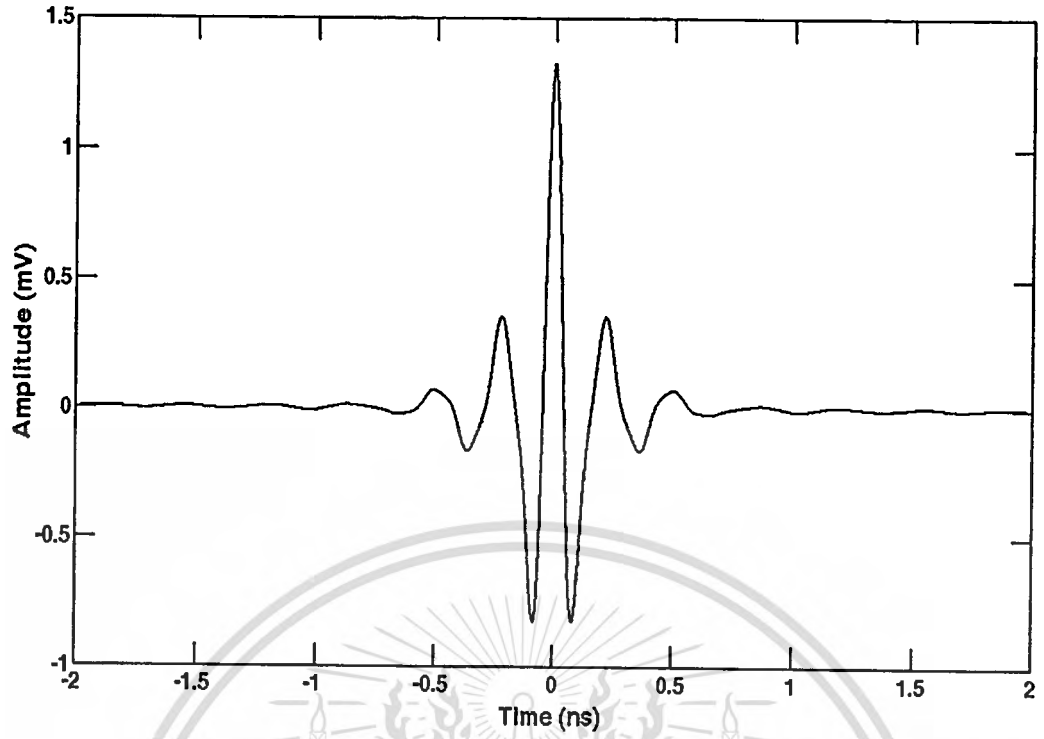

Figure A.33 Output waveform with root raised cosine passband transmitted waveform and isotropic template satisfying the FCC spectral mask for indoor limit.

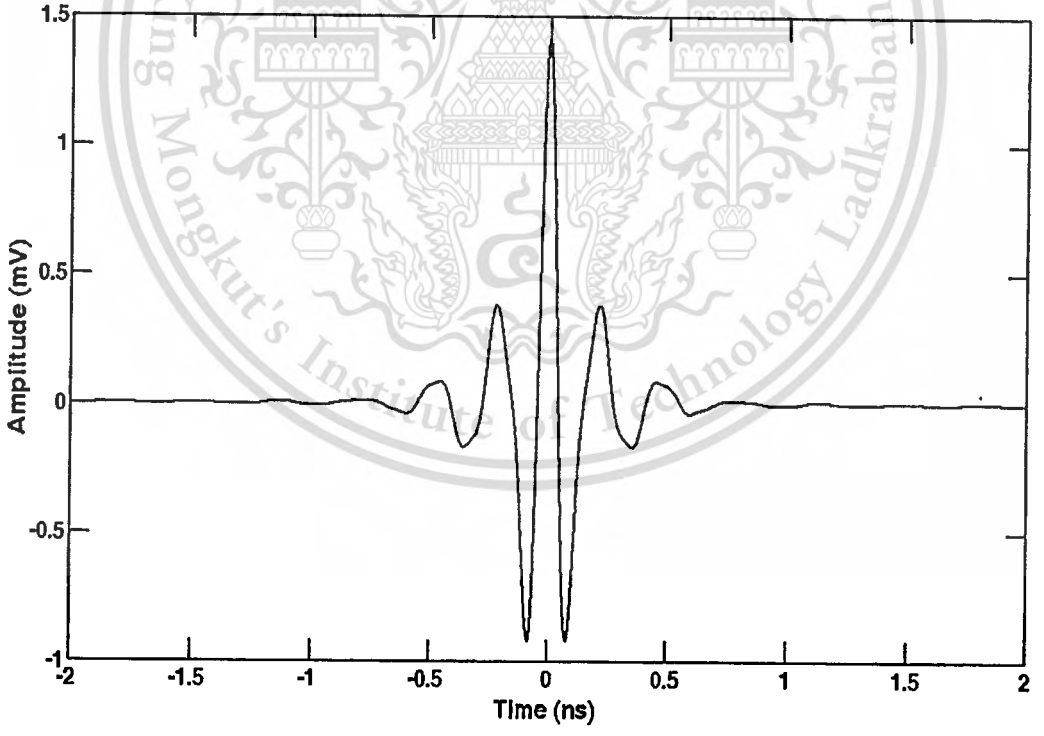

Figure A.34 Output waveform with root raised cosine passband transmitted waveform and isotropic template satisfying the FCC spectral mask for outdoor limit.

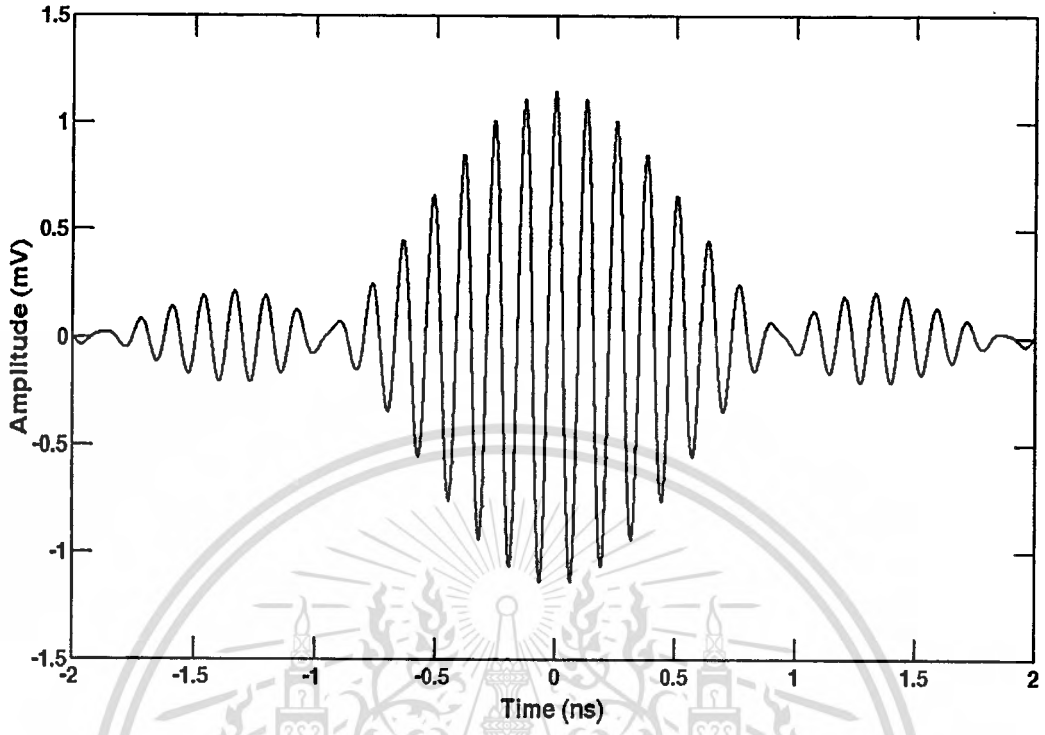

Figure A.35 Output waveform with root raised cosine passband transmitted waveform and isotropic template satisfying the common frequency band spectral mask.

A.4 Waveform Distortion

In this section, waveform distortion of each case is evaluated using Equation (5.16) and shown. The waveform distortion of rectangular passband waveform satisfying the FCC spectral masks for indoor and outdoor limits is shown in Figure A.36. Figure A.37 shows the waveform distortion of rectangular passband waveform satisfying the common frequency band spectral mask. The waveform distortions of root raised cosine passband waveforms satisfying the FCC spectral masks for indoor and outdoor limits are shown in Figures A.38 and A.39, respectively. Figure A.40 shows the waveform distortion of root raised cosine passband waveform satisfying the common frequency band spectral mask.

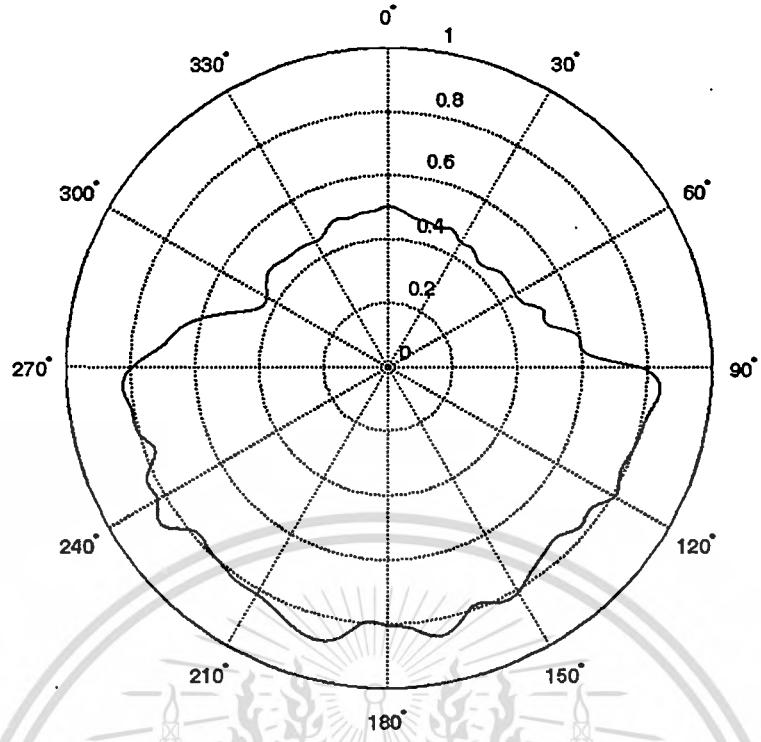

Figure A.36 Waveform distortion of rectangular passband waveform satisfying the FCC spectral masks for indoor and outdoor limits.

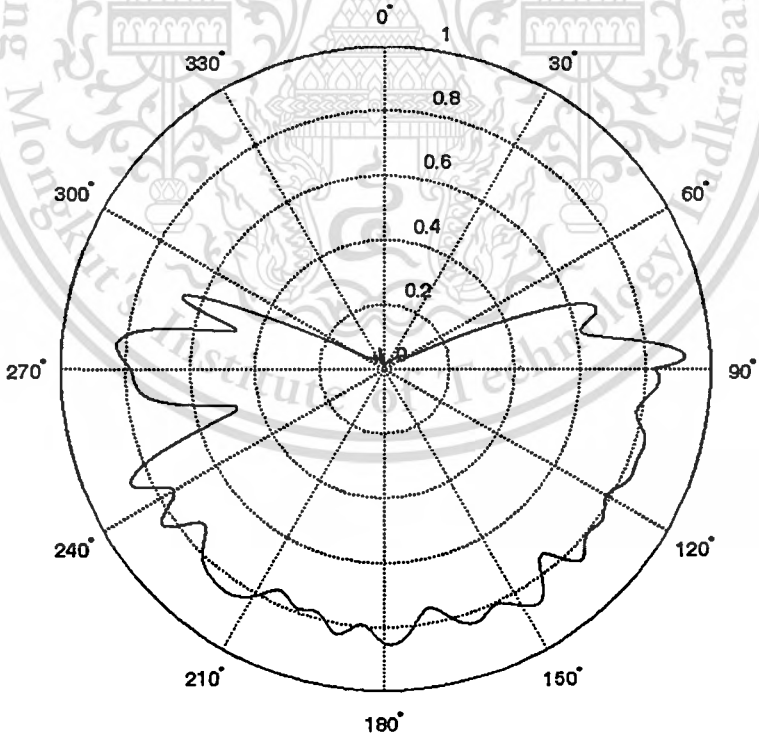

Figure A.37 Waveform distortion of rectangular passband waveform satisfying the common frequency band spectral masks.

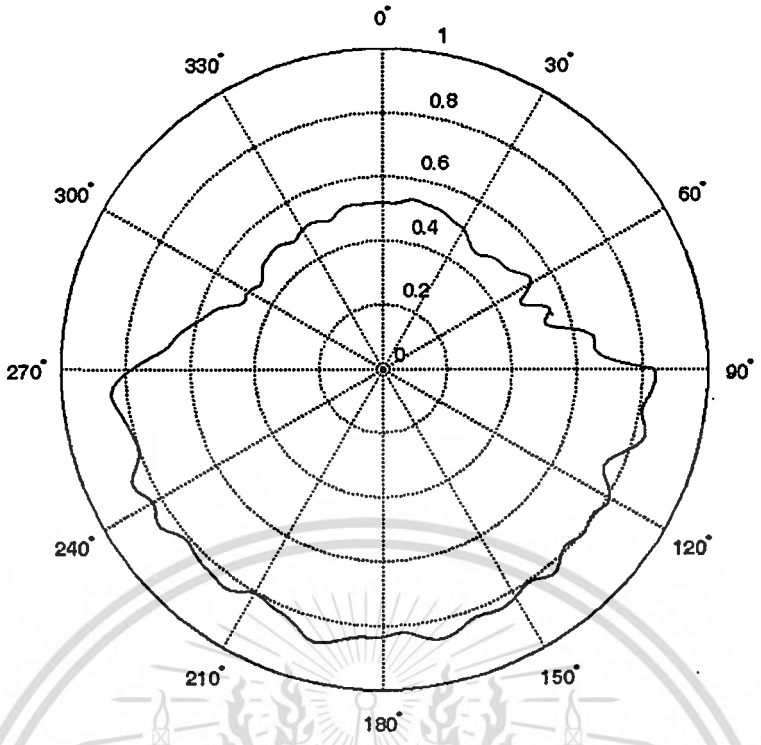

Figure A.38 Waveform distortion of root raised cosine passband waveform satisfying the FCC spectral mask for indoor limit.

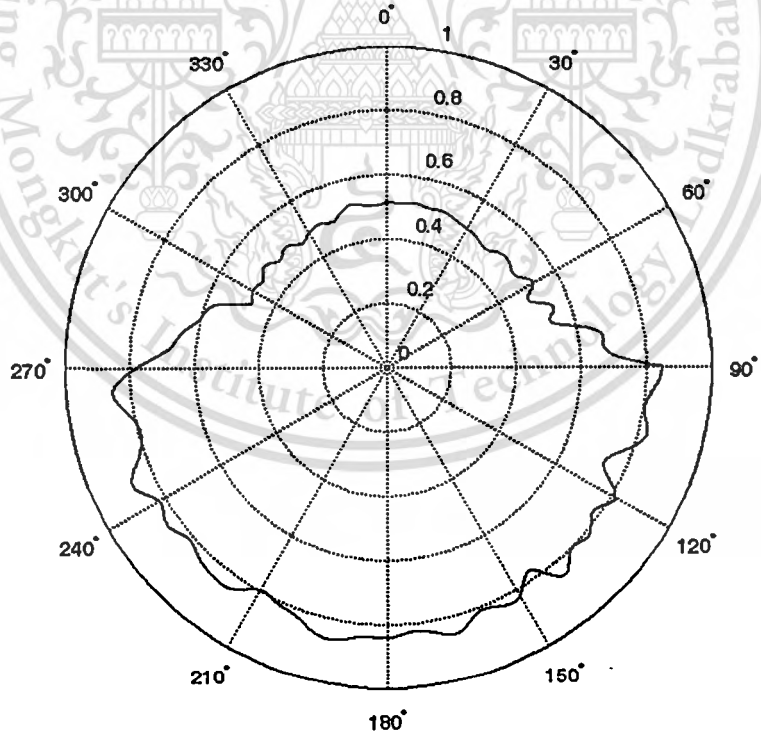

Figure A.39 Waveform distortion of root raised cosine passband waveform satisfying the FCC spectral mask for outdoor limit.

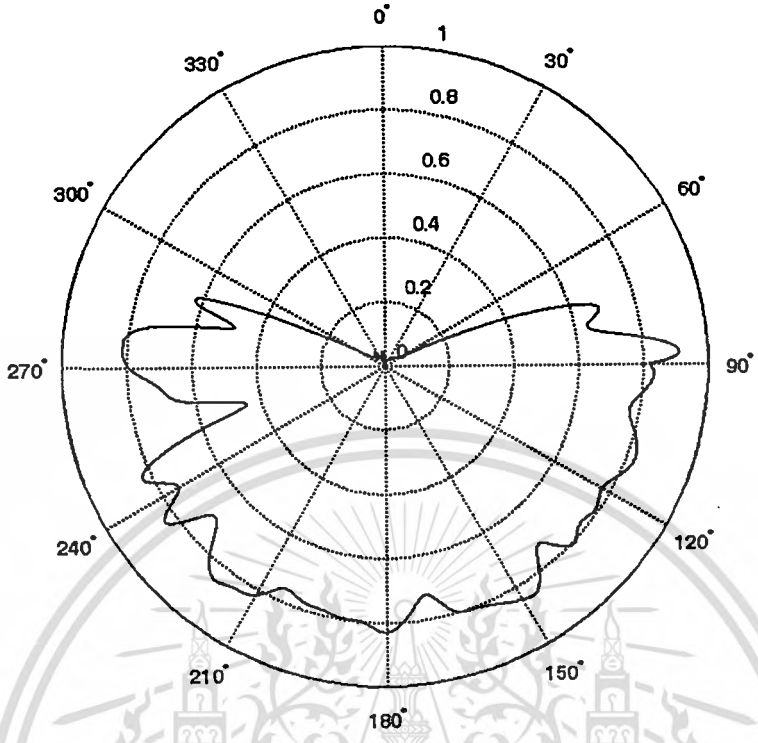

Figure A.40 Waveform distortion of root raised cosine passband waveform satisfying the common frequency band spectral mask.

A.5 Transmission Gain

Transmission gains of correlation receivers for both received signal and isotropic templates are considered. For correlation receiver with received signal template, the transmission gain is evaluated using Equation (5.17). The transmission gain of rectangular passband waveform with received signal template satisfying the FCC spectral masks for indoor and outdoor limits is shown in Figure A.41. Figure A.42 shows the transmission gain of rectangular passband waveform with received signal template satisfying the common frequency band spectral mask. The transmission gains of root raised cosine passband waveforms with received signal template satisfying the FCC spectral masks for indoor and outdoor limits are shown in Figures A.43 and A.44, respectively. Figure A.45 shows the transmission gain of root raised cosine passband waveform with received signal template satisfying the common frequency band spectral mask.

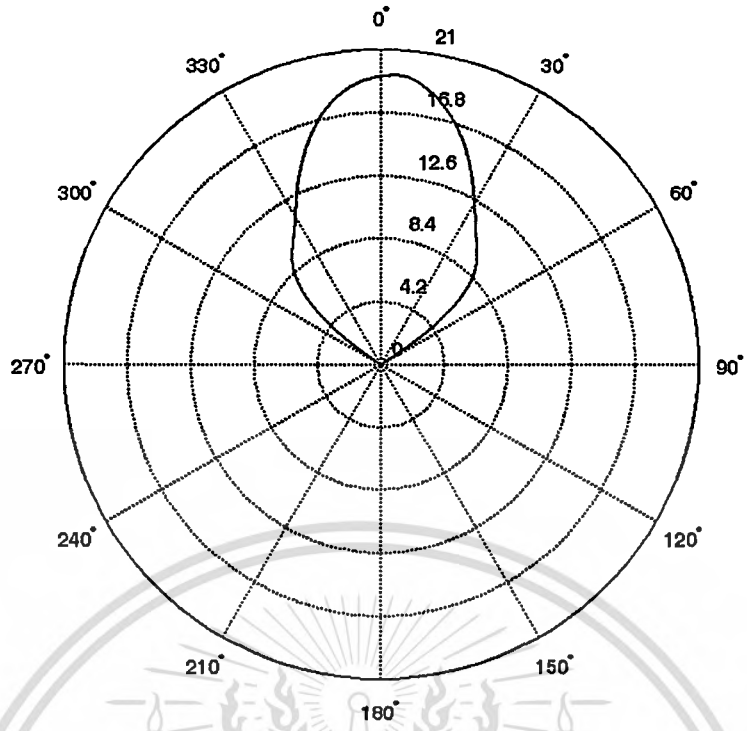

Figure A.41 Transmission gain of rectangular passband waveform with received signal template satisfying the FCC spectral masks for indoor and outdoor limits.

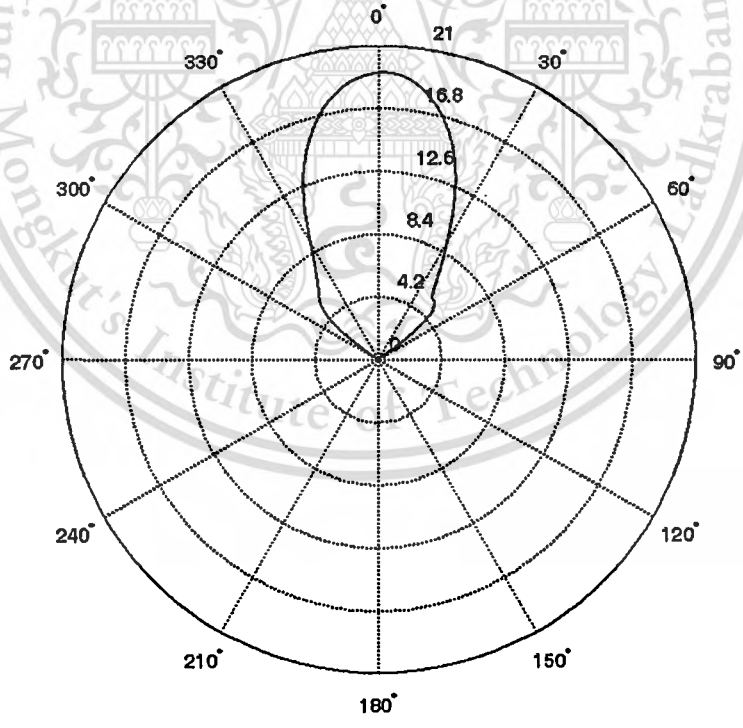

Figure A.42 Transmission gain of rectangular passband waveform with received signal template satisfying the common frequency band spectral mask.

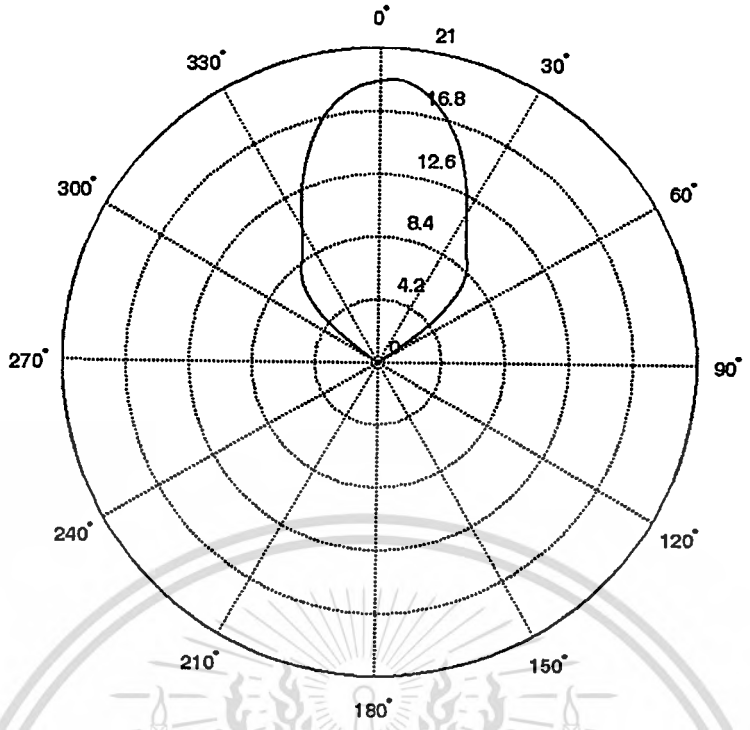

Figure A.43 Transmission gain of root raised cosine passband waveform with received signal template satisfying the FCC spectral mask for indoor limit.

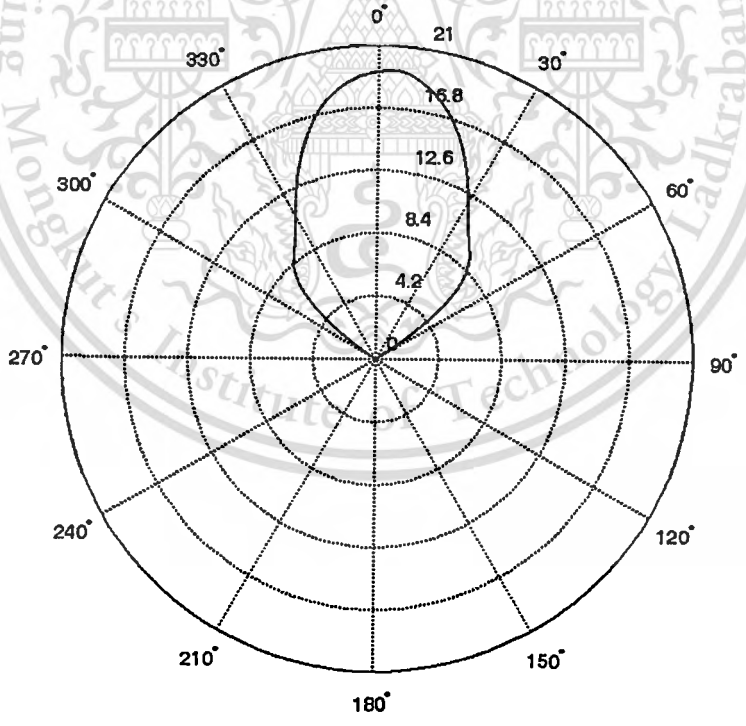

Figure A.44 Transmission gain of root raised cosine passband waveform with received signal template satisfying the FCC spectral mask for outdoor limit.

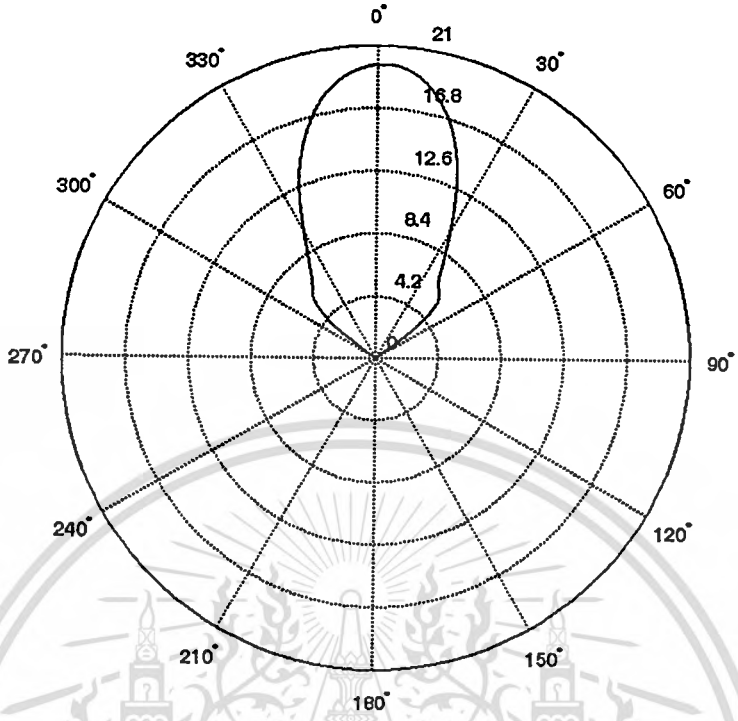

Figure A.45 Transmission gain of root raised cosine passband waveform with received signal template satisfying the common frequency band spectral mask.

Finally, transmission gain of correlation receivers with isotropic template is evaluated using Equation (5.18). The transmission gain of rectangular passband waveform with isotropic template satisfying the FCC spectral masks for indoor and outdoor limits is shown in Figure A.46. Figure A.47 shows the transmission gain of rectangular passband waveform with isotropic template satisfying the common frequency band spectral mask. The transmission gains of root raised cosine passband waveforms with isotropic template satisfying the FCC spectral masks for indoor and outdoor limits are shown in Figures A.48 and A.49, respectively. Figure A.50 shows the transmission gain of root raised cosine passband waveform with isotropic template satisfying the common frequency band spectral mask.

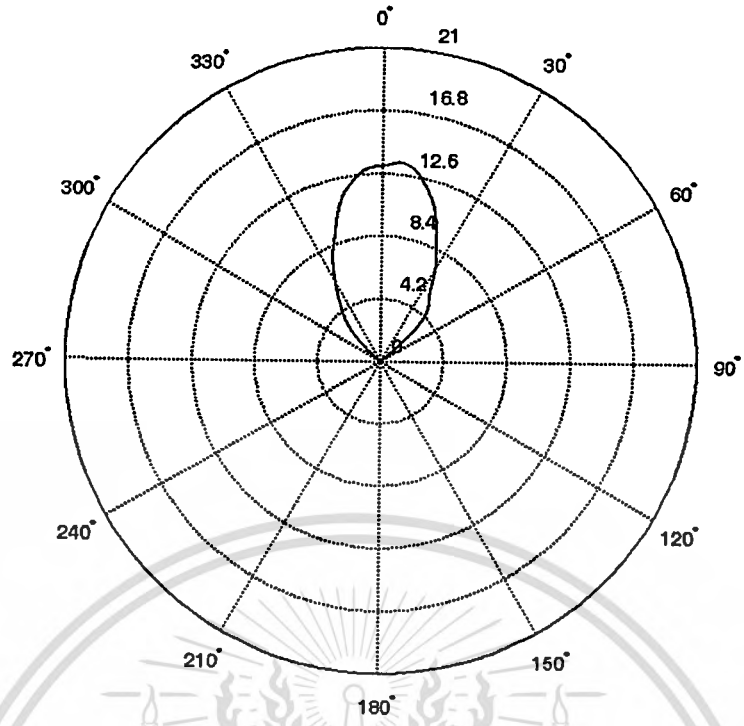

Figure A.46 Transmission gain of rectangular passband waveform with received signal template satisfying the FCC spectral masks for indoor and outdoor limits.

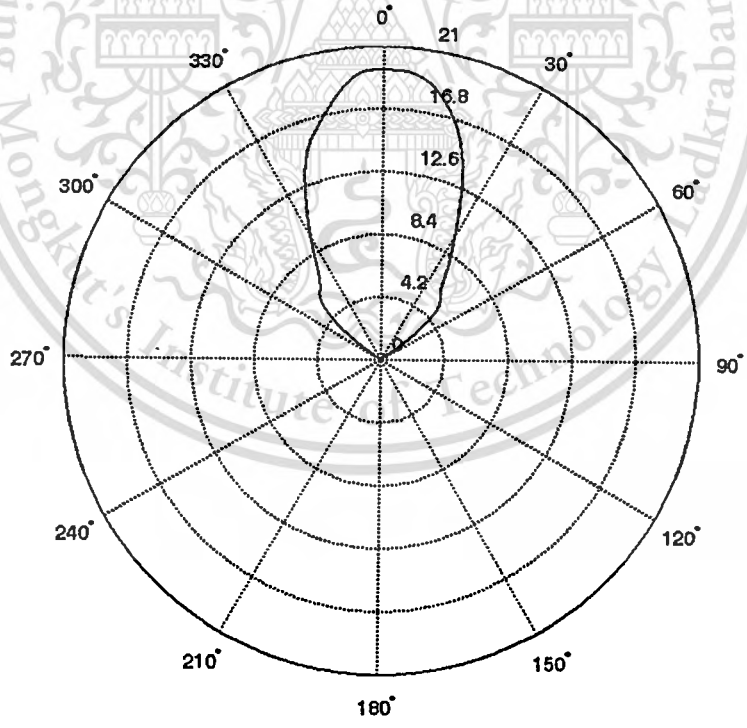

Figure A.47 Transmission gain of rectangular passband waveform with received signal template satisfying the common frequency band spectral mask.

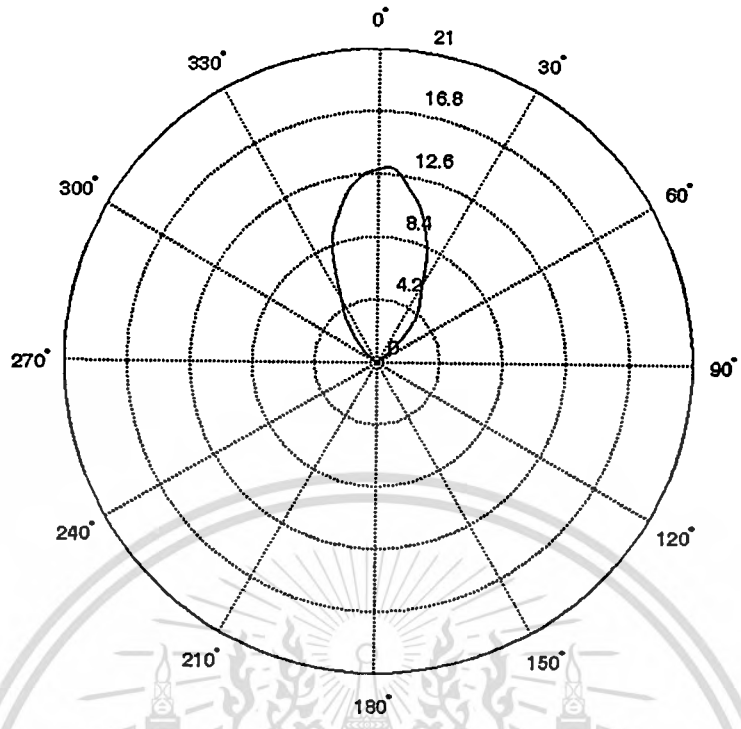

Figure A.48 Transmission gain of root raised cosine passband waveform with received signal template satisfying the FCC spectral mask for indoor limit.

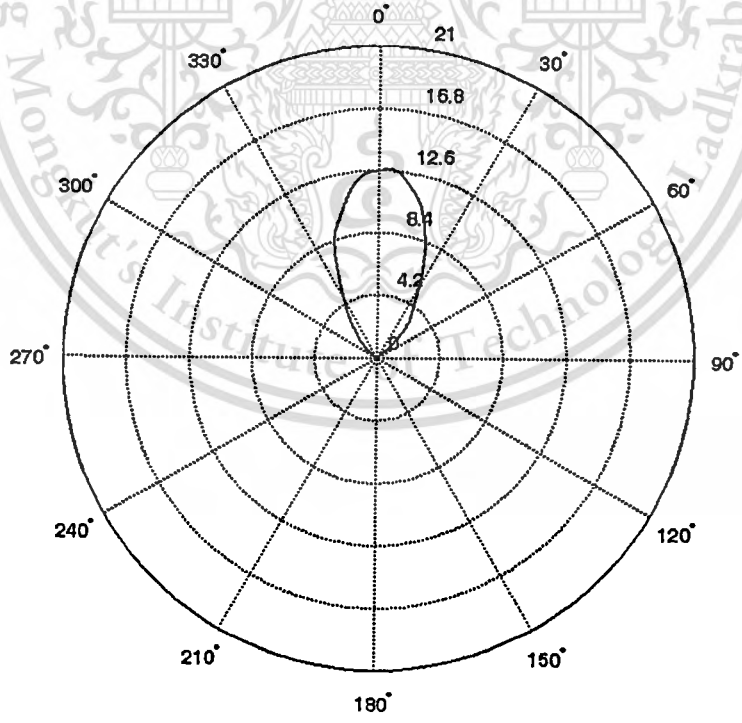

Figure A.49 Transmission gain of root raised cosine passband waveform with received signal template satisfying the FCC spectral mask for outdoor limit.

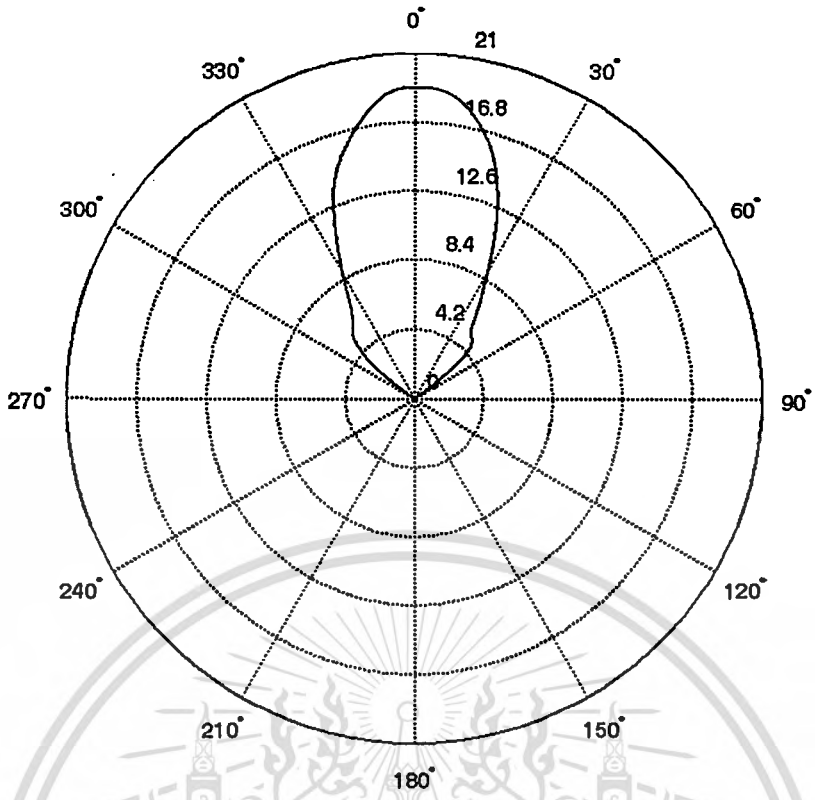

Figure A.50 Transmission gain of root raised cosine passband waveform with received signal template satisfying the common frequency band spectral mask.

RELATED PUBLICATIONS

[1] Sathaporn Promwong, **Pichaya Supanakoon** and Jun-ichi Takada, "Waveform Distortion and Transmission Gain on Ultra Wideband Impulse Radio," IEICE Transactions on Communications, vol. E93-B, no. 10, Oct. 2010.

[2] **Pichaya Supanakoon**, Sathaporn Promwong and Jun-ichi Takada, "Novel Waveform Distortion Parameter for Ultra Wideband Impulse Radio Systems," 2011 International Symposium on Antennas and Propagation (ISAP), ThG3-4, 25-28 Oct. 2011.

[3] **Pichaya Supanakoon**, Sathaporn Promwong and Jun-ichi Takada, "Closed Form Formulas of Correlation Coefficient for Ultra Wideband Impulse Radio Systems," 2011 International Symposium on Antennas and Propagation (ISAP), ThG3-5, 25-28 Oct. 2011.

平成5年4月14日第三種郵便物認可　平成22年9月25日印刷　平成22年10月1日発行　第226号（毎月1回1日発行）　ISSN 0916-8516

on Communications

■ *Special Section on Advanced Technologies in Antennas and Propagation in Conjunction with Main Topics of ISAP2009*

(continued over leaf)

A PUBLICATION OF THE COMMUNICATIONS SOCIETY
The Institute of Electronics, Information and Communication Engineers
Kikai-Shinko-Kaikan Bldg., 5-8, Shibakoen 3 chome, Minato-ku, TOKYO, 105-0011 JAPAN
URL:http://search.ieice.org/cs/

VOL.E93-B NO.10
OCTOBER 2010

2644

IEICE TRANS. COMMUN., VOL.E93–B, NO.10 OCTOBER 2010

PAPER Special Section on Advanced Technologies in Antennas and Propagation in Conjunction with Main Topics of ISAP2009

Waveform Distortion and Transmission Gain on Ultra Wideband Impulse Radio

Sathaporn PROMWONG[†a)], *Member*, **Pichaya SUPANAKOON**[†], *Student Member*, *and* **Jun-ichi TAKADA**[††], *Senior Member*

SUMMARY A waveform of an ultra wideband impulse radio (UWB-IR) system can be extremely distorted through a channel even for free-space transmission because of antenna dispersion. This highly degrades the link budget performance. Therefore, the understand of antenna characteristics, which effects on waveform distortion, is necessary. This paper studies the waveform distortion due to antenna in free space transmission in UWB-IR system. The link budget is usually evaluated by using the Friis' transmission formula. However, it is not directly applicable to the UWB-IR transmission system. The link budget evaluation formula attended from conventional Friis' transmission formula that takes into account the transmitted waveform, its distortion due to the antennas, the channel and the correlation receiver is proposed. Since the antenna is significant pulse-shaping filters in UWB-IR system, the example kind of the log-periodic dipole antenna (LPDA) is experimentally examined, especially focused on the effect of the template waveforms.

key words: *ultra wideband impulse radio (UWB-IR), Friis' transmission formula, antenna, distortion, transmission gain*

1. Introduction

Recently, an ultra wideband impulse radio (UWB-IR) system draws much attention due to its potential low cost and low power consumption properties. In UWB-IR system, any frequency selectivity causes distortion of the transmitting pulse shape. Antennas usually act as significant pulse-shaping filters and cause extreme waveform distortion. Consequently, this will increase the complexity of the detection mechanism at the receiver [1]. Moreover, low cost, geometrically small and still efficient structures are required for the typical wireless applications. Therefore, the knowledge of waveform distortion due to antenna is important to design and improve the performances of UWB-IR system.

The link budget between transmitter (Tx) output and receiver (Rx) output is significant parameter for considering the performances of UWB-IR system. For narrowband wireless systems, Friis' transmission formula is used for the line-of-sight (LOS) link budget evaluation [2]. However, it is not directly applicable to the UWB-IR system as the bandwidth of the pulse is extremely wide and the output signal-to-noise ratio (SNR) depends on the template waveform of the correlation receiver. Moreover, the effect of the waveform distortion shall be quantitatively considered in the link budget evaluation. Therefore, Friis' transmission formula is necessary to extend for UWB-IR system. Several researches such as [3] claimed that the received waveform at Rx antenna terminal is simply considered in the term of derivative of transmitted waveform at Tx antenna terminal. These models are easy and provide initial vision of received waveform, but they are not sufficient for analysis and design. There are some researches about more accurate modeling of link budget for UWB-IR system [4]–[11]. The link budget model composed with input admittance of transmitter, transmission impedance and frequency transfer function of receiver is proposed in [4]. The other models are factorized in the term of the frequency transfer function of each factor. The model composed with frequency transfer functions of Tx antenna and Rx antenna based on radar-range equation is proposed in [5]. The model composed with frequency transfer functions of Tx antenna/channel and Rx antenna is proposed in [6]. Next, the models in the terms of the antenna frequency transfer functions in transmission with reciprocity theorem are developed in [7]–[9]. The other models composed with frequency transfer functions of Tx antenna, channel and Rx antenna are proposed in [10], [11]. Note that these models have the same significance but have the different notation, factorization and definition of each factor. Moreover, the most models do not consider a correlation receiver [4]–[6], [8]–[11]. Although the correlation receiver is included in the model of [7], it does not consider the optimum correlation receiver, which can be considered as the upper boundary of best performance.

The purpose of this paper is to propose a more generalized link budget model for studying the waveform distortion due to antenna on free space transmission in UWB-IR system. We develop the free space link budget evaluation scheme in the term of frequency transfer function for UWB-IR system that takes into account the transmitted waveform, its distortion due to the antennas, the channel and the correlation receiver. This model is based on the Friis' transmission formula, adapted to the UWB-IR transmission system, in the sense that we derive the equivalent frequency transfer function of UWB-IR system [12]–[14]. Rectangular passband waveform is used as the UWB-IR transmitted waveform. Experimental investigations are done for log-periodic dipole antenna (LPDA). The distortion quantities in the terms of waveform distortion and transmission gain

Manuscript received January 5, 2010.
Manuscript revised May 8, 2010.

[†]The authors are with the Department of Telecommunication Engineering, Faculty of Engineering, King Mongkut's Institute of Technology Ladkrabang, Bangkok 10520, Thailand.

[††]The author is with the Graduate School of Engineering, Tokyo Institute of Technology, Tokyo, 152-8550 Japan.

a) E-mail: kpsathap@kmitl.ac.th

DOI: 10.1587/transcom.E93.B.2644

are defined and shown. This scheme provides some useful physical insights and optimized design procedure with clear and accessible description of the UWB-IR link budget comprised of practical antenna. Furthermore, these distortion quantities can be used as reference for performance evaluation of UWB-IR antenna.

The rest of this paper is organized as follows. In Sect. 2, the theory of free space link budget evaluation underlying this paper is explained. Next, the experimental evaluation and its results are shown in Sects. 3 and 4, respectively. Finally, conclusion is discussed in Sect. 5.

2. Model and Theory of Free Space Link Budget Evaluation

In this paper, the short range communication in LOS scenario is assumed, where other multipath components are often less influential to the channel response. Therefore, the propagation channel is assumed to be free space, although it is rather straightforward to extend the discussion to double-directional channel model [15], [16].

2.1 Transmission System Model for UWB-IR System

The Friis' transmission formula [2] has been widely used to evaluate a link budget for the narrowband LOS channels. The Friis' transmission gain $G_{\text{Friis}}(f)$ is defined as

$$\begin{aligned} G_{\text{Friis}}(f) &= \frac{P_{\text{r}}(f)}{P_{\text{t}}(f)}, \\ &= G_{\text{f}}(f,d)G_{\text{r}}(f,\boldsymbol{\Omega}_{\text{r}})G_{\text{t}}(f,\boldsymbol{\Omega}_{\text{t}})\eta_{\text{p}}(f), \end{aligned} \tag{1}$$

where f is the operating frequency, d is the separation between Tx and Rx antennas, $P_{\text{t}}(f)$ and $P_{\text{r}}(f)$ respectively are the input power to the Tx antenna and the output power from the Rx antenna, $G_{\text{t}}(f,\boldsymbol{\Omega}_{\text{t}})$ and $G_{\text{r}}(f,\boldsymbol{\Omega}_{\text{r}})$ respectively are effective gain of Tx and Rx antennas, $G_{\text{f}}(f,d)$ is the free space propagation gain and $\eta_{\text{p}}(f)$ is the polarization matching efficiency. The free space propagation gain can be written as

$$G_{\text{f}}(f,d) = \left(\frac{c}{4\pi df}\right)^2, \tag{2}$$

where c is the velocity of light.

Figure 1(a) shows the block diagram of Eq. (1). In Fig. 1(a), $P_{\text{t}}^{\text{e.i.r.p}}(f,\boldsymbol{\Omega}_{\text{t}})$ is the effective isotropic radiation power from Tx antenna toward $\boldsymbol{\Omega}_{\text{t}}$ direction and $P_{\text{r}}^{\text{e.i.r.p}}(f)$ is the effective isotropic received power at Rx antenna.

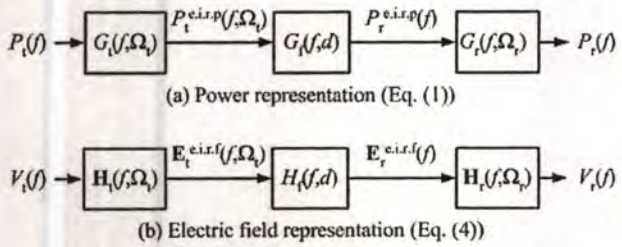

Fig. 1 Block diagram of Friis" transmission formula.

It is noted, however, that Eq. (1) is satisfied only at some frequency, and is not directly applicable to the UWB-IR transmission system. The formula shall be extended to take into account the transmitted waveform, its distortion due to the antennas, the channel and the correlation receiver [12]–[14].

For UWB-IR system, the free space link budget is formulated in the term of frequency transfer function that takes into account the transmitted waveform, its distortion due to the antennas, the channel and the correlation receiver. The free space transfer function $H_{\text{f}}(f,d)$ can be written as

$$H_{\text{f}}(f,d) = \frac{c}{4\pi fd}e^{-\text{j}2\pi fd/c}. \tag{3}$$

Free space channel transfer function $H_{\text{c}}(f)$ including the antennas is obtained by using the extension of Friis' transmission formula as

$$H_{\text{c}}(f) = H_{\text{f}}(f,d)\,\mathbf{H}_{\text{t}}(f,\boldsymbol{\Omega}_{\text{t}})\cdot\mathbf{H}_{\text{r}}(f,\boldsymbol{\Omega}_{\text{r}}), \tag{4}$$

where $\mathbf{H}_a(f,\boldsymbol{\Omega}_a)$ $(a = \text{r}\,or\,\text{t})$ is a complex transfer function vector of the antenna relative to the isotropic antenna towards the $\boldsymbol{\Omega}_a = (\theta_a, \varphi_a)$ direction, i.e.

$$\begin{aligned} \mathbf{H}_a(f,\boldsymbol{\Omega}_{\text{a}}) &= \mathbf{H}_a(f,\theta_a,\varphi_a) \\ &= \hat{\boldsymbol{\theta}}_a H_{a\theta}(f,\theta_a,\varphi_a) + \hat{\boldsymbol{\varphi}}_a H_{a\varphi}(f,\theta_a,\varphi_a), \end{aligned} \tag{5}$$

which has the relation as

$$\frac{1}{4\pi}\int_0^{2\pi}\int_0^{\pi}\|\mathbf{H}_a(f,\theta_a,\varphi_a)\|^2\sin\theta\,\text{d}\theta\,\text{d}\varphi = \eta_a, \tag{6}$$

where η_a is the antenna efficiency, so that the value is normalized by that for isotropic antenna†. Unit vectors $\hat{\boldsymbol{\theta}}_a$, $\hat{\boldsymbol{\varphi}}_a$ express the polarization and are defined with respect to the local polar coordinates of the antennas. The following relations can be easily derived as

$$\hat{\boldsymbol{\theta}}_{\text{r}} = \hat{\boldsymbol{\theta}}_{\text{t}}, \tag{7}$$

$$\hat{\boldsymbol{\varphi}}_{\text{r}} = -\hat{\boldsymbol{\varphi}}_{\text{t}}. \tag{8}$$

By introducing vector notation, $\eta_{\text{p}}(f)$ in Eq. (1) is implicitly taken into account.

For the identical Tx and Rx antennas satisfying Eqs. (7) and (8), the complex transfer functions of Tx and Rx antennas can be written as††

†It is noted that Eq. (2) is often used in the free space link budget evaluation, although it is not correct in the electromagnetic theory [9]. The dependency of f is not really the propagation loss, but is due to the change of reception area of Rx antenna for the same gain. In other words, this is the compensation of the use of the relative gain of the antennas, i.e. $G_{\text{t}}(f,\boldsymbol{\Omega}) = G_{\text{r}}(f,\boldsymbol{\Omega})$, when the same antenna is used as Tx and Rx antennas.

††The factorization of channel transfer function H_{c} of Eq. (4) and the complex transfer functions of identical Tx and Rx antennas of Eq. (9) are mathematically corrected in the sense of identical Tx and Rx antennas should have same gain. However, the factors H_{t}, H_{f} and H_{r} cannot separate physically. In physical situation, H_{t} transfers the transmitting voltage (V) to the electrical field (V/m) and H_{r} transfers the electric field (V/m) to received voltage (V). Physically, the factors H_{t} and H_{r} should have different unit and form.

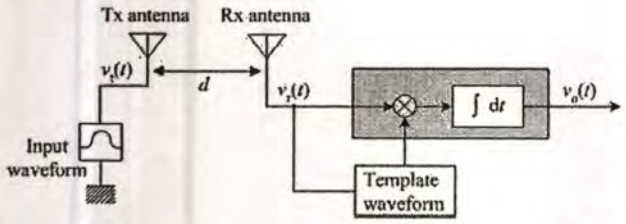

Fig. 2 Block diagram of transmission system model for UWB-IR signal.

$$H_t(f) = H_r(f) = \sqrt{\frac{H_c(f)}{H_f(f,d)}}. \tag{9}$$

Figure 1(b) shows the block diagram of Eq. (4). In Fig. 1(b), $\mathbf{E}_t^{\text{e.i.r.f}}(f, \Omega_t)$ is the effective isotropic radiated field vector from Tx antenna toward Ω_t direction and $\mathbf{E}_r^{\text{e.i.r.f}}(f)$ is the effective isotropic received field vector of Rx antenna.

The receiver input waveform $v_r(t)$ is given by

$$v_r(t) = \int_{-\infty}^{\infty} H_c(f)V_t(f)e^{j2\pi ft}\mathrm{d}f, \tag{10}$$

where $V_t(f)$ is the spectrum of the transmitted waveform.

2.2 Correlation Receiver

Let us consider a correlation receiver shown in Fig. 2. The output SNR is dependent on the choice of the template waveform. The correlator output $v_o(\tau)$ is therefore expressed as

$$v_o(\tau) = \int_{-\infty}^{\infty} v_r(t)h_w(t-\tau)\mathrm{d}t, \tag{11}$$

where $h_w(t)$ is the template waveform and τ corresponds to the timing of the template waveform. The optimum timing τ_o is chosen as

$$\tau_o = \arg\max_{\tau} v_o(\tau). \tag{12}$$

Hereafter $h_w(t)$ is normalized as

$$\int_{-\infty}^{\infty} |h_w(t)|^2\mathrm{d}t = 2B, \tag{13}$$

where B is the signal bandwidth, so that the output noise power is a constant as N_0B, where $N_0/2$ is the power spectral density of additive white Gaussian noise (AWGN).

Under the constraint of Eq. (13), $h_{wm}(t)$ maximizes $v_o(\tau_o)$ when $h_{wm}(t)$ is a time-reversed and scaled version of $v_r(t)$, i.e.

$$h_{wm}(t) = \frac{\sqrt{2B}v_r(\tau_o - t)}{\sqrt{\int_{-\infty}^{\infty} |v_r(t)|^2\mathrm{d}t}}, \tag{14}$$

where τ_o is usually chosen so that $h_{wm}(t) = 0$ for $t < 0$ to satisfy the causality. $h_{wm}(t)$ is called the received signal template waveform hereafter. It is noted that the link budget evaluation is identical to that in [13] when $h_{wm}(t)$ is used as the receiver template.

2.3 Feasibility of the Optimum Correlation Receiver

It is obvious from Eq. (14) that the received signal template waveform is not the simple time-reversed version of the transmitted waveform, but includes the frequency characteristics of the antennas and the free space propagation. Therefore, it is not always feasible to adapt the template waveform to the angular-dependent antenna characteristics, since the waveform shall be generated at the clock rate at least twice as high as the highest frequency of the signal. Therefore, we consider a canonical template waveform $h_{wc}(t)$. In this paper $h_{wc}(t)$ is chosen, which is optimum for the isotropic and the constant gain antennas, i.e.

$$h_{wc}(t) = \frac{\sqrt{2B}v_{r\text{-iso}}(\tau_o - t)}{\sqrt{\int_{-\infty}^{\infty} |v_{r\text{-iso}}(t)|^2\mathrm{d}t}}, \tag{15}$$

where the receiver input voltage for the case of isotropic antennas used in both sides $v_{r\text{-iso}}(t)$ can be written as

$$v_{r\text{-iso}}(t) = \int_{-\infty}^{\infty} H_f(f,d)V_t(f)e^{j2\pi ft}\mathrm{d}f. \tag{16}$$

2.4 Waveform Distortion

The waveform distortion is considered in the term of distortion between received waveform and received waveform for the case of isotropic antennas used in both side and it can be written as

$$W = 1 - \frac{\max\left|\int_{-\infty}^{\infty} v_r^*(t)\cdot v_{r-iso}(t+\tau)\mathrm{d}t\right|}{\sqrt{\int_{-\infty}^{\infty} |v_r(t)|^2\mathrm{d}t \cdot \int_{-\infty}^{\infty} |v_{r-iso}(t)|^2\mathrm{d}t}}, \tag{17}$$

where * is the complex conjugate operator, $v_r(t)$ is the received waveform in time domain and can be evaluated by using inverse Fourier transform of its spectral density

$$v_r(t) = \int_{-\infty}^{\infty} V_r(f)e^{j2\pi ft}\mathrm{d}f. \tag{18}$$

This quantity is equal to 0 when two waveforms are identical and it is increased when the waveform is more differ from another.

2.5 Transmission Gain

The transmission gain in this paper is defined as the peak amplitude of the correlator output with the considered antennas normalized by that with that for the pair of isotropic antennas. Due to the normalization of template waveforms in Eqs. (14) and (15), this gain value represents the gain of SNR ratio. Therefore, the transmission gain of the received signal template case G_{wm} in dBi can be written as

$$G_{wm} = \frac{\max\left|\int_{-\infty}^{\infty} v_r(t)h_{wm}(t-\tau)\mathrm{d}t\right|}{\max\left|\int_{-\infty}^{\infty} v_{r\text{-iso}}(t)h_{wc}(t-\tau)\mathrm{d}t\right|}. \tag{19}$$

Similarly, the transmission gain of the isotropic template case G_{wc} in dBi can be written as

$$G_{wc} = \frac{\max\left|\int_{-\infty}^{\infty} v_r(t)h_{wc}(t-\tau)\mathrm{d}t\right|}{\max\left|\int_{-\infty}^{\infty} v_{r\text{-iso}}(t)h_{wc}(t-\tau)\mathrm{d}t\right|}. \quad (20)$$

The difference between the transmission gain of the received signal and the isotropic template cases also indicates the distortion quantity of the waveform. Different from the original Friis' transmission formula, the optimum transmission gain of UWB-IR signal can not be simply expressed by the product of antenna indices.

3. Experimental Evaluation of Example UWB-IR Antenna Link

In this section, the LOS link with the LPDA is evaluated based on the previous section.

3.1 Transmitted Waveforms

The effect of the waveform distortion is more obvious when the bandwidth is wider. We considered the transmitted waveforms that fully cover the Federal Communications Commission (FCC) frequency band, i.e., 3.1–10.6 GHz [17] and common frequency band available among the FCC of USA, European Conference of Postal and Telecommunications Administrations/Electronic Communications Committee (CEPT/ECC) of Europe and Ministry of Internal Affairs and Communications (MIC) of Japan, i.e., 7.25–8.5 GHz [18].

In this paper, the rectangular passband waveforms is used as the transmitted waveform. The rectangular passband waveform is the waveform with rectangular spectrum and its spectral density is defined as

$$V_{t,re}(f) = \begin{cases} 1 & ||f| - f_c| \le \frac{f_b}{2} \\ 0 & \text{otherwise} \end{cases}, \quad (21)$$

where f_c is the center frequency and f_b is the spectral bandwidth. For satisfying the FCC spectral masks for indoor and outdoor limits, f_c and f_b are set to 6.85 and 7.50 GHz, respectively. For satisfying the common frequency band spectral mask, f_c and f_b are set to 7.875 and 1.250 GHz, respectively.

For analysis of waveform distortion, the root raised cosine passband waveform is used to compare with the rectangular passband waveform. Its spectral density is defined as

$$V_{t,ro}(f) = \begin{cases} 1 & ||f| - f_c| \le \frac{1-\alpha}{2T} \\ A & \frac{1-\alpha}{2T} < ||f| - f_c| \le \frac{1+\alpha}{2T} \\ 0 & \text{otherwise} \end{cases}, \quad (22)$$

where

$$A = \sqrt{\frac{1}{2}\left[\ 1 + \cos\left(\frac{\pi T}{\alpha}\left[|f| - f_c| - \frac{1-\alpha}{2T}\right]\right)\ \right]},$$

$T = 1/f_b$ is the reciprocal of the symbol-rate and $\alpha = 0.3$ is the roll-off factor. For satisfying the FCC spectral mask, the center frequency f_c is set to 6.85 GHz. The spectral bandwidth f_b is set to 6.37 and 5.94 GHz for satisfying FCC spectral masks for indoor and outdoor limits. For satisfying the common frequency band spectral mask, f_c and f_b are set to 7.877 and 0.975 GHz, respectively.

Table 1 Experimental setup parameters.

Parameter	Value
Frequency range	3 GHz to 11 GHz
Number of frequency points	1601
Dynamic range	80 dB
Tx antenna height	1.75 m
Rx antenna height	1.75 m
Distance between Tx and Rx	3 m
Rx rotation range	0° to 360°
Rx rotation step	5°
Rx rotation cut	E- or H-plane

3.2 Experimental Setup and Measurement Model

The UWB-IR radio channel transfer function was measured as S_{21} in frequency domain by using a vector network analyzer (VNA) in an anechoic chamber. The VNA was operated in the response measurement mode, where Port-1 was the Tx port and Port-2 was the Rx port, respectively. Both Tx and Rx antennas were fixed at the height of 1.75 m and separated by 3 m.

The experimental parameters are listed in Table 1. It is noted that the calibration of VNA is done at the connectors of the cables to be connected to the antennas. Therefore, all the impairments of the antenna characteristics are included in the measurement results.

3.3 Data Processing

The waveform transmission was simulated by using $V_t(f)$ defined in Sect. 3.1, $H_c(f)$ measured in Sect. 3.2 and the correlation receiver presented in Sects. 2.2 and 2.3. As the template waveforms, we considered the received signal template waveform $h_{wm}(t)$ which was optimized for each transmission channel setup, i.e. antennas and their pointing directions, as well as the isotropic template waveform $h_{wc}(t)$ designed for the isotropic antennas and independent of antenna setup. The waveform distortions defined in Sect. 2.4 is evaluated. The UWB-IR transmission gain presented in the next section was normalized by the transmission gain of the isotropic antennas at both Tx and Rx sides as defined in Sect. 2.5.

3.4 Results

A log-periodic dipole antenna (LPDA) is also used at broadband. It also has a frequency-independent gain. The dispersion characteristic of the LPDA is rather big, since the phase center changes with frequency due to the resonance of the dipole elements [19]. We used a commercial LPDA, Watkins–Johnson's AR7–15A, shown in Fig. 3. The antenna

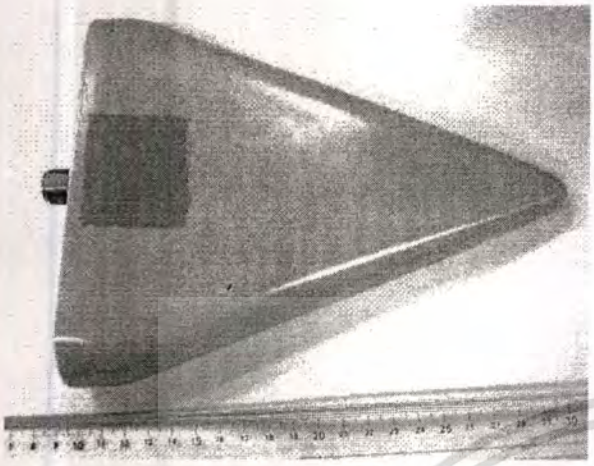

Fig. 3 Log-periodic dipole antenna (Watkins–Johnson AR7–15A).

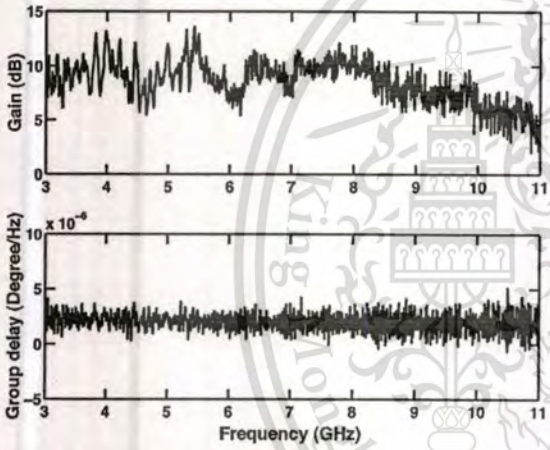

Fig. 4 Gain and group delay of LPDA–LPDA link at 0° pointing angle.

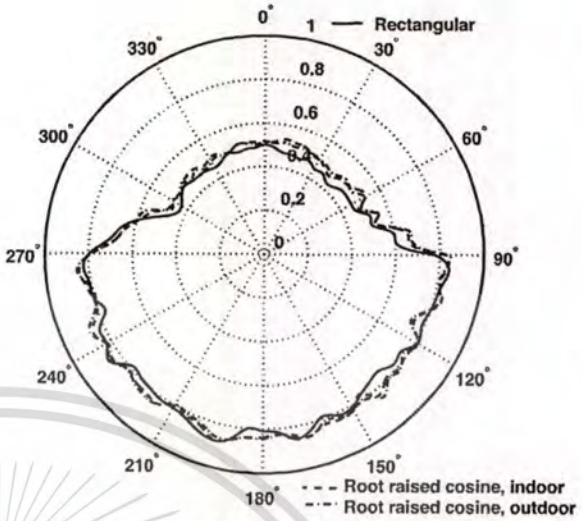

Fig. 5 Waveform distortion of waveform satisfying FCC spectral mask for LPDA-LPDA link.

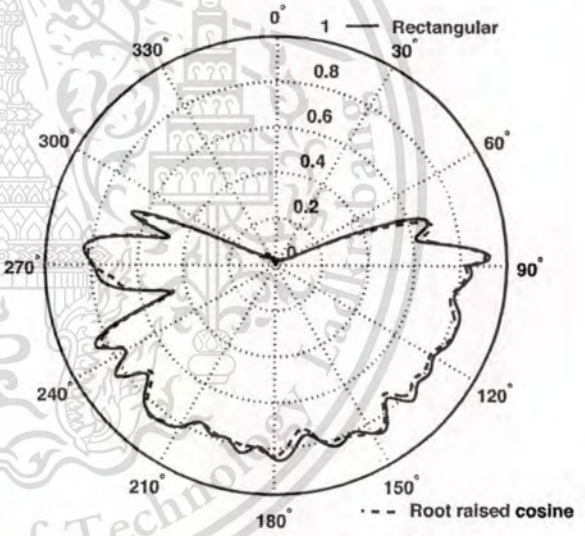

Fig. 6 Waveform distortion of waveform satisfying common frequency band spectral mask for LPDA-LPDA link.

has been designed to operate in the range of 1 to 12.4 GHz.

The channel transfer function of LPDA–LPDA link was measured and evaluated as function of the antenna pointing angle in the E-plane with rotation of both antennas. Gain and group delay of LPDA–LPDA link at 0° pointing angle are shown in Fig. 4. As well known, the constant gain and group delay are need for the distortionless case. The standard deviation of gain and group delay are 1.74 dB and 7.45×10^{-7} degree/Hz in FCC frequency band (3.1–10.6 GHz), while the standard deviation of gain and group delay are 0.85 dB and 7.43×10^{-7} degree/Hz in common frequency band (7.25–8.5 GHz). That means the distortion in FCC frequency band is more than that in common frequency band. However, the UWB-IR signal is detected using correlation receiver in time domain. Therefore, the quantity of distortion is should be derived in time domain. In this paper, the distortion quantities in the terms of waveform distortion and transmission gain are evaluated.

Figures 5 and 6 show the waveform distortions of waveforms satisfying FCC and common frequency band spectral masks, respectively. Averagely, the waveform distortion of waveform satisfying FCC spectral mask is more than that satisfying common frequency band spectral mask, especially at 0° pointing angle. That is because the bandwidth of FCC frequency band is much wider than that of common frequency band. The trend of frequency dispersion is higher. As shown in Fig. 4, the standard deviations of gain and group delay in FCC frequency band are more than that in common frequency band.

The transmission gain of waveform satisfying FCC spectral mask compared with transmission gain at 6.85 GHz, which is center frequency of FCC frequecy band, is shown in Fig. 7. Figure 8 shows the transmission gain of waveform satisfying common frequency band spectral mask compared with transmission gain at 7.875 GHz, which is center frequency of common frequecy band. As is known, an LPDA

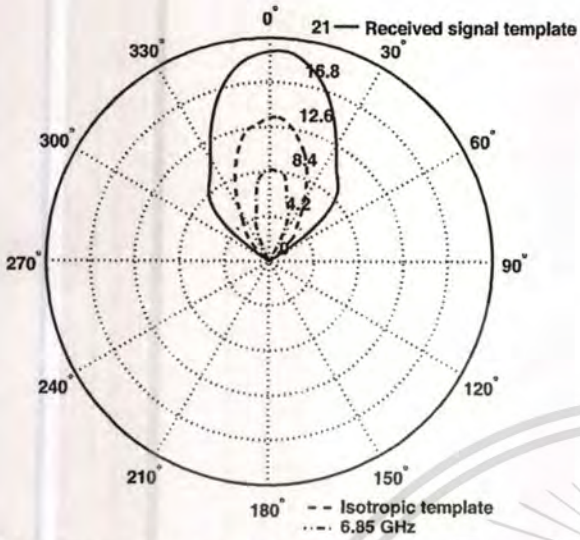

Fig. 7 Transmission gain satisfying FCC spectral mask compared with transmission gain at 6.85 GHz for LPDA–LPDA link.

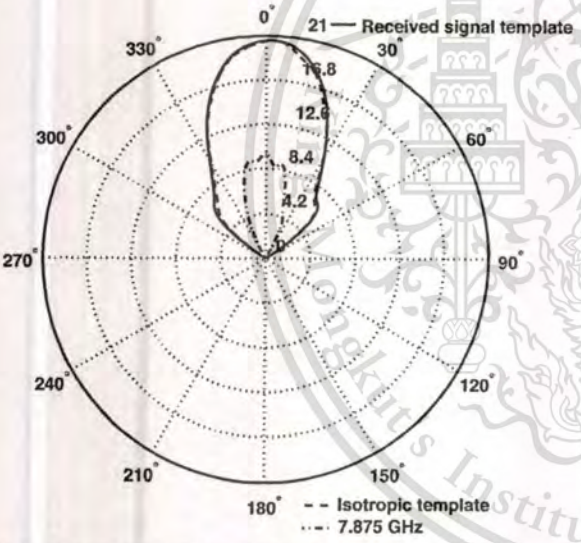

Fig. 8 Transmission gain satisfying common frequency band spectral mask compared with transmission gain at 7.875 GHz for LPDA–LPDA link.

is uni-directional and its gain is high. The difference between transmission gains used received signal and isotropic templates satisfying FCC spectral mask is clearly more than that satisfying common frequency band spectral mask. The difference between transmission gains used received signal and isotropic templates indicates the distortion quantity. Therefore, the difference of transmission gain correspond to the waveform distortion in the same way. As seen from the results, the waveform distortion and the difference of transmission gain are large for FCC spectral mask and small for common frequency band spectral mask. For comparison between proposed UWB-IR transmission gains and conventional transmission gains at their center frequencies, the proposed UWB-IR transmission gains are clearly higher than conventional transmission gains at their center frequencies. That is because the proposed UWB-IR transmission gains consider correlation receiver and include the SNR gain of correlation receiver satisfying the conditions of Eqs. (14) and (15).

4. Discussion

From these results, the UWB-IR transmission gain, using both the received signal and the isotropic template waveforms, gives us the quantitative measurement of the link budget. Since we have chosen the broadband antennas, the trend of the narrowband gain is reflected in the UWB-IR transmission gain. Another issue is the distortion due to the antennas. It is obvious that although LPDA antenna has higher transmission gain, the distortion due to the LPDA antenna is high. Due to the higher spectral bandwidth, the waveform distortion and transmission gain satisfying FCC spectral mask are more than that satisfying common frequency band spectral mask.

5. Conclusion

This paper has presented how to evaluate the link budget of UWB-IR transmission gain, which includes the transmitted waveform, the antennas, the free space propagation, and the correlation receiver. By using the proposed definition, we have evaluated example LPDA. This scheme may be effective especially to evaluate the deployable antenna with non-ideal frequency characteristics of return loss and directivity, as the overall performance can be evaluated only by the term of the UWB-IR transmission gain.

Note that the formulation presented in [13] is a special case for the optimum template waveform in this paper. Therefore, the IEEE 802.15.3a path loss model presented in [20] is also a special case of the formulation presented in this paper, by considering the rectangular frequency spectrum, the frequency independent isotropic antenna and the received signal template.

This approach can be easily extended to the multipath environment as well. There are two key issues: One is the focus of this paper, i.e. the antenna transfer function is angular-dependent. The other one is that the propagation channel is also angular dependent at both Tx and Rx. In the context of UWB-IR system, just a few studies have been done with respect to the former aspect, and almost none for the latter. Although Ref. [7] treated both antenna and multipath channels, it only considered the impulse response of the whole channel. However, the impulse response itself is influenced by the antennas, and the formulation for multipath environment is not sufficient. The authors are working on the double-directional modeling of UWB-IR channel in parallel to this study [15], [16]. Due to this background, the authors are planning to treat the multipath environment by using this approach in future. The use of the rake receiver may solve the antenna distortion and delay spread of propagation environment simultaneously.

Acknowledgement

The authors would like to thank Mr. Kimio Sakurai and Mr. Wataru Hachitani of Tokyo Institute of Technology for his help in the experiments, Prof. Koichi Ito and Dr. Kazuyuki Saito of Chiba University for letting us use their LPDA.

References

[1] K. Siwiak, "Impact of ultra wide band transmissions on a generic receiver," Proc. 2001 Spring IEEE Veh. Tech. Conf. (VTC), vol.2, pp.1181–1183, Rhodes, Greece, May 2001.
[2] H.T. Friis, "A note on a simple transmission formula," Proc. IRE, vol.34, no.5, pp.254–256, May 1946.
[3] H.F. Harmuth, Antennas and Waveguides for Nonsinusoidal Waves, Academic Press, Orlando, 1984.
[4] A.O. Boryssenko and D.H. Schaubert, "Antenna link transfer function factorization applied to optimized channel design," IEEE Trans. Antennas Propag., vol.54, no.10, pp.2878–2889, Oct. 2006.
[5] D. Lamensdorf and L. Susman, "Baseband-pulse-antenna techniques," IEEE Antennas Propag. Mag., vol.36, no.1, pp.20–30, Feb. 1994.
[6] A.H. Mohammadian, A. Rajkotia, and S.S. Soliman, "Characterization of UWB transmit-receive antenna system," Proc. IEEE Conf. Ultra Wideband Syst. Tech. (UWBST) 2003, pp.157–161, Reston, USA, Nov. 2003.
[7] A. Sibille, "A Framework for analysis of antenna effect in UWB communications," Proc. 2005 Spring IEEE Veh. Tech. Conf. (VTC), vol.1, pp.48–52, Texas, USA, June 2005.
[8] W. Sörgel and W. Wiesbeck, "Influence of the antennas on the ultra-wideband transmission," EURASIP J. Applied Signal Processing, pp.296–305, 2005.
[9] J. Kunisch, "Implications of Lorentz reciprocity for ultra-wideband antennas," Proc. IEEE. Int. Conf. Ultrawideband (ICUWB), pp.214–219, Sept. 2007.
[10] Z.N. Chen, X.H. Wu, H.F. Li, N. Yang, and M.Y.W. Chia, "Considerations for source pulses and antennas in UWB radio systems," IEEE Trans. Antennas Propag., vol.52, no.7, pp.1739–1748, July 2004.
[11] Y. Duroc, A. Ghiotto, T.P. Vuong, and S. Tedjini, "UWB antenna: Systems with transfer function and impulse response," IEEE Trans. Antennas Propag., vol.55, no.5, pp.1449–1451, May 2007.
[12] J. Takada, S. Promwong, and W. Hachitani, "Extension of Friis' transmission formula for ultra-wideband systems," IEICE Technical Report, WBS2003-8/MW2003-20, May 2003.
[13] S. Promwong, and J. Takada, "Free space link budget estimation scheme for ultra wideband impulse radio with imperfect antennas," IEICE Electronics Express, vol.1, no.7, pp.188–192, July 2004.
[14] S. Promwong, W. Hachitani, and J. Takada, "Free space link budget evaluation of UWB-IR systems," Proc. 2004 Int. Workshop Ultra Wideband Syst./Conf. Ultra Wideband Syst. Tech. (Joint UWBST & IWUWBS 2004), pp.312–316, Kyoto, Japan, May 2004.
[15] J. Takada, K. Haneda, and H. Tsuchiya, "Joint DOA/DOD/DTOA estimation system for UWB double directional channel modeling," in ed. S. Changran, Advance in Direction of Arrival Estimation, pp.345–362, Artech House, Norwood, MA, USA, 2006.
[16] K. Haneda, J. Takada, and T. Kobayashi, "Double directional ultra wideband channel characterization in a line-of-sight home environment," IEICE Trans. Fundamentals, vol.E88-A, no.9, pp.2264–2271, Sept. 2005.
[17] Federal Communications Commission, "Revision of part 15 of the commissions rules regarding UWB transmission systems," First Report, FCC 02-48, April 2002.
[18] W. Hirt and M. Weisenhorn, "Overview and implications of the emerging global UWB radio regulatory framework," Proc. 2006 IEEE Int. Conf. on Ultra-Wideband, pp.581–586, Sept. 2006.
[19] H.G. Schantz, "Dispersion and UWB antennas," Proc. 2004 Int. Workshop Ultra Wideband Syst./Conf. Ultra Wideband Syst. Tech. (Joint UWBST & IWUWBS 2004), Kyoto, Japan, May 2004.
[20] J. Foerster, "Channel modeling sub-committee report final," IEEE P802.15-02/368r5-SG3a, Nov. 2002.

Sathaporn Promwong was born in Chiang-Mai, Thailand. He received the B. Ind. Tech. degree in Electronic Technology, M.E. degree in Electrical Engineering from King Mongkut's Institute of Technology Ladkrabang, Bangkok, Thailand, and Ph.D. degree in Communications and Integrated Systems from Tokyo Institute of Technology, Tokyo, Japan in 1994, 1999, and 2009 respectively. Since 1995, he has joined in the department of Information Engineering, now he has joined in the school of Telecommunication Engineering, Faculty of Engineering, King Mongkut's Institute of Technology Ladkrabang. His research is interested in the area of Ultra Wideband (UWB) systems, antenna and radio wave propagation. He is a member of the ECTI and IEEE.

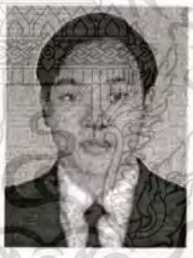

Pichaya Supanakoon received the B.E. degree in Telecommunication Engineering and M.E. degree in Electrical Engineering both from King Mongkut's Institute of Technology Ladkrabang, Bangkok, Thailand, in 1998 and 2000, respectively. Since 1999, he has been with the Department of Information Engineering, now he has joined in the school of Telecommunication Engineering, Faculty of Engineering, King Mongkut's Institute of Technology Ladkrabang. From 2004, he has been an Assistance Professor at King Mongkut's Institute of Technology Ladkrabang. His research interests are in ultra wideband (UWB) communications, electromagnetic field computation and radio wave propagation. He is a student member of the IEEE and ECTI.

Jun-ichi Takada received the B.E., M.E. and D.E. degrees from Tokyo Institute of Technology, Tokyo Japan in 1987, 1989, and 1992, respectively. He was with Chiba University in 1992 to 1994. Since 1994 he has been with Tokyo Institute of Technology, and he is currently a Professor. His current interests are wireless propagation and channel modeling, array signal processing, cognitive radio system, and ICT applications in international development. He received Achievement Award of IEICE in 2008.

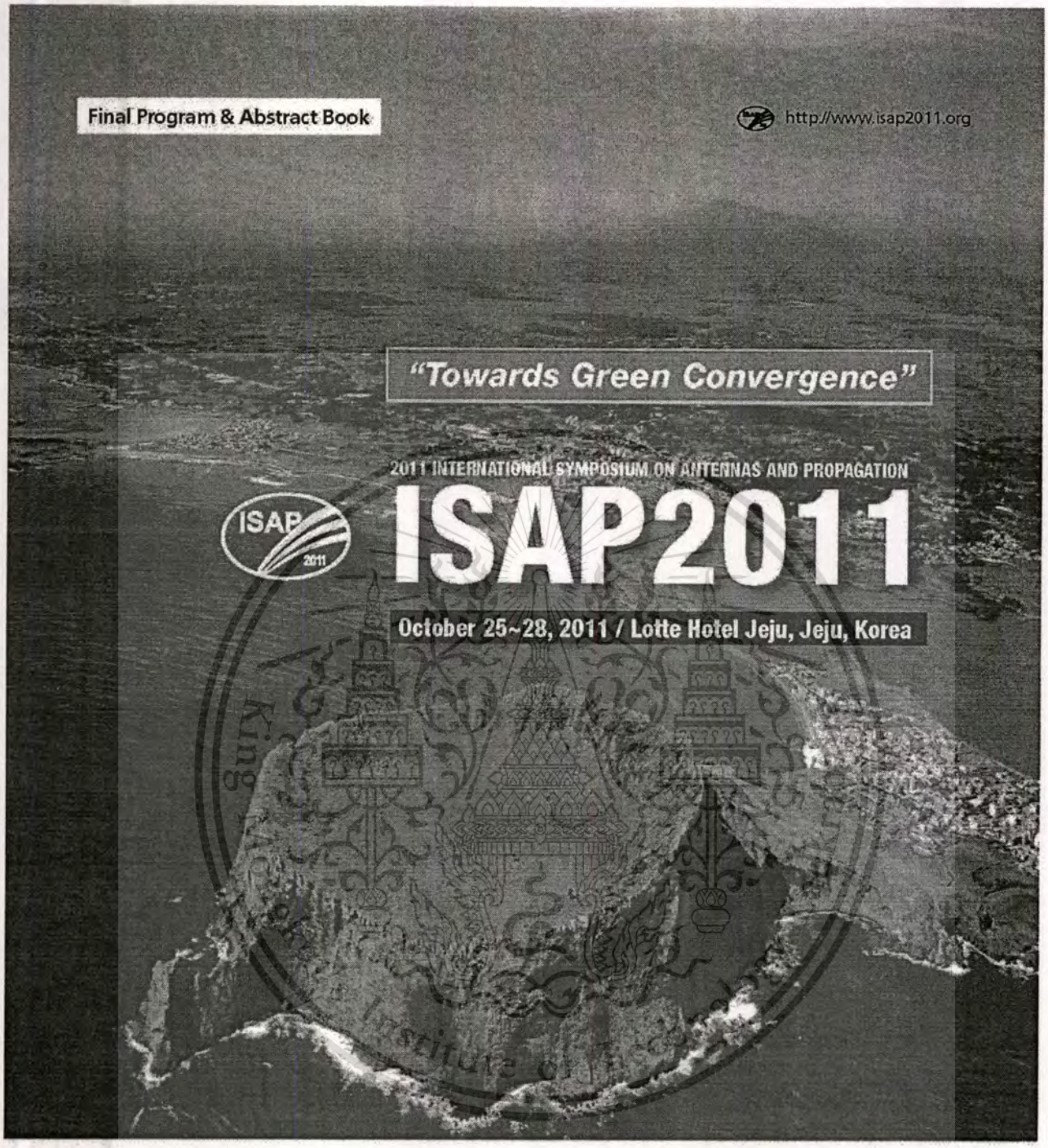

Organized & Sponsored by

- Korean Institute of Electromagnetic Engineering and Science (KIEES)

Co-Sponsored by

- Institute of Electronics, Information and Communication Engineers (IEICE)

Technically Co-Sponsored by

- Antennas and Propagation Society of the Institute of Electrical and Electronics Engineers (IEEE/AP-S)
- Antennas Society of CIE (CIE-AS)
- International Union of Radio Science (URSI)
- The Institute of Electronics Engineers of Korea (IEEK)
- IEEE AP-S Seoul Chapter

KIEES · CIE · IEEE AP-S · CIE-AS · IEEE AP-S Seoul Chapter · URSI · IEEK

Novel Waveform Distortion Parameter for Ultra Wideband Impulse Radio Systems

#Pichaya Supanakoon†, Sathaporn Promwong† and Jun-ichi Takada††

† Department of Telecommunication Engineering, Faculty of Engineering,
King Mongkut's Institute of Technology Ladkrabang, Bangkok 10520, Thailand.
Email: {kspichay, kpsathap}@kmitl.ac.th

†† Graduate School of Engineering, Tokyo Institute of Technology,
2-12-1-S6-4, O-okayama, Meguro-ku, Tokyo, 152-8550, Japan.
Email: takada@ide.titech.ac.jp

Abstract

Study of waveform distortion is necessary for designing optimum ultra wideband impulse radio (UWB-IR) systems because the distortion of waveform degrades the performance of correlation receiver. In this paper, the novel quantitative parameter of waveform distortion that is peak to average loss ratio is proposed and derived in the closed form formula for UWB-IR transmissions. The peak to average loss ratio is defined as the ratio between peak power loss and average power loss from transmitter (Tx) to receiver (Rx). The free space and ground reflection channels are considered. The results obtained from proposed formula are compared with measurement. This proposed parameter is useful to define the quantity of waveform distortion in UWB-IR systems.

Keywords : ultra wideband impulse radio (UWB-IR), waveform distortion

1 Introduction

For ultra wideband impulse radio (UWB-IR) transmission, very high peak short pulse with very low duty cycle allow to obtain the ultra low power consumption. The peak power loss and average power loss from transmitter (Tx) and receiver (Rx) are equal for the distortionless condition. However, the distortion of UWB-IR waveform due to frequency and time dispersion of channel cases the difference. Therefore, the ratio between peak power loss and average power loss from Tx to Rx can be defined as the quantity of waveform distortion.

In this paper, the novel quantitative parameter that is peak to average loss ratio is proposed and derived in the closed form formula for UWB-IR transmissions. The peak to average loss ratio is defined as the ratio between peak power loss and average power loss from Tx to receiver Rx. The free space and ground reflection channels are considered. The measurement was done for the ground reflection channel. The results obtained from proposed formula are shown and compared with measurement.

2 Peak to Average Loss Ratio

For deriving the peak to average loss ratio, the transmitted waveform is defined as rectangular passband waveform [1]. The expression of this waveform in time domain v_t and its spectral density V_t are

$$v_t(t) = \frac{1}{f_b}[f_H \mathrm{sinc}(2f_H t) - f_L \mathrm{sinc}(2f_L t)], \quad (1)$$

$$V_{\mathrm{t}}(f) = \begin{cases} \frac{1}{2f_{\mathrm{b}}} & ||f| - f_{\mathrm{c}}| \leq \frac{f_{\mathrm{b}}}{2} \\ 0 & ||f| - f_{\mathrm{c}}| > \frac{f_{\mathrm{b}}}{2} \end{cases}, \tag{2}$$

where t is the time, f is the frequency, f_{c} is the center frequency, f_{b} is the spectral bandwidth, $f_{\mathrm{L}} = f_{\mathrm{c}} - f_{\mathrm{b}}/2$ is the lowest frequency, $f_{\mathrm{H}} = f_{\mathrm{c}} + f_{\mathrm{b}}/2$ is the highest frequency and $\mathrm{sinc}(x) = \sin(\pi x)/(\pi x)$.

The spectral density of received waveform V_{r} is calculated by using multiplication between frequency transfer function of channel H_{c} and V_{t}. Subsequently, the received waveform in time domain v_{r} is calculated by using inverse Fourier transform of its spectral density, which can be respectively written as

$$V_{\mathrm{r}}(f) = H_{\mathrm{c}}(f) \cdot V_{\mathrm{t}}(f), \tag{3}$$

$$v_{\mathrm{r}}(t) = \int_{-\infty}^{\infty} V_{\mathrm{r}}(f) \cdot e^{j2\pi ft} \mathrm{d}f. \tag{4}$$

In this paper, the Tx and Rx antennas are assumed to be isotropic antennas and H_{c} is considered for free space and ground reflection channels.

The peak to average loss ratio PAR in dB is defined as the ratio between peak power loss and average power loss from Tx to Rx, which can be written as

$$PAR = 10 \log \left\{ \frac{\max[v_{\mathrm{t}}^2(t)]}{\max[v_{\mathrm{r}}^2(t)]} \cdot \frac{\int_{-\infty}^{\infty} |V_{\mathrm{r}}(f)|^2 \mathrm{d}f}{\int_{-\infty}^{\infty} |V_{\mathrm{t}}(f)|^2 \mathrm{d}f} \right\}. \tag{5}$$

This proposed definition is used to derive the closed form formula for free space and ground reflection channels.

2.1 Free Space Channel

The extension of Friis' transmission formula [2] is used to characterize the UWB-IR free space channel. The frequency transfer function of free space channel $H_{\mathrm{c,f}}$ can be written as

$$H_{\mathrm{c,f}}(f) = \frac{c}{4\pi |f| d} e^{-j2\pi fd/c}, \tag{6}$$

where c is the velocity of light and d is the distance from Tx to Rx.

From definition of peak to average loss ratio in Eq. (5), the closed form formula of peak to average loss ratio for free space channel PAR_{f} can be derived as

$$PAR_{\mathrm{f}} = 20 \log \left[\frac{f_{\mathrm{b}}}{\sqrt{f_{\mathrm{H}} f_{\mathrm{L}}} \ln \left(\frac{f_{\mathrm{H}}}{f_{\mathrm{L}}} \right)} \right]. \tag{7}$$

2.2 Ground Reflection Channel

The frequency transfer function of ground reflection channel $H_{\mathrm{c,g}}$ is the addition between frequency transfer function of direct and reflection paths, and can be written as

$$H_{\mathrm{c,g}}(f) = \frac{c}{4\pi |f| d'} e^{-j2\pi fd'/c} + \Gamma \frac{c}{4\pi |f| d''} e^{-j2\pi fd''/c}, \tag{8}$$

where Γ is the reflection coefficient of ground $d' = \sqrt{(h_{\mathrm{t}} - h_{\mathrm{r}})^2 + d^2}$ and $d'' = \sqrt{(h_{\mathrm{t}} + h_{\mathrm{r}})^2 + d^2}$ are distances of direct and reflection paths, h_{t} and h_{r} are the heights of Tx and Rx antennas, respectively.

From definition of peak to average loss ratio in Eq. (5), the closed form formula of peak to average loss ratio for ground reflection channel PAR_{g} can be derived as

$$PAR_{\mathrm{g}} = 10\log\left\{\frac{f_{\mathrm{b}}^2(d''^2+\Gamma^2 d'^2) - 2\Gamma f_{\mathrm{L}} f_{\mathrm{H}} f_{\mathrm{b}} d' d'' \left[\mathrm{Cd}\left(\frac{2\pi\Delta d}{c}\right) + \frac{2\pi\Delta d}{c}\mathrm{Sid}\left(\frac{2\pi\Delta d}{c}\right)\right]}{f_{\mathrm{L}} f_{\mathrm{H}}\left[d''\ln\left(\frac{f_{\mathrm{H}}}{f_{\mathrm{L}}}\right) + \Gamma d'\mathrm{Cid}\left(\frac{2\pi\Delta d}{c}\right)\right]^2}\right\}, \tag{9}$$

where $\Delta d = d'' - d'$ is the different distance between direct and reflection paths, $\mathrm{Cid}(x) = \mathrm{Ci}(xf_{\mathrm{H}}) - \mathrm{Ci}(xf_{\mathrm{L}})$, $\mathrm{Sid}(x) = \mathrm{Si}(xf_{\mathrm{H}}) - \mathrm{Si}(xf_{\mathrm{L}})$, $\mathrm{Cd}(x) = \frac{1}{f_{\mathrm{H}}}\cos(xf_{\mathrm{H}}) - \frac{1}{f_{\mathrm{L}}}\cos(xf_{\mathrm{L}})$, $\mathrm{Ci}(x) = -\int_x^\infty \frac{1}{\tau}\cos(\tau)\mathrm{d}\tau$, and $\mathrm{Si}(x) = \int_0^x \frac{1}{\tau}\sin(\tau)\mathrm{d}\tau$ are cosine integral and sine integral functions.

3 Measurement

The measurement equipment, setup and parameters are the same as in [3]. The frequency transfer function of ground reflection channel was measured using a vector network analyzer (VNA). The measurement was done in the open area that is the soccer field of King Mongkuts Institute of Technology Ladkrabang (KMITL), Thailand. The metallic plate was laid on the ground between Tx and Rx antennas for the perfect reflection condition ($\Gamma = -1$). The measurement setup is shown in Fig. 1.

The biconical antennas were used as Tx and Rx antennas. Both Tx and Rx antennas were fixed at the height of $h_{\mathrm{t}} = h_{\mathrm{r}} = 0.75$ m with horizontal polarization for focusing the signal from direct and ground reflection paths. The measurement distance d was ranged from 1 to 5 m with 0.25 m distance increment step. The frequency transfer functions of Tx and Rx antennas were evaluated by using three-antenna method [4] and were used to remove from the measurement frequency transfer functions of the ground reflection channels. The center frequency of waveform f_{c} is fixed at 4.1 GHz. The two cases of signal bandwidths are investigated, that are $f_{\mathrm{b}} = 0.5$ and 1.4 GHz. Therefore, the lowest frequencies f_{L} are equal to 3.85 and 3.40 GHz, while the highest frequencies f_{H} are equal to 4.35 and 4.80 GHz for fist and second cases, respectively.

4 Results

For free space channel, parameters f_{c} is fixed at 6.85 GHz and f_{b} is varied from 500 MHz to 7.5 GHz. Figure 2 shows the peak to average loss ratio for free space channel. At narrow bandwidth, the peak to average loss ratio is approached to zero. In other word, there is slight distortion of narrow bandwidth waveform for free space channel. The maximum peak

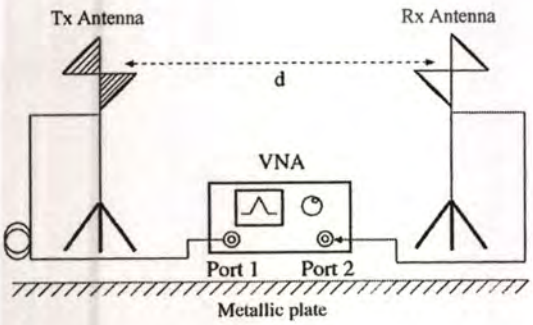

Figure 1: Measurement setup.

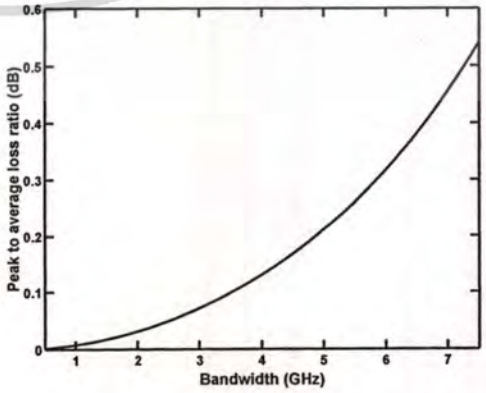

Figure 2: Peak to average loss ratio along 500 MHz to 7.5 GHz bandwidth for free space channel.

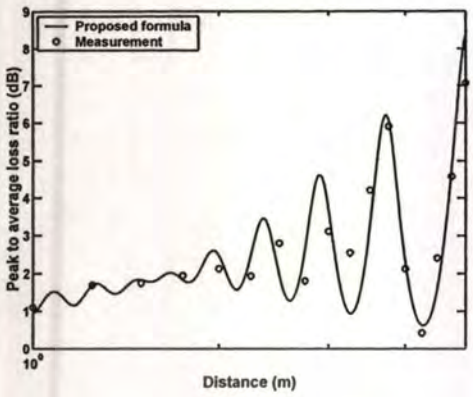

Figure 3: Comparison between peak to average loss ratio from proposed formula and measurement with 500 MHz bandwidth.

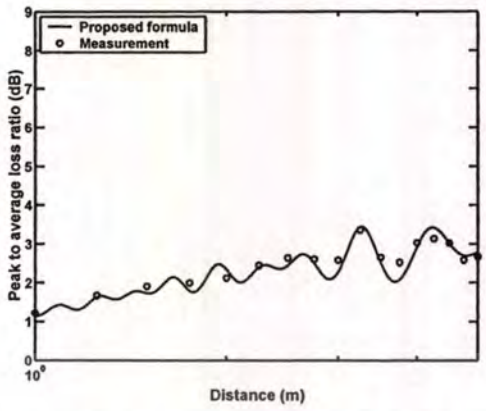

Figure 4: Comparison between peak to average loss ratio from proposed formula and measurement with 1.4 GHz bandwidth.

to average loss ratio is 0.54 dB at 7.5 GHz bandwidth. The distortion of waveform is caused by frequency dispersion. That is the magnitude of frequency transfer function of free space channel is not constant along frequency.

For ground reflection channel, the analyzed parameters are the same as measurement. Figures 3 and 4 show the comparison between peak to average loss ratio from proposed formula and measurement with 500 MHz and 1.4 GHz bandwidths, respectively. Unlike with free space channel, the peak to average loss ratio of wide bandwidth is less than that of narrow bandwidth because the main waveform distortion causes from time dispersion or multipath fading. Therefore, the UWB-IR systems are robust to multipath fading more than narrowband systems. The distortion of waveform is also dependent on distance.

5 Conclusions

In this paper, the novel quantitative parameter that is peak to average loss ratio is proposed and derived in the closed form formula for UWB-IR transmissions. From the results, the proposed formula corresponds with measurement. For free space channel, the waveform distortion is caused by frequency dispersion and is higher when bandwidth is increased. On the other hand, the waveform distortion is caused by time dispersion and is lower when bandwidth is increased for ground reflection channel. In addition, the waveform distortion is dependent on distance and is much more than free space channel. This proposed parameter is useful to define the quantity of waveform distortion in UWB-IR systems.

References

[1] P. Supanakoon, K. Wansiang, S. Promwong and J. Takada, "Simple waveform for UWB communication," *Electrical Engineering/Electronics, Computer, Telecommunication, and Information Technology International Conference (ECTI-CON)*, pp. 626-629, 12-13 May 2005.

[2] J. Takada, S. Promwong and W. Hachitani, "Extension of Friis' transmission formula for ultra wideband systems," *Technical Report of IEICE*, WBS2003-8/MW2003-20, May 2003.

[3] S. Promwong, P. Supanakoon and J. Takada, "Ground refection transmission loss evaluation scheme for ultra wideband impulse radio," *ECTI-EEC Transactions on Electrical Engineering, Electronics, and Communications*, vol. 5, no. 1, pp. 18-24, Jan. 2007.

[4] S. Promwong, W. Hachitani and J. Takada, "Free space link budget evaluation of UWB-IR systems," *International Workshop on Ultra Wideband System Joint with Conference on Ultra Wideband Systems and Technologies (UWBST & IWUWBS)*, pp. 312-316, May 2004.

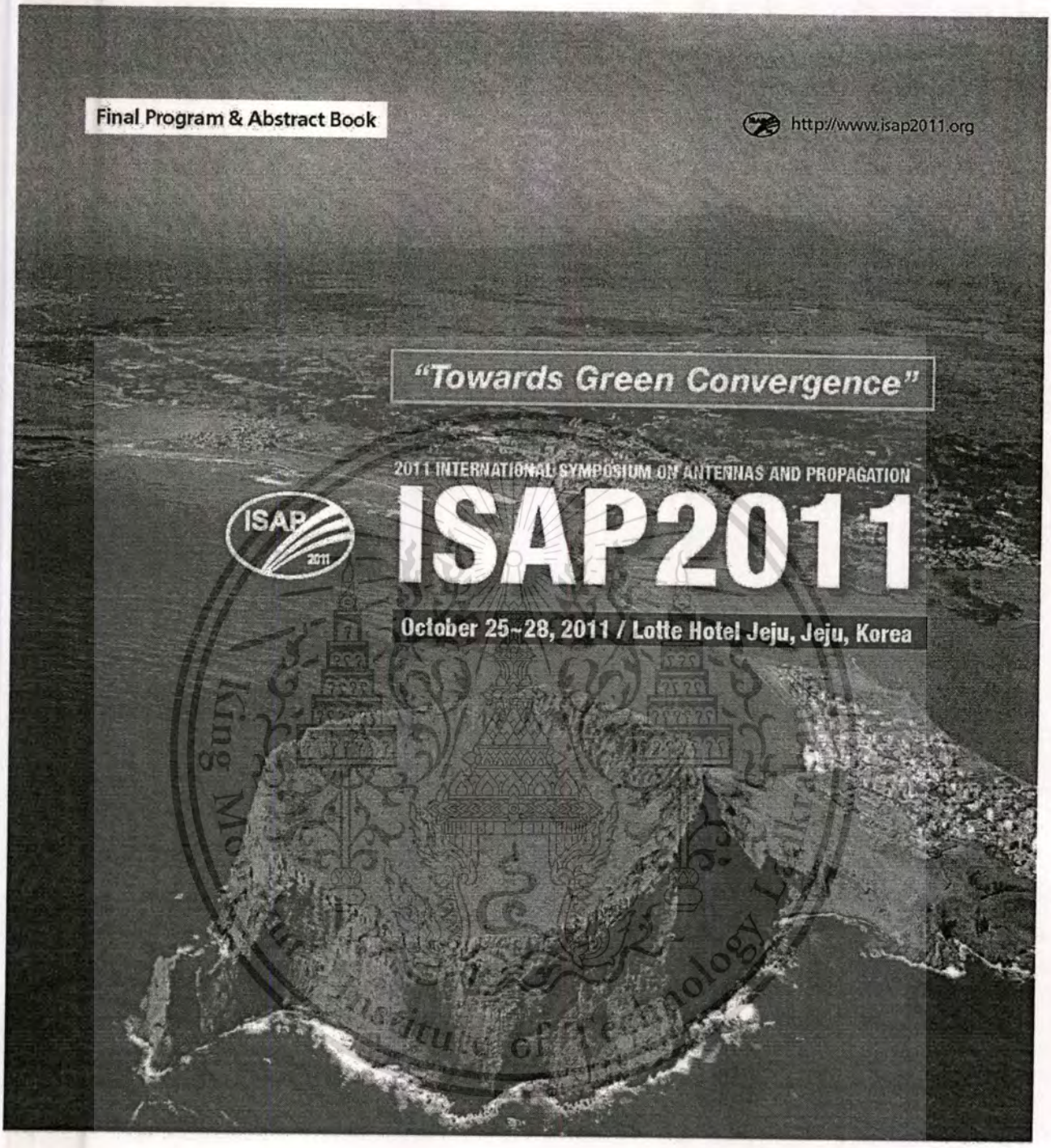

Organized & Sponsored by

- Korean Institute of Electromagnetic Engineering and Science (KIEES)

Co-Sponsored by

- Institute of Electronics, Information and Communication Engineers (IEICE)

Technically Co-Sponsored by

- Antennas and Propagation Society of the Institute of Electrical and Electronics Engineers (IEEE/AP-S)
- Antennas Society of CIE (CIE-AS)
- International Union of Radio Science (URSI)
- The Institute of Electronics Engineers of Korea (IEEK)
- IEEE AP-S Seoul Chapter

Closed Form Formulas of Correlation Coefficient for Ultra Wideband Impulse Radio Systems

#Pichaya Supanakoon†, Sathaporn Promwong† and Jun-ichi Takada††

† Department of Telecommunication Engineering, Faculty of Engineering,
King Mongkut's Institute of Technology Ladkrabang, Bangkok 10520, Thailand.
Email: {kspichay, kpsathap}@kmitl.ac.th

†† Graduate School of Engineering, Tokyo Institute of Technology,
2-12-1-S6-4, O-okayama, Meguro-ku, Tokyo, 152-8550, Japan.
Email: takada@ide.titech.ac.jp

Abstract

Correlation coefficient is a important parameter that indicates the efficiency of correlation receiver for Ultra Wideband Impulse Radio (UWB-IR) systems. The correlation coefficient is also used to analyze the waveform distortion. In this paper, the closed form formulas of correlation coefficient are derived using the rectangular passband waveform and the extension of Friss' transmission formula. The free space and ground reflection channels are considered. The results obtained from proposed formulas are compared with measurement. For ground reflection channel, the proposed formula of correlation efficient corresponds with measurement.

Keywords : ultra wideband impulse radio (UWB-IR), correlation coefficient

1 Introduction

Ultra wideband Impulse Radio (UWB-IR) is promising technique to achieve very high capacity, low cost and low power consumption properties for wireless systems. The Federal Communications Commission (FCC) in United States of America (USA) specified that UWB-IR signal has frequency spectrum ranging from 3.1 GHz to 10.6 GHz. The FCC defined that UWB-IR signal has fractional bandwidth equal to or greater than 0.20, or occupied bandwidth equal to ro greater than 500 MHz [1].

For UWB-IR correlation receiver with transmitted template signal, the correlation coefficient used to identify the receiver efficiency. The correlation coefficient is equal to 1 means the efficiency is 100%. In other word, that is the special case of correlation receiver, which is called as matched filter receiver. The transmitted template signal is identical with received signal. the correlation coefficient is decreased when the template signal is more differ. If the correlation coefficient is equal to 0, that means the template signal is orthogonal with received signal. There is no signal that can detect from the receiver. The correlation coefficient is also applied to analyze the waveform distortion [2].

In this paper, the closed form formulas of correlation coefficient are derived using the rectangular passband waveform [3] and the extension of Friss' transmission formula [4]-[5]. The free space and ground reflection channels are considered. The measurement was done for the ground reflection channel. The results obtained from proposed formula are shown and compared with measurement.

The rest of this paper is organized as follows. In section 2, correlation coefficient formulas are derived. Next, measurement and results are explained in sections 3 and 4, respectively. Finally, the conclusions are given in section 5.

2 Derivation of Correlation Coefficient Formulas

For deriving the correlation coefficient, the transmitted waveform is defined as rectangular passband waveform [3]. The expression of this waveform in time domain v_t and its spectral density V_t are

$$v_t(t) = \frac{1}{f_b}[f_H \mathrm{sinc}(2f_H t) - f_L \mathrm{sinc}(2f_L t)], \tag{1}$$

$$V_t(f) = \begin{cases} \frac{1}{2f_b} & ||f| - f_c| \le \frac{f_b}{2} \\ 0 & ||f| - f_c| > \frac{f_b}{2} \end{cases}, \tag{2}$$

where t is the time, f is the frequency, f_c is the center frequency, f_b is the spectral bandwidth and $\mathrm{sinc}(x) = \sin(\pi x)/(\pi x)$. This waveform has 1 V maximum amplitude at time zero.

Subsequently, the received waveform v_r in time domain can be evaluated using

$$v_r(t) = \int_{-\infty}^{\infty} H_c(f) \cdot V_t(f) \cdot e^{j2\pi ft} \mathrm{d}f, \tag{3}$$

where H_c is frequency transfer function of channel. The transmitter and receiver antennas are assumed to be isotropic antenna.

The correlation coefficient is defined as

$$C = \frac{\max |\int_{-\infty}^{\infty} v_r^*(t) \cdot v_t(t+\tau)\mathrm{d}t|}{\sqrt{\int_{-\infty}^{\infty} |v_r(t)|^2 \mathrm{d}t \cdot \int_{-\infty}^{\infty} |v_t(t)|^2 \mathrm{d}t}}, \tag{4}$$

where * is the complex conjugate operator. This definition is used to derive the closed form formula for free space and ground reflection channels.

2.1 Free Space Channel

The extension of Friis' transmission formula [4]-[5] is used to characterize the UWB-IR free space channel. The frequency transfer function of free space channel $H_{c,f}$ can be written as

$$H_{c,f}(f) = \frac{c}{4\pi |f| d} e^{-j2\pi fd/c}, \tag{5}$$

where c is the velocity of light and d is the distance.

The closed form formula of correlation coefficient for free space channel C_f can be derived as

$$C_f = \frac{\sqrt{f_L f_H}}{f_b} \ln\left(\frac{f_H}{f_L}\right). \tag{6}$$

2.2 Ground Reflection Channel

The frequency transfer function of ground reflection channel $H_{c,g}$ is the addition between frequency transfer function of direct and reflection paths, and can be written as

$$H_{c,g}(f) = \frac{c}{4\pi |f| d'} e^{-j2\pi fd'/c} + \Gamma \frac{c}{4\pi |f| d''} e^{-j2\pi fd''/c}, \tag{7}$$

where Γ is the reflection coefficient of ground, $d' = \sqrt{(h_t - h_r)^2 + d^2}$ and $d'' = \sqrt{(h_t + h_r)^2 + d^2}$ are distances of direct and reflection paths, h_t and h_r are the heights of Tx and Rx antennas, respectively.

The closed form formula of correlation coefficient for ground reflection channel C_g can be derived as

$$C_g = \frac{\frac{1}{f_b}\left\{\frac{1}{d'}\ln\left(\frac{f_H}{f_L}\right)+\frac{\Gamma}{d''}\left[\mathrm{Ci}\left(\frac{2\pi f_H \Delta d}{c}\right)-\mathrm{Ci}\left(\frac{2\pi f_L \Delta d}{c}\right)\right]\right\}}{\sqrt{\frac{1}{f_L f_H f_b d' d''}\left\{\frac{f_b(d''^2+\Gamma^2 d'^2)}{d' d''}-2\Gamma \mathrm{Cr}\left(\frac{2\pi\Delta d}{c}\right)-\frac{4\pi\Gamma f_L f_H \Delta d}{c}\left[\mathrm{Si}\left(\frac{2\pi f_H \Delta d}{c}\right)-\mathrm{Si}\left(\frac{2\pi f_L \Delta d}{c}\right)\right]\right\}}}, \quad (8)$$

where $\Delta d = d'' - d'$ is the difference between direct and reflection paths, $\mathrm{Cr}(x) = f_L \cos(x f_H) - f_H \cos(x f_L)$, $\mathrm{Ci}(x) = -\int_x^\infty \frac{1}{\tau}\cos(\tau)\mathrm{d}\tau$ and $\mathrm{Si}(x) = \int_0^x \frac{1}{\tau}\sin(\tau)\mathrm{d}\tau$ are cosine integral and sine integral functions, respectively.

3 Measurement

The measurement equipment, setup and parameters are the same as in [6]. The frequency transfer function of ground reflection channel was measured using a vector network analyzer (VNA). The measurement was done in the open area that is the soccer field of King Mongkuts Institute of Technology Ladkrabang (KMITL), Thailand. The metallic plate was laid on the ground between Tx and Rx antennas for the perfect reflection condition ($\Gamma = -1$).

The biconical antennas were used as Tx and Rx antennas. Both Tx and Rx antennas were fixed at the height of $h_t = h_r = 0.75$ m with horizontal polarization for focusing the signal from direct and ground reflection paths. The measurement distance d was ranged from 1 to 5 m with 0.25 m distance increment step. The frequency transfer functions of Tx and Rx antennas were evaluated by using three-antenna method [7] and were used to remove from the measurement frequency transfer functions of the ground reflection channels. The center frequency of waveform f_c is fixed at 4.1 GHz. The two cases of signal bandwidths are investigated, that are $f_b = 0.5$ and 1.4 GHz.

4 Results

For free space channel, parameters f_c is fixed at 6.85 GHz and f_b is varied from 500 MHz to 7.5 GHz. Figure 1 shows the correlation coefficient. At narrow bandwidth, the correlation coefficient is approached to 1. The efficiency of correlation receiver is almost to 100%. The minimum correlation coefficient is 0.94 at 7.5 GHz bandwidth. The comparison between transmitted and received waveforms for this case is shown in Fig. 2. The efficiency of receiver is very good for free space channel. That means the waveform is slightly distorted in free space channel.

For ground reflection channel, the analyzed parameters are the same as measurement. Figures 3 and 4 show the comparison between correlation coefficeint from proposed formula and measurement with 500 MHz and 1.4 GHz bandwidths, respectively. The efficiency is significantly decreased compared with free space channel because of multipath fadding. The wide bandwidth has effect from multipath fadding along distance less than narrow bandwidth.

5 Conclusions

In this paper, the closed form formulas of correlation coefficient are derived using the rectangular passband waveform and the extension of Friss' transmission formula. The proposed formula corresponds with measurement. For free space channel, the efficiency of correlation receiver is very good and is more than 94%. On the other hand, the efficiency is significantly decreased for ground reflection channel because of multipath fadding. Averagely, the efficiency of correlation receiver is reduced to 77% and 78% with 500 MHz and 1.4 GHz bandwidths, respectively.

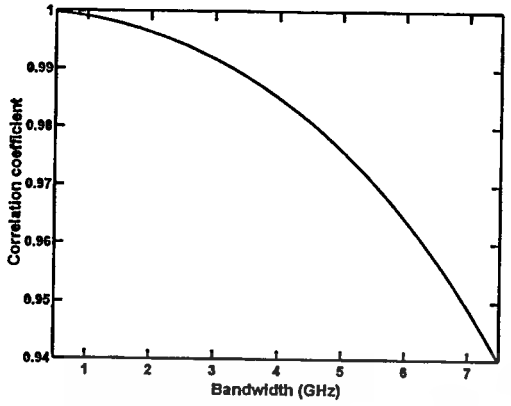

Figure 1: Correlation coefficient along 500 MHz to 7.5 GHz bandwidth for free space channel.

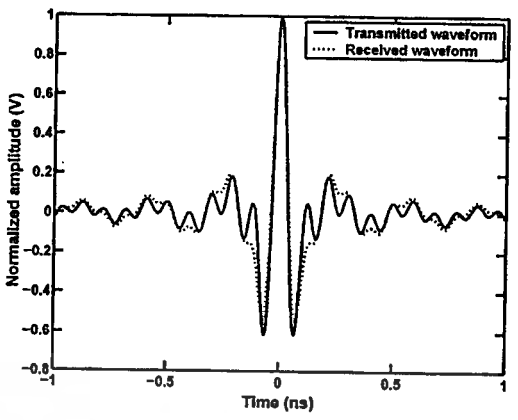

Figure 2: Comparison between transmitted and received waveforms with 7.5 GHz bandwidth.

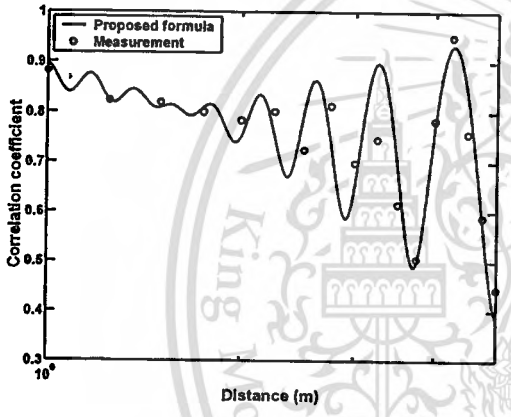

Figure 3: Comparison between correlation coefficient from proposed formula and measurement with 500 MHz bandwidth.

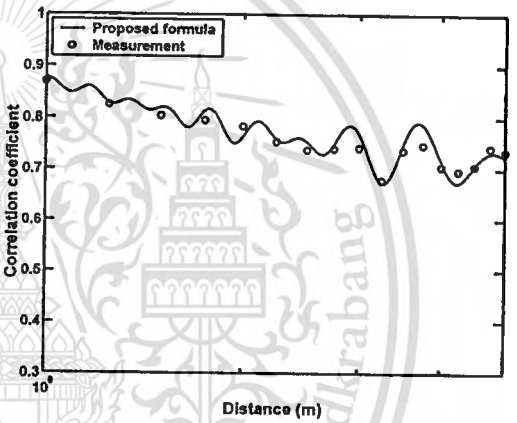

Figure 4: Comparison between correlation coefficient from proposed formula and measurement with 1.4 GHz bandwidth.

References

[1] Federal Communications Commission, "Revision of part 15 of the commission's rules regarding UWB transmission systems," First Report, FCC 02-48, Apr. 2002.

[2] S. Promwong, P. Supanakoon, J. Takada, "Waveform distortion and transmission gain on ultra wideband impulse radio," *IEICE Transactions on Communications*, vol. E93-B, no. 10, pp. 2644-2650, Oct. 2010.

[3] P. Supanakoon, K. Wansiang, S. Promwong and J. Takada, "Simple waveform for UWB communication," *Electrical Engineering/Electronics, Computer, Telecommunication, and Information Technology International Conference (ECTI-CON)*, pp. 626-629, 12-13 May 2005.

[4] J. Takada, S. Promwong and W. Hachitani, "Extension of Friis' transmission formula for ultra wideband systems," *Technical Report of IEICE*, WBS2003-8/MW2003-20, May 2003.

[5] S. Promwong and J. Takada, "Free space link budget estimation scheme for ultra wideband impulse radio with imperfect antennas," *IEICE Electronics Express*, vol. 1, no. 7, pp. 182-192, July 2004.

[6] S. Promwong, P. Supanakoon and J. Takada, "Ground refection transmission loss evaluation scheme for ultra wideband impulse radio," *ECTI-EEC Transactions on Electrical Engineering, Electronics, and Communications*, vol. 5, no. 1, pp. 18-24, Jan. 2007.

[7] S. Promwong, W. Hachitani and J. Takada, "Free space link budget evaluation of UWB-IR systems," *International Workshop on Ultra Wideband System Joint with Conference on Ultra Wideband Systems and Technologies (UWBST & IWUWBS)*, pp. 312-316, May 2004.

AUTHOR BIOGRAPHY

Pichaya Supanakoon was burn in Bangkok, Thailand. He received the B.E. degree in Telecommunication Engineering and M.E. degree in Electrical Engineering both from King Mongkut's Institute of Technology Ladkrabang, Bangkok, Thailand, in 1998 and 2000, respectively. Since 1999, he has been with the Department of Information Engineering, now he has joined in the Department of Telecommunication Engineering, Faculty of Engineering, King Mongku'ts Institute of Technology Ladkrabang. From 2004, he has been an Assistance Professor at King Mongkut's Institute of Technology Ladkrabang. His research interests are in ultra wideband impulse radio (UWB-IR) systems, electromagnetic field computation and radio wave propagation.